

**SYNTHESIS OF NOVEL POLYPEPTIDE-SILICA HYBRID MATERIALS
THROUGH SURFACE-INITIATED *N*-CARBOXYANHYDRIDE
POLYMERIZATION**

A Dissertation

by

JONATHAN DAVID LUNN

Submitted to the Office of Graduate Studies of
Texas A&M University
in partial fulfillment of the requirements for the degree of
DOCTOR OF PHILOSOPHY

May 2010

Major Subject: Chemical Engineering

**SYNTHESIS OF NOVEL POLYPEPTIDE-SILICA HYBRID MATERIALS
THROUGH SURFACE-INITIATED *N*-CARBOXYANHYDRIDE
POLYMERIZATION**

A Dissertation

by

JONATHAN DAVID LUNN

Submitted to the Office of Graduate Studies of
Texas A&M University
in partial fulfillment of the requirements for the degree of

DOCTOR OF PHILOSOPHY

Approved by:

Chair of Committee,	Daniel Shantz
Committee Members,	Michael Pishko
	David Bergbreiter
	James Batteas
Head of Department,	Michael Pishko

May 2010

Major Subject: Chemical Engineering

ABSTRACT

Synthesis of Novel Polypeptide-Silica Hybrid Materials through Surface-initiated
N-carboxyanhydride Polymerization. (May 2010)

Jonathan David Lunn, B.S., Texas A&M University;

M.S., Texas A&M University

Chair of Advisory Committee: Dr. Daniel F. Shantz

There is an increasing demand for materials that are physically robust, easily recovered, and able to perform a wide variety of chemical functions. By combining hard and soft matter synergistically, organic-inorganic hybrid materials are potentially useful for a number of applications (e.g. catalysis, separations, sensing). In this respect, organic/ordered mesoporous silica (OMS) hybrids have attracted considerable attention, with an increasing emphasis on complex organic moieties achieved through multi-step reactions and polymerizations. It is on this front that we have focused our work, specifically in regard to polypeptides.

Polypeptides are well suited organic components for hybrids as they provide a wide range of possible side chain chemistries (NH₂, -SH, -COOH, -OH, etc.), chirality, and have conformations that are known to be responsive to external stimuli (pH, electrolytes, solvents, etc.). Our work has shown that *N*-carboxyanhydride chemistry offers a facile single step approach to the incorporation of dense polypeptide brushes in OMS. Modifying the initiator loading, pore size, pore topology, and monomer identity

significantly impacted the properties of the obtained composites and peptide brush layers.

Extending this work, a synthesis paradigm for preferentially grafting poly-L-lysine to the external and internal surfaces of SBA-15, a widely used OMS material, was developed. We observed that the pores of these hybrids could be opened and closed by the reversible swelling of the polypeptide layer. Similarly, novel bifunctional hybrids were synthesized by grafting polypeptides to the external surface of monodisperse OMS spheres that contain a thiol-functionalized core. The accessibility of the internal thiols to a fluorescent dye shows the potential of these hybrids for applications such as controlled uptake/release.

To my loving wife, Nataly

ACKNOWLEDGEMENTS

I would like to thank Dr. Daniel F. Shantz for his support and guidance throughout the course of my graduate studies. He has been a great teacher and mentor. I also thank my committee members, Dr. David Bergbreiter, Dr. Michael Pishko and Dr. James Batteas. I am indebted to my colleagues in the Shantz groups for their help, advice, scrutiny and collaborations. I specifically thank Dr. Seunguk Yeu for his many interesting and fruitful discussions. I thank God for providing me with the ability, will, and opportunity to complete this degree. Lastly, I thank my family and friends and, especially my wife, Nataly, for her love and encouragement.

TABLE OF CONTENTS

	Page
ABSTRACT	iii
DEDICATION	v
ACKNOWLEDGEMENTS	vi
TABLE OF CONTENTS	vii
LIST OF FIGURES.....	ix
LIST OF TABLES	xiv
 CHAPTER	
I INTRODUCTION.....	1
1.1. Introduction.....	1
1.2. Hybrid Materials	2
1.3. Silica-based Materials.....	6
1.4. OMS Hybrids.....	25
1.5. Polymer Synthesis.....	30
1.6. Surface Grafting.....	68
1.7. Research Hypothesis and Objectives.....	73
II EXPERIMENTAL METHODS	75
2.1. Introduction.....	75
2.2. Synthetic Procedures.....	75
2.3. Analytical Methods.....	93
III INITIAL WORK.....	115
3.1. Introduction.....	115
3.2. Experimental.....	116
3.3. Results.....	116
3.4. Conclusions.....	126
IV POLYPEPTIDE—OMS HYBRID MATERIALS.....	127
4.1. Introduction.....	127

CHAPTER	Page
4.2. Experimental.....	127
4.3. Results.....	128
4.4. Discussion.....	151
4.5. Conclusions.....	153
V SURFACE SELECTIVE GRAFTING	154
5.1. Introduction.....	154
5.2. Selective Grafting of Polylysine Only	155
5.3. Selective Grafting of Polylysine and Thiols	162
5.4. Summary	174
VI POLYPEPTIDE/THIOL—OMS SPHERE HYBRIDS	176
6.1. Introduction.....	176
6.2. Experimental.....	177
6.3. Results.....	178
6.4. Conclusions.....	190
VII CONCLUSIONS AND FUTURE WORK	192
7.1. Conclusions.....	192
7.2. Future Work.....	194
REFERENCES.....	199
APPENDIX A	215
APPENDIX B	221
APPENDIX C	227
VITA	228

LIST OF FIGURES

FIGURE	Page
1.1 Diagram clarifying the distinction between hybrid materials, nanocomposites and composites	3
1.2 Common hybrid synthesis routes derived from sol-gel chemistry	4
1.3 Polymerization behavior of aqueous silica.....	11
1.4 Simulated structures from various growth models with corresponding fractal dimensions	12
1.5 pH dependence of hydrolysis, condensation, and dissolution.....	14
1.6 Pictorial representation of the MFI zeolite framework along [010] plane	17
1.7 TEM images of (a) MCM-41, (b) MCM-48.	19
1.8 Comparison between MCM-41 and SBA-15	21
1.9 TEM image of SBA-15	21
1.10 Characteristic features of KIT-6: a) XRD pattern; b) TEM image; c) N ₂ adsorption isotherm; and d) pore size distributions at different synthesis temperatures	22
1.11 Some examples of free-radical initiators.....	49
1.12 Persistent radicals used in NMP	54
1.13 Examples of Cu ligands in ATRP	57
1.14 Free energy change (ΔG_o^{298}) and relative values of K_{ATRP} for homolytic bond cleavage of alkyl bromides deduced from DFT calculations at 25°C relative to methyl 2-bromopropionate ($K_{ATRP}=1$).....	58
1.15 R leaving group ability and Z group influence over addition and fragmentation	61
1.16 The most common ROMP catalysts.....	67

FIGURE	Page
1.17 Graphic depiction of adsorbed vs. covalently attached polymers.....	69
1.18 Pictorial representation of surface grafting approaches	70
1.19 Examples of surface bound initiators for the grafting from approach	71
2.1 A visual representation of Bragg's Law.....	95
2.2 The XRD pattern of MCM-48.....	95
2.3 The six IUPAC classification of adsorption isotherms	97
2.4 Typical FT-IR spectrometer instrument configuration	101
2.5 Examples of molecules with and without permanent dipole moments.....	102
2.6 Potential well for the harmonic oscillator	104
2.7 Normal modes of vibration for carbon dioxide.....	105
2.8 Types of vibration for a methylene group.....	106
2.9 Tabulated IR absorption band ranges by functional group	107
2.10 Simplified schematic of photoemission spectroscopy	108
2.11 Schematic of the photoemission process for XPS.....	110
2.12 XPS spectrum of Sn	112
3.1 Survey and C 1s XPS scans of PZLK and APTMS grafted from silicon	117
3.2 CD spectra of PZLK grafted from silicon.....	118
3.3 Survey (left) and C 1s (right) XPS scans of Fmoc-spaced PZLK and APTMS grafted from silicon.....	120
3.4 CD spectra of Fmoc-spaced PZLK on silicon.....	121
3.5 XPS survey scans of APTMS and PZLK on colloidal silica	123

FIGURE	Page
3.6 FT-IR and CD of the PZLK grafted from colloidal silica.....	124
3.7 FT-IR of various polypeptides grafted to MCM-41: Polyglycine, Poly-L-alanine, PZLK, APTMS-MCM-41.....	125
4.1 PXRD of MCM-41, SBA-15, and KIT-6.....	129
4.2 Adsorption isotherms of MCM-41, SBA-15, and KIT-6.....	130
4.3 IR spectra of the Poly-Z-L-lysine—MCM-41 composites.....	135
4.4 IR spectra of the protected (top) and deprotected (•HBr) (bottom) 0.75mmol APTMS/g SiO ₂ Poly-Z-L-lysine—MCM-41 composite.....	136
4.5 ¹³ C{ ¹ H} CP MAS NMR of the side chain protected and deprotected (•HBr) 0.75mmol APTMS/g MCM-41 Poly-Z-L-lysine composite.....	137
4.6 XPS of the Poly-Z-L-lysine—MCM-41 composites: 0.75mmol APTMS/g; 0.50mmol APTMS/g; and 0.25mmol APTMS/g.....	139
4.7 MALDI-TOF MS of peptide from the 0.25mmol APTMS/g SBA-15 Poly-Z-L-lysine composite.....	140
4.8 MALDI-TOF MS of peptide from the 0.50mmol APTMS/g SBA-15 Poly-Z-L-lysine composite.....	141
4.9 MALDI-TOF MS of peptide from the 0.75mmol APTMS/g SBA-15 Poly-Z-L-lysine composite.....	141
4.10 IR spectra of the Poly-L-alanine—SBA-15 composites: 0.75mmol APTMS/g; 0.50mmol APTMS/g; and 0.25mmol APTMS/g.....	146
4.11 IR spectra of the Poly-L-alanine—MCM-41 and KIT-6 composites, both containing 0.5mmol ATPMS/g SiO ₂	146
4.12 XPS of the Poly-L-alanine—SBA-15 composites: 0.75mmol APTMS/g; 0.50mmol APTMS/g; and 0.25mmol APTMS/g.....	147
4.13 MALDI-TOF MS of peptide from the 0.25mmol APTMS/g SBA-15 Poly-L-alanine composite.....	148

FIGURE	Page
4.14 MALDI-TOF MS of peptide from the 0.50mmol APTMS/g SBA-15 Poly-L-alanine composite.....	149
4.15 MALDI-TOF MS of peptide from the 0.75mmol APTMS/g SBA-15 Poly-L-alanine composite.....	149
4.16 MALDI-TOF MS of peptide from the 0.75mmol APTMS/g MCM-41 Poly-L-alanine composite.....	150
4.17 MALDI-TOF MS of peptide from the 0.75mmol APTMS/g KIT-6 Poly-L-alanine composite.....	150
5.1 Pictorial representations of externally and internally grafted poly-Z-L-lysine SBA-15 hybrids with thiols grafted to the opposite surface.....	155
5.2 XPS spectra of I1 and X1	157
5.3 IR spectra of the externally and internally poly-Z-L-lysine grafted SBA-15, showing spectra for the precursor materials, and both protected and deprotected hybrids.....	159
5.4 Nitrogen adsorption isotherms of the externally and internally poly-Z-L-lysine grafted SBA-15.....	161
5.5 XPS spectra of externally grafted MPTMS to SBA-15 by various methods: MW approach; 24 hours reflux w/ water; and 2h stirring at RT.....	163
5.6 Confocal images of A) I2 and B) X2 dyed with NHS-fluorescein and BODIPY-TMR thiosulfate; C) XPS spectra of I2 and X2	166
5.7 IR spectra of PZK-X2-10 and PZK-I2-10	167
5.8 SEM images of the samples prepared <i>via</i> microwaves.....	169
5.9 A) Plot of N/Si and C/Si atomic ratios for poly-Z-L-lysine grafted samples; B) XPS spectra of PZK-I2-5 (top) and PZK-X2-5	170
5.10 A) Nitrogen adsorption isotherms of I2 , PK-I2-5 , and PK-I2-10 ; B) Nitrogen adsorption isotherms of the neutral PK-I2-10 and protonated PK-I2-10 H+	171

FIGURE	Page
5.11 A) Nitrogen adsorption isotherms of X2 , PK-X2-5 , and PK-X2-10 ; B) Nitrogen adsorption isotherms of the neutral PK-X2-10 and protonated PK-X2-10 H+	173
5.12 IR of neutral and protonated A) PK-X-10 and B) PK-I-10	175
6.1 XRD and SEM of OMS spheres: A) XRD pattern of as-made OMS spheres with thiol core and B) SEM image of NH₂/SH-MMSS	179
6.2 Nitrogen adsorption isotherm of NH₂/SH-MMSS	180
6.3 XPS spectra and confocal microscopy of NH₂/SH-MMSS : A) XPS spectra comparing OMS spheres that were amine-functionalized and extracted, with those that were extracted without additional functionalization; and B) A confocal image of spheres dyed with NHS-fluorescein and BODIPY-TMR thiosulfate.....	181
6.4 A) IR and B) XPS spectra of PZK/SH-MMSS before and after deprotection.....	183
6.5 A) IR and B) XPS spectra of PBG/SH-MMSS before and after deprotection.....	184
6.6 A) IR and B) XPS spectra of PZK&PBG/SH-MMSS before and after deprotection.....	185
6.7 SEM images of the OMS spheres before and after polymerization	188
6.8 Confocal images showing the uptake of amine and thiol-selective dyes in the various hybrids	189

LIST OF TABLES

TABLE	Page
1.1 Susceptibility of various types of monomers to free-radical, cationic and anionic polymerization.....	35
1.2 Initiating systems for vinyl ethers and isobutene	44
1.3 Reactivity of transition metals investigated in ROMP with respect to olefins	66
4.1 Tabulated nitrogen adsorption results for the poly-Z-L-lysine—OMS composites	131
4.2 Elemental composition.....	133
4.3 Catalytic results for the nitroaldol reaction between <i>p</i> -nitrobenzaldehyde and nitromethane	142
4.4 Tabulated nitrogen adsorption results for the poly-L-alanine—OMS composites.....	144
5.1 Adsorption and TGA data of hybrids synthesized from X1 and I1	158
5.2 Adsorption and TGA data of MW samples.....	167
6.1 Adsorption and TGA data of OMS sphere hybrids.....	187

CHAPTER I

INTRODUCTION

1.1 Introduction

Throughout history, humans have striven to develop new materials to fit the needs of daily life and expanding civilization, frequently by physically combining known materials. An early example of such a material, ancient Egyptians would construct bricks by mixing chopped straw into Nile alluvium (a mixture of silt, clay). This straw had a high organic acid content which made the clay more workable and plastic and prevented shrinkage upon drying.¹ Such materials are termed *composites*.

A composite is a material derived from two or more materials, generally with significantly different chemical and physical properties. The components maintain their individual character on a small scale; while on a larger scale create a new material with unique properties and characteristics. Materials are generally chosen in order to profit from the favorable characteristics – and likewise counteract the unfavorable characteristics – of the individual components. A superior material is thus created through synergy. Commonly encountered composite materials are asphalt concrete, composed of mineral aggregate and a complex mixture of hydrocarbon binders, and plywood, composed of wood veneers and adhesives. Both of these materials have enhanced strength and durability compared to their parent materials, as is frequently the desired outcome.

This dissertation follows the style of *Chemistry of Materials*.

Whereas most composites combine macroscopic materials or phases, *nanocomposite* materials represent a special subgroup in which one or more of the components has a dimension 1-100nm. By increasing interfacial interaction between components, nanocomposites possess novel properties unattainable in the bulk or with substituents of larger dimensions. For example, polymers infused with nanoparticles exhibit dramatically reduced light scattering than those with larger particles and as a result have very interesting optical characteristics.²

1.2 Hybrid Materials

A term sometimes used interchangeably with nanocomposite is *hybrid material* or simply “hybrid”. A hybrid material, however, can be distinguished from a nanocomposite in that it is a molecular dispersion rather than a dispersion of a nanometer-scale (1-100nm) phase,² as is the case when colloidal inorganic particles are dispersed in a polymer matrix or porous silicates are filled with a polymeric phase (i.e. no individual bonding to the surface). That means, frequently, the dispersed component has dimensions smaller than 1nm and is not a nanocomposite. These definitions become blurred when the dispersed molecules are macromolecular species with nanometer-scale dimensions (See Figure 1.1 for clarification). For the purpose of this dissertation we will continue to refer to such materials as hybrids.

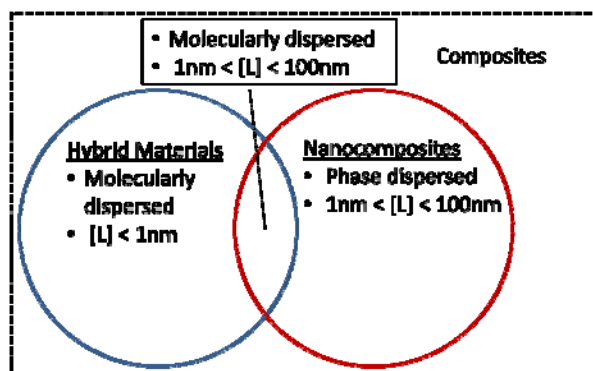


Figure 1.1 Diagram clarifying the distinction between hybrid materials, nanocomposites and composites.

Most relevant to the following discussion are those composed of organic and inorganic species. These materials are most commonly organic moieties bound to silicates. Isolating chemically specific functional moieties on physically rigid surfaces, not only maximizes the interactions between the two components, but also external species making them potentially useful in a variety of applications, such as, complex separations, highly selective catalysis, and sensing. As there is an increasing demand for materials that are physically robust, easily recovered, and able to perform a wide variety of chemical functions, such materials have received considerable attention among researchers. Clays and layered silicates intercalated with organic cations are an early and still prevalent example of hybrid materials.³ By exchanging alkali cations with varying sizes of organic cations, the spacing between layers can be made to expand or contract making them potentially useful for membrane separations and other applications. Ancient Mayans, though ignorant of the chemistry involved, also used clays impregnated with indigo as dyes for wall paintings.³

Hybrid materials can be synthesized through a wide variety of techniques. The use of pre-existing silicates and inorganic materials such as those just described are still used; however, the use of sol-gel chemistry for silica matrix construction permits the greatest degree of design flexibility and variety of materials that can be synthesized. Common synthesis techniques derived from sol-gel chemistry have been outlined by Gomez-Romero and Sanchez and are shown in Figure 1.1.3. Relevant approaches to this work will be discussed in more detail below.

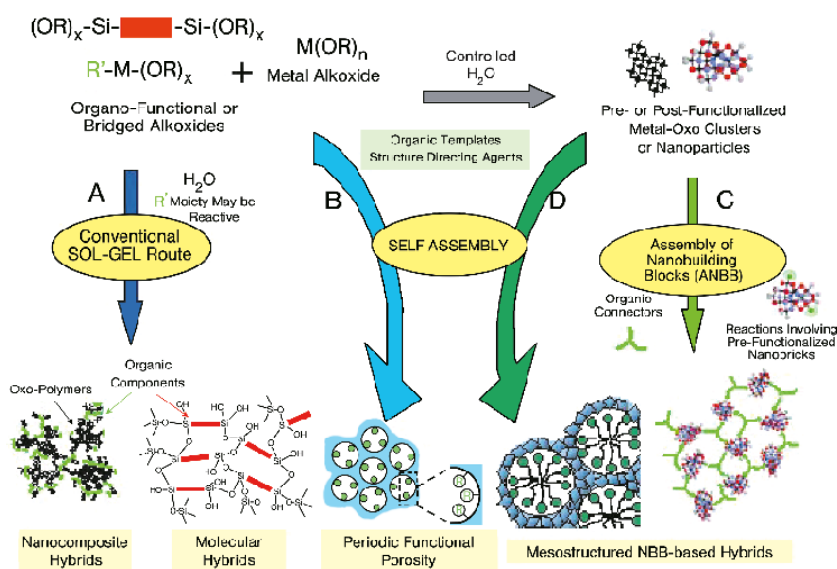


Figure 1.2 Common hybrid synthesis routes derived from sol-gel chemistry.³

Polymers, though most commonly used as hybrid or nanocomposite matrices, have more recently been used as the organic modifier of silica-based hybrids. These studies initially focused only on functionalizing planar and colloidal surfaces with polymers, but over the past few years have transitioned to porous silicates as well.

Polymers are interesting organic modifiers for hybrids as they dramatically increase the number of functional sites compared to simple functional groups, have diverse chemistries, and have very unique physical properties.

Since the discovery of *N*-carboxyanhydrides (NCAs) by Hermann Leuchs in 1906,⁴⁻⁶ NCAs have been used to synthesize a diverse set of materials from step-wise constructed peptides⁷ to drug-delivery devices,^{8,9} polymeric brushes¹⁰ and as templates for inorganic oxides.¹¹⁻¹⁴ As polypeptides are chiral, responsive to external stimuli (pH, electrolytes, solvent and temperature) and offer a wide range of side chain chemistries (thiols, amines, carboxylic acids, etc.), they are very suitable organic components in hybrid materials for possible applications such as chiral separations, solid asymmetric catalysts, drug delivery and sensing.

This dissertation explores hybrid materials resulting from the grafting of polypeptides from silica, primarily ordered mesoporous silica (OMS). The synthesis of these hybrids involves two principal steps, silica matrix synthesis through sol-gel chemistry followed by the covalent attachment of polypeptides through a surface-initiated polymerization. As a result, this work may be understood with respect to two seemingly distinct fields: sol-gel chemistry derived materials and polymer synthesis. In order to fully appreciate the presented findings, an understanding of both is helpful. First, sol-gel chemistry will be discussed, including OMS synthesis and development of simple OMS-hybrid materials. This discussion will be followed by a detailed overview of polymer chemistry and grafting to surfaces. Finally, the objectives of this dissertation work and initial hypotheses will be presented.

1.3 Silica-based Materials

1.3.1 *Sol-gel Chemistry*

First capturing the interest of scientists in the mid-1800s studying silica gels, the sol-gel method is a means of synthesizing metal oxide frameworks and particles, primarily silica, *via* polycondensation of the monomeric metal oxide species in solution — silicic acid, $\text{Si}(\text{OH})_4$, in the case of silica.¹⁵ The term sol-gel is derived from the potential products and intermediates of this process: sols and gels. Sols are dispersions of colloidal particles in solution, and gels, rather than distinct particles, are rigid interconnected porous (submicron) networks and polymeric species. Sol-gel chemistry allows us to synthesize new siliceous (and inorganic oxide) materials using chemical methods, in contrast to previous approaches of manipulating naturally occurring solids. As this dissertation focuses on hybrids of silica and silica is sufficiently complex on its own, the summary below will be limited to silica.

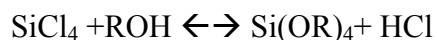
1.3.2 *General Considerations*

As mentioned above silica is a polymer; it is synthesized through the polycondensation of its monomer, silicic acid, $\text{Si}(\text{OH})_4$. Two factors which distinguish the polycondensation of silica acid from the polycondensation reactions of organic polymers (as we will see below) are: a) silicon is the major player rather than carbon; and b) there are four reactive groups, rather than two in the case of the typical organic polymer (notable exceptions being resins and dendrimers, for example). These two factors bring about a fundamental difference in the way silica polymerizes. According

to Iler,¹⁶ one of the early pioneers in silica chemistry, in contrast to traditional organic polymerizations which form chains which branch and crosslink, polymerization in sol-gels occurs in three main steps: 1) particle formation through monomer polymerization; 2) particle growth; and, depending upon solution conditions, 3) particles link to form chains, networks, and eventually a gel. That is to say, rather than forming chains, sol-gels form dense particles (in aqueous solutions) and subsequent reactions involve monomer to surface interactions or surface to surface interactions rather than those between isolated functional groups.

1.3.3 Precursor Materials

“Sol-gels” are formed by means of two principal methods: 1) hydrolysis and polycondensation of molecular precursors, most commonly tetraalkoxysilanes; or 2) dissolution/polycondensation or direct gelation of a solution of colloidal particles (such as the commercially available Ludox®) or other solid precursor. The first approach is more simplistic for fundamental scientific studies, as it does not depend upon the dissolution rate of the solid precursor. The most prevalent tetraalkoxysilanes used in the literature are tetraethoxysilane (TEOS) and tetramethoxysilane (TMOS), both synthesized by reacting the respective anhydrous alcohol with tetrachlorosilane (Scheme 1.1). It should be noted that the bulkier and more branched the alkyl group of the alkoxide, the more stable the silane is toward hydrolysis and alcohol condensation.

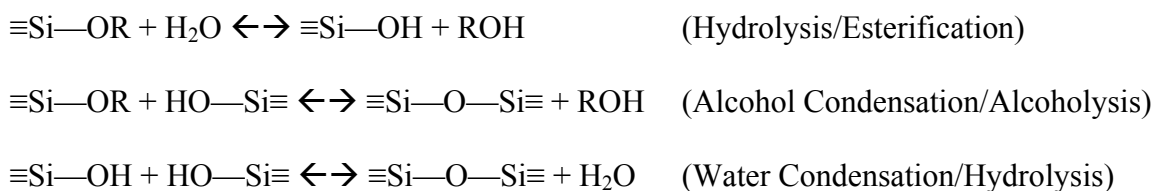


Scheme 1.1 Tetraalkoxysilane synthesis from tetrachlorosilane

In many cases, it is desired to reduce the number of hydrolysable bonds (e.g., for linear silicon polymers, such as, polydimethylsiloxane) or to incorporate an organic functional group. For this purpose, alkoxide groups may be substituted with alkyl groups. A wide variety of organosilanes are commercially available.

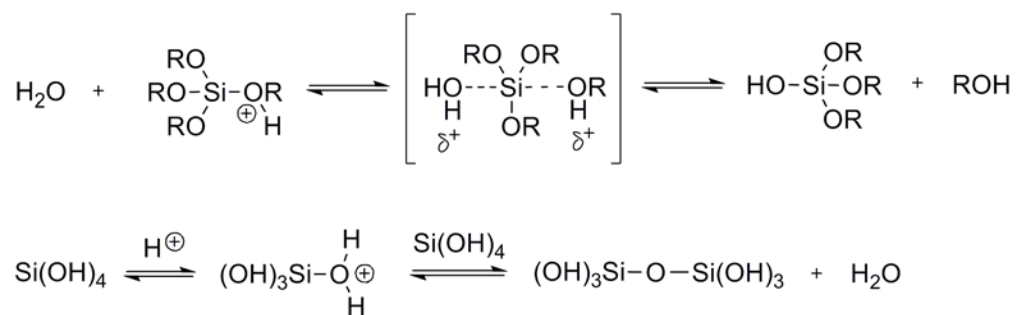
1.3.4 Hydrolysis and Condensation

Upon mixing with water, usually accompanied by a catalyst such as acid or base, tetraalkoxysilanes undergo hydrolysis to form silicic acid. The silanol, as a nucleophile, reacts with an electrophilic silicon from another silane to form a siloxane bond, either to produce water or alcohol as a byproduct in a condensation reaction. A minimum water-to-tetraalkoxysilane ratio of two is required for complete hydrolysis and condensation, though this ratio is typically over four. The principal reactions are shown below in Scheme 1.2.

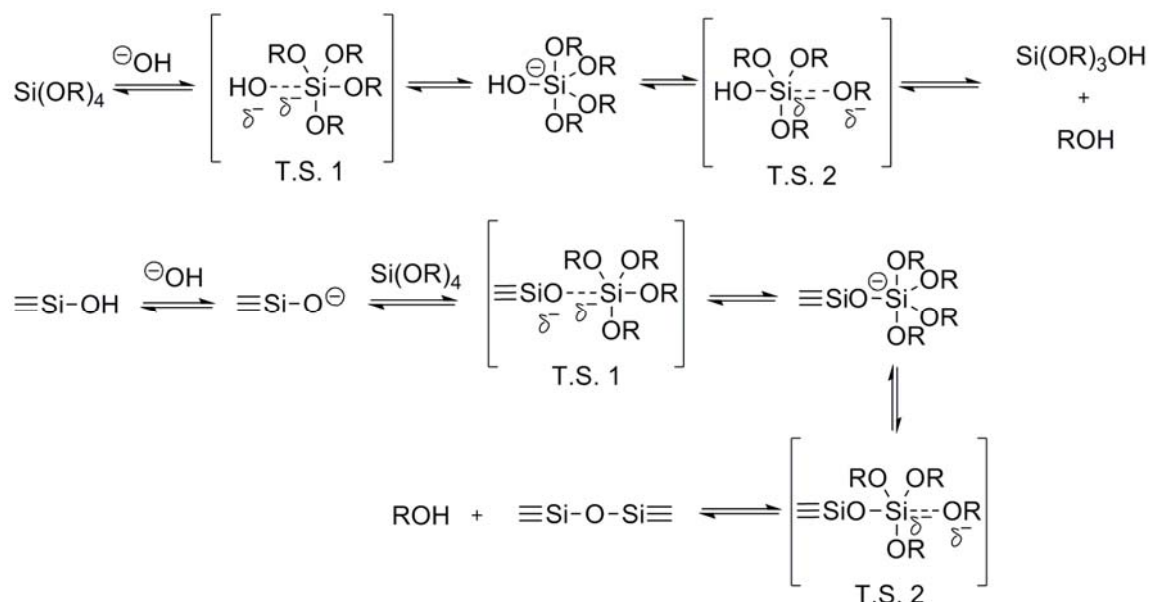


Scheme 1.2 Principle reactions in the sol-gel process.¹⁵

Hydrolysis and condensation occur *via* S_N2-type mechanisms for both acid and base catalysis.¹⁵ In the acid-catalysis mechanisms, the alkoxy or hydroxyl group attached to silicon is first protonated, activating it for nucleophilic attack by water or a silanol in hydrolysis and condensation, respectively (Scheme 1.3a). Conversely, in the base-catalyzed mechanisms, silanes are attacked directly by hydroxyl ion for hydrolysis and by silanolate ion for condensation (Scheme 1.3b). Interestingly, both base-catalyzed mechanisms pass through a pentacoordinate silicon intermediate with a formal negative charge.



Scheme 1.3a Acid-catalyzed hydrolysis (top) and condensation (bottom) mechanisms.¹⁵



Scheme 1.3b Base-catalyzed hydrolysis (top) and condensation (bottom) mechanisms.¹⁵

1.3.5 Particle Formation and Gelation

As discussed by Iler¹⁶ and Brinker¹⁵, at the onset of hydrolysis in aqueous silicates, silicate rings are rapidly formed which grow through monomer addition into dense particles on the range of 1-5nm. These primary particles serve as nuclei for growth through Oswald ripening from numerous small and highly soluble particles to fewer larger and much less soluble particles. Factors, such as pH, dilution, temperature, and the presence of salts, fluoride ion or organic compounds influence the size of these elementary particles and what comes of them: whether larger colloids or gels are formed and their corresponding physical characteristics (morphology, porosity, etc.) (Figure 1.3).

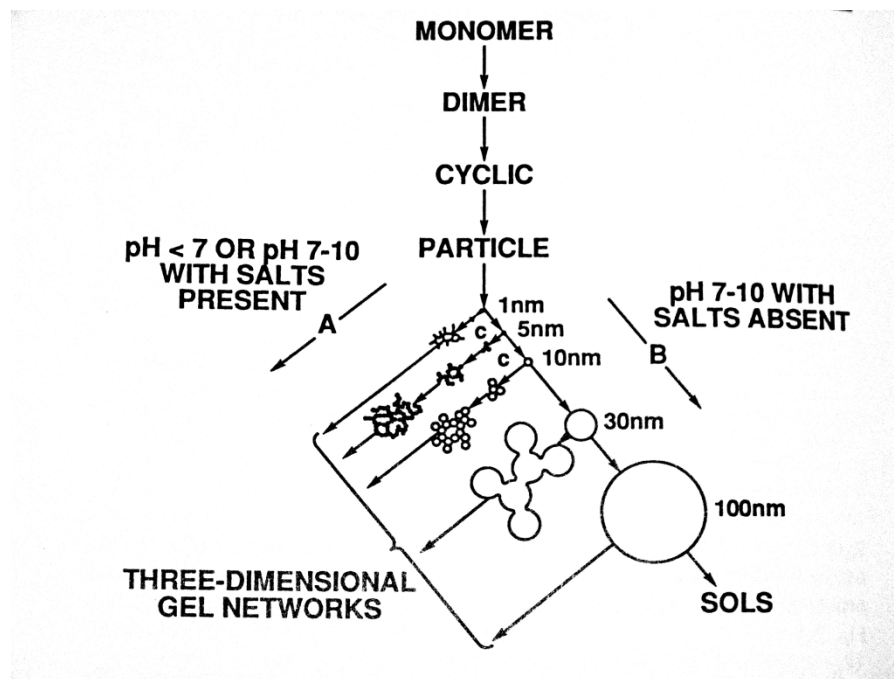


Figure 1.3 Polymerization behavior of aqueous silica.¹⁶

1.3.5.1 Growth Models

There are two sets of growth models that have been developed for aqueous silicate systems to explain experimental observation: monomer-cluster growth and cluster-cluster growth.¹⁵ The cluster-cluster growth model is the limiting case in which clusters react exclusively with each other in the absence of available monomer. Monomer-cluster growth is another limiting case in which monomer is continually available and reacts exclusively with pre-formed clusters. Within these two sets of models there are the reaction and diffusion-limited cases. Diffusion-limited cluster-cluster aggregation (DLCA) occurs when the reaction rate is fast compared to that of diffusion and the clusters react upon the first collision. This model leads to aggregates

with a low fractal dimension ($d_f \sim 1.8$) as simulated by Meakin¹⁷ (Figure 1.4). Reaction-limited cluster-cluster aggregation is the opposite case, in which a collision does not necessarily correspond to a reaction and leads to slightly higher fractal dimensions ($d_f \sim 2.09$). Diffusion-limited monomer-cluster aggregation (DLMCA) and reaction-limited monomer-cluster aggregation (RLMCA) describe the equivalent cases for monomer-cluster growth, which lead to higher fractal dimensions, $d_f \sim 2.5$ and $d_f \sim 3$, respectively. From these growth models/mechanisms, a range of structures can be obtained from more linear in the case of DLCA to spherical for RLMCA.



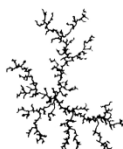
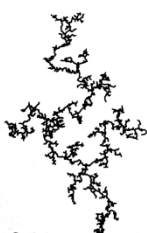
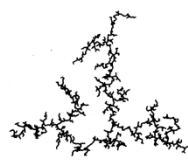
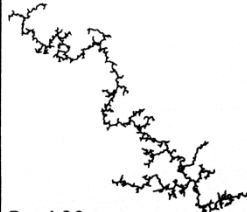
	REACTION-LIMITED	BALLISTIC	DIFFUSION-LIMITED
MONOMER-CLUSTER	EDEN  $D = 3.00$	VOLD  $D = 3.00$	WITTEN-SANDER  $D = 2.50$
CLUSTER-CLUSTER	RLCA  $D = 2.09$	SUTHERLAND  $D = 1.95$	DLCA  $D = 1.80$

Figure 1.4 Simulated structures from various growth models with corresponding fractal dimensions ($D = d_f$).^{15,17}

1.3.5.2 *Low pH (pH<2)*

Both Brinker¹⁵ and Iler¹⁶ divide the pH dependence of silica polymerization into three regions: $\text{pH} < 2$; $2 < \text{pH} < 7$; and $\text{pH} > 7$. As the isoelectric point of silica is at approximately a pH of 2, acid catalysis occurs at $\text{pH} < 2$ and base catalysis at $\text{pH} > 2$. At low pH values (< 2), below the isoelectric point, hydrolysis and condensation occur through acid catalysis as described above. The hydrolysis rate is much higher than the condensation rate. The high hydrolysis rate is likely due to the fact that the electron-donating alkoxy groups promote hydrolysis through the stabilization of the protonated intermediate, whereas, the more electron withdrawing hydroxyl and siloxane bonds destabilize it. After complete conversion of alkoxy silane to silicic acid, small colloidal particles are formed and further condensation occurs as described by the RLCA model. Aggregation occurs as the silanols on the particle surfaces are neutral and lack electrostatic repulsion needed for a stable suspension. As depolymerization does not occur appreciably at low pHs, the clusters bind irreversibly resulting in a three-dimensional gel network (Figure 1.4). Figure 1.5 shows the dependence of pH on hydrolysis, condensation and dissolution.

1.3.5.3 *High pH (pH>7)*

High pH systems at sufficient dilutions ($\text{H}_2\text{O}/\text{Tetraalkoxysilane} > 4$) follow the RLMCA model leading to non-fractal spherical structures (Figure 1.4). Upon hydrolysis, small colloidal particles form, as in the low pH scenario. However, at high pHs, the acidic surface silanols deprotonate resulting in electrostatic repulsion and stable

sols. Silica is soluble at higher pH values; silanes with only one siloxane bond (Q1 sites) are preferentially dissolved resulting in the dual effect of creating a continuous monomer supply and enabling restructuring of the surface (Figure 1.5). High pH systems when accompanied by ammonia can form monodisperse spheres as occurs in the Stöber Process¹⁸ with varying sizes depending primarily on the ratio between ammonia and silica.

1.3.5.4 Intermediate pH ($2 < \text{pH} < 7$)

As one might expect, systems of intermediate pH values can form structures which share features of both limiting cases. At pH values closer to 2, the structures are more akin to the networks of small particles seen for low pH values; for those closer to 7, structures of higher fractal dimensions (Figure 1.4).

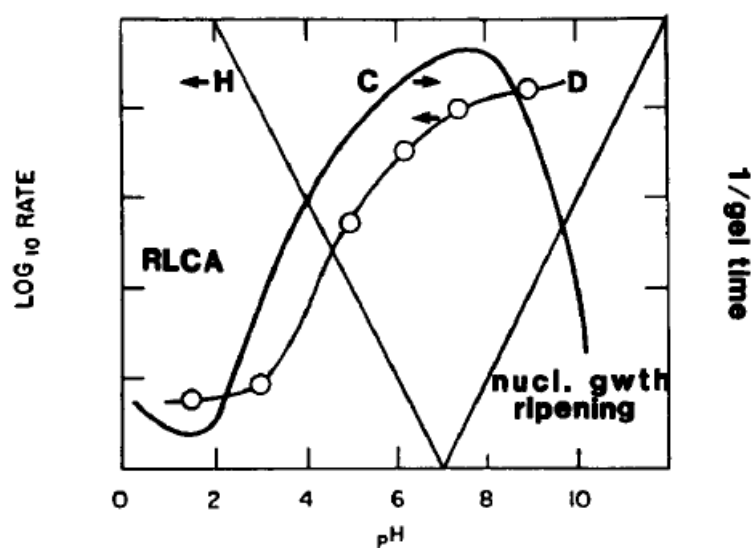


Figure 1.5 pH dependence of hydrolysis (H), condensation (C), and dissolution (D).¹⁵

1.3.5.5 Other Contribution Factors

The presence of salts, fluoride ion and cosolvents can significantly alter the behavior described above. Salts or charged organic compounds shield the negatively charged surfaces, which stabilize sols causing them to aggregate at pH values in which they would otherwise be stable. Fluoride ion makes silanols more acidic, which can promote dissolution and restructuring of silicates at low pH values. Cosolvents, depending on their polarity and other properties, can enhance or decrease the solubility of silica.

1.3.6 Porous Silicates

One of the greatest achievements of sol-gel chemistry is the ability to synthesize a large variety of porous materials with different pore sizes, molecular structures, and inherent properties. Porous inorganic materials that can be used in applications such as catalysis and separations have been intensely studied over the last 50 years due to their potential stability, ease of recovery and high surface areas. These materials can be divided into three categories according to pore size: microporous ($< 2\text{nm}$), mesoporous ($2\text{-}50\text{nm}$), and macroporous ($> 50\text{nm}$). It should be noted, however, that materials do not always belong exclusively to one category and may have a broad range of pore sizes or shapes.

Amorphous oxides, while widely used industrially, are complex due to their inherent disorder. From a fundamental viewpoint, inorganic solids which are crystalline, or at least ordered, should be easier to understand and are useful for specialty

applications where tight control of pore size and physical properties is desired. With this in mind, zeolites have received considerable interest in the latter half of the last century and ordered mesoporous silicas in the last two decades.

1.3.6.1 Zeolites

Discovered in 1756 by the Swedish mineralogist A.F. Cronstedt, zeolites are crystalline silicates and aluminosilicates with high surface areas and uniform micropores resulting from their crystal structure. Zeolites have shown to be very useful in applications such as ion-exchange, separations by size exclusion and catalytic cracking. Though there are approximately 40 naturally occurring zeolitic structures, Barrer and Denny first realized the potential of sol-gel chemistry for zeolite synthesis in 1961 with the synthesis of a Zeolite A (LTA) analog using a silica sol at high pH accompanied by tetramethylammonium cations.¹⁹

Today, synthetic protocols for numerous zeolitic frameworks exist (including naturally occurring varieties) with diverse crystal structures, pore connectivities and chemical properties. Zeolite synthesis is typically performed at high pH combining a silica source, such as those discussed above (e.g. tetraalkoxysilane, sodium silicate, silica sol or solid silica precursor), an alumina source, and alkali/organic cations, followed by aging at elevated temperatures (~100-200° C) for a period of days to months. Once filtered and rinsed, alkali cations can be removed through ion exchange and organic cations by calcination.

Charge matching of the zeolite framework with the employed cation(s), as well as the cation shape, are extremely important in zeolite synthesis and the type of cation used highly influences the type of zeolite (if any) formed. Such cations are referred to frequently in the literature as templates or structure-directing agents (SDAs).²⁰ Due to the importance of charge matching, smaller alkali cations are good templating agents for high aluminum content zeolites which contain a large number of acid sites and larger organic cations with lower charge densities for intermediate ($2 < \text{Si/Al} < 5$) to high silica zeolites ($5 < \text{Si/Al}$). Though in many cases, cations are selective to specific zeolitic phases, their precise role and the zeolite nucleation mechanism in general are still subject to rigorous investigation.²¹⁻²⁴ For high silica zeolites, these investigations mainly focus on understanding the mechanistic aspects of the synthesis of silicalite-1 (MFI), believed to be a “model” zeolite as it is purely siliceous, easy to synthesize, and uses simple tetraalkylammonium cations (TAAs) as SDAs (Figure 1.6). Though the mechanism is still highly debatable, recent work indicates silicalite-1 is formed by the nucleation of amorphous elementary particles with an adsorbed layer(s) of TAA in a cluster-cluster type growth mechanism followed/accompanied by restructuring.^{25,26}

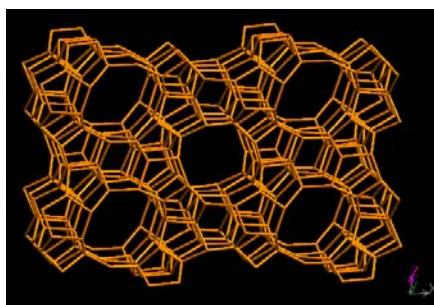


Figure 1.6 Pictorial representation of the MFI zeolite framework along [010] plane.

Despite having a wide range of applications, current and potential, zeolites are limited by their small pore sizes, which are usually less than 2nm. Though small pore sizes are a strength in cases where size and shape selectivity for small molecules are desired, as is relevant in catalysis and membrane separations, there are many cases where the admittance of larger molecules is desirable. This desire led to the development of larger pore zeolites such as VPI-5 in the late 1980s and ultimately to the discovery of ordered mesoporous silicas by Mobil Corporation, published in 1992.

1.3.6.2 Ordered Mesoporous Silicas

Ordered mesoporous silicas (OMS) are siliceous materials that, though they are not crystalline, possess mesopores with long range ordering. The mesophases can be arranged in a number of topologies: cubic, hexagonal, and cubic bicontinuous, for example. Synthesis mixtures are prepared by combining a tetraalkoxysilane (or some other silica source), an organic SDA, and either an acid or base. The mixture is heated for period of time, typically on the order of days, followed by aging (if required), then filtered and washed. To remove the organic structure-directing agent, the resulting powder is either calcined at a high temperature or extracted. OMS synthesis is very similar to zeolite synthesis in that a structure-directing agent is involved. The biggest difference between them, however, is the type of SDA employed: SDAs for OMS are much larger and typically self-assemble into micellar structures. Since, the initial discovery, numerous OMS materials have been synthesized. The OMS materials used in this dissertation are described below.

1) MCM-41

The first types of OMS were developed by the Mobil Corporation in the early 1990's when Mobil researchers experimented with longer chain alkyltrimethylammonium salts and are referred to as M41S. They discovered that the alkyltrimethylammonium salts self-assemble into 2D and 3D structures which in turn act as templates for silica polymerization. The most well known and widely studied of this OMS type is MCM-41. MCM-41 has hexagonally arranged cylindrical pores ($p6mm$) which can vary from 2.5-10 nm in diameter depending on the length of the alkyl chain in the template. It is formed under basic conditions, typically, using cetyltrimethylammonium bromide (CTAB) as the template. Using CTAB, a typical pore size for MCM-41 is 4nm. Both molecular and solid silica precursors may be used as silica is readily dissoluble in this pH region. Another M41S material, MCM-48, is cubic and its pore network can be represented by the $Ia3d$ space group.²⁷ Figure 1.7 compares the TEM images of MCM-41 and MCM-48.

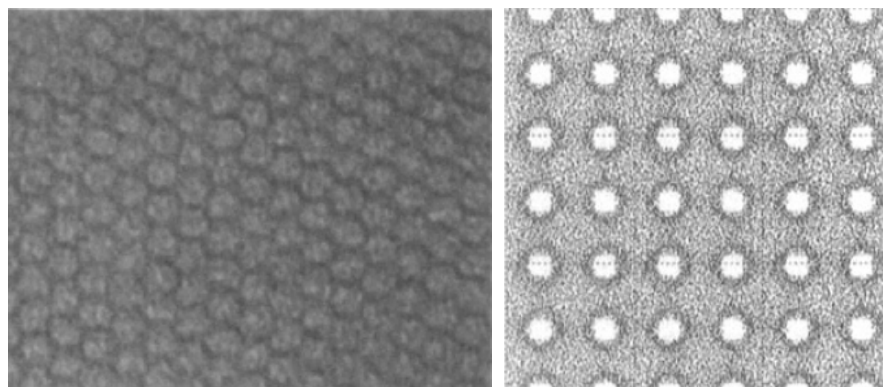


Figure 1.7 TEM images of (a) MCM-41 ($d_p = 4.0\text{nm}$),²⁸ (b) MCM-48 ($d_p = 3.0\text{nm}$).²⁷

2) SBA-15

SBA-15 is another ordered mesoporous silica. It is one of a series of mesoporous materials developed in the mid-late 1990's by Stucky and coworkers at the University of California at Santa Barbara.^{29,30} It has a hexagonal pore network, a $p6mm$ space group like MCM-41, and accessible pore diameters in the range of 6-20 nm (See Figure 1.8). A typical pore size for SBA-15 is 8nm. A TEM image of SBA-15 is shown in Figure 1.9. SBA-15 is synthesized under acidic conditions using a triblock copolymer, Pluronic P123, as a structure-directing agent. Pluronic P123 is made up of two blocks of twenty hydrophilic ethylene oxide (EO) units separated by one block of seventy hydrophobic propylene oxide (PO) units ($EO_{20}PO_{70}EO_{20}$). For SBA-15 and other OMS syntheses under acid conditions only molecular precursors can be used as silica does not readily dissolve (without fluoride ion). One significant difference between the resulting structures of SBA-15 and MCM-41 is the unordered micropores that SBA-15 possesses resulting from inclusion of Pluronic in the pore walls. Other differences in SBA-15 from MCM-41 include thicker pore walls, larger pores, and higher hydrothermal stability. Just as MCM-41 has a cubically ordered counterpart (MCM-48), SBA-15 has a cubic counterpart designated SBA-16 ($Im\bar{3}m$).

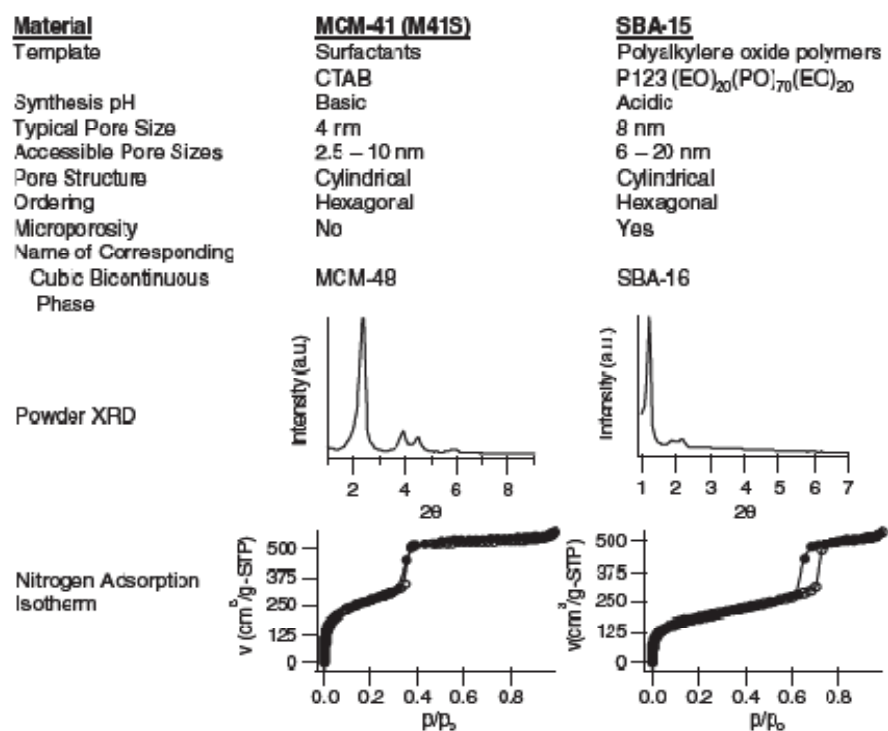


Figure 1.8 Comparison between MCM-41 and SBA-15.³¹

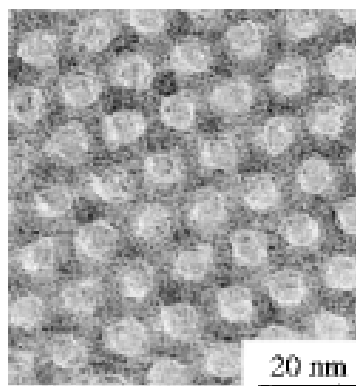


Figure 1.9 TEM image of SBA-15.³⁰

3) *KIT-6*

KIT-6 is another OMS material developed at the Korea Advanced Institute of Science and Technology in 2003 by Ryoo's group.³² Its structure is similar to that of MCM-48 in that it can be represented by the *Ia3d* space group. It has pore diameters in the range of 4-12nm. KIT-6 is formed under similar conditions as SBA-15 with the notable difference being the use of butanol as a cosolvent. Characteristic features of KIT-6 are shown below in Figure 1.10.

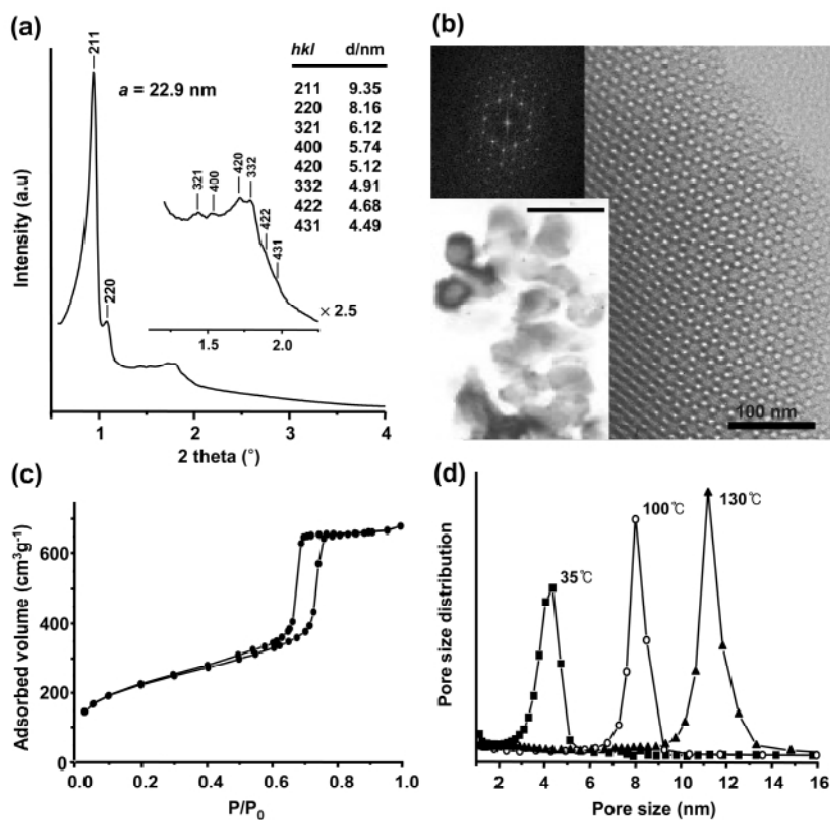
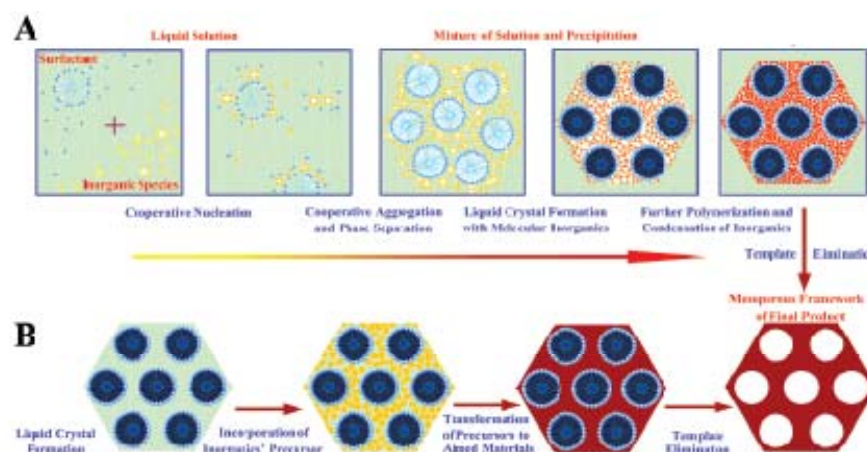


Figure 1.10 Characteristic features of KIT-6: a) XRD pattern; b) TEM image; c) N_2 adsorption isotherm; and d) pore size distributions at different synthesis temperatures.³²

4) OMS Formation

Two related general mechanistic models exist for OMS formation: a) liquid-crystal templating; and b) cooperative self-assembly (Scheme 1.4).³³ Liquid-crystal templating, the original mechanism proposed by Mobil researchers occurs in three steps: liquid-crystal formation; incorporation of inorganic precursor within the crystal; inorganic precursor polymerization to form the final structure. Cooperative self-assembly, rather than occurring in distinct steps, occurs in a concerted fashion with the inorganic species adhering to micelles, cooperatively forming the ordered structure, followed by further condensation/polymerization resulting in the OMS material.



Scheme 1.4 Proposed mechanisms of OMS synthesis: A) cooperative self-assembly; and B) liquid-crystal templating.³³

Two factors that play important roles in OMS formation are a) the packing parameter of the SDA; and b) charge matching of the silica species, SDAs and accompanying counter-ions. The packing parameter g is defined as $g = V/a_0l$, where V is

the total volume occupied by the SDA, including associated solvent molecules, a_0 is the effective area of the head group, and l is the kinetic length of the SDA; The packing parameter has a profound impact on the type of micellar structure formed: values close to 1 prefer a lamellar structure; $1/2 - 2/3$ prefer cubic $Ia3d$; $1/2$, hexagonal ($p6m$); and $1/3$, cubic ($Pm3n$). By manipulating the volume of the head and tail portions of the SDA, one can in principle promote the formation of a desired mesophase. An example of this concept is the synthesis of KIT-6; the addition of butanol is believed to swell the inner hydrophobic block of Pluronic micelles, raising the packing parameter, and transitioning the mesophase from hexagonal to cubic ($Ia3d$).

Galen Stucky and coworkers proposed in 1994 a set of possible OMS formation pathways in relation to the charge matching of silica species, SDAs and associated counter-ions.³⁴ As in zeolite synthesis, the proper charge balance is extremely important. Two sets of pathways were proposed: 1) direct pathways, where silica precursor is directly associated with an SDA of opposite charge (S^+I^- for basic conditions with a cationic SDA and S^-I^+ for acid conditions with an anionic SDA); and 2) mediated pathways, where counter-ions aid the interaction between a silica species and SDA of the similar charge ($S^-X^+I^-$ and $S^+X^-I^+$). S, I, and X indicate the SDA, the inorganic species and counter-ion, respectively, with positive (+) or negative (-) charges. Recall from above, condensation and hydrolysis proceed through positively charged intermediates (S^+) for acidic conditions and negatively charged intermediates (S^-) for basic conditions.

MCM-41 is a classical example of the S^+I^- pathway, as CTAB is a cationic surfactant and the synthesis is performed under basic conditions. SBA-15 and KIT-6 proceed through the mediated pathway, $(S^0H^+)(XI^-)$, as under acid conditions both the ethylene oxide block of the non-ionic Pluronic and silica are protonated. A neutral-neutral interaction pathway (S^0I^0) in which the SDA and silica associate through H-bonding was proposed and tested by Pinnavaia and coworkers, leading to mesoporous materials without long-range ordering.³⁵

1.4 OMS Hybrids

As mentioned in Sublevel 1.2, organic-inorganic hybrid materials may be synthesized by attaching an organic modifier to a silica or inorganic matrix. By doing so, a synergistic material combining chemical specificity (organic functional group) with mechanical robustness and structure (inorganic) is created. Hybrid materials constructed from porous silicates with high surface areas and large pores are especially relevant for catalysis, separations and sensing, among other applications.

While macroporous silicas ($d_p > 20\text{nm}$) can be easily modified, their surface area is low. On the other end of the spectrum, microporous materials ($d_p < 2\text{nm}$) have pore diameters that are too small for larger organic components and guest species. Mesoporous materials ($2\text{nm} < d_p < 20\text{nm}$), thus, represent a compromise between both regimes. As noted above, the additional aspect of order makes these materials not only easier to understand from a fundamental research perspective but also allows more control over the resulting properties of the materials as is needed for specialty

applications. In this regard, OMS have been extensively studied as supports for hybrid materials as they possess an ordered pore structure containing uniformly sized pores, a variety of pore connectivities, and surfaces that can be easily functionalized using a the wealth of previously developed silane chemistry.^{31,36} These material properties facilitate analysis of the hybrid material by microscopy, powder X-ray diffraction (PXRD), and porosimetry, and allow a relatively straightforward determination of how organic incorporation modifies the porosity and other properties of the parent OMS.

1.4.1 Hybrid Classes

Organic moieties can be bound to OMS surfaces through either weak bonding (Class I) or strong bonding (Class II). Class I hybrids are typically characterized by H-bonding, van der Waals or weak electrostatic interactions and class II hybrids by covalent, coordinative or strong ionic bonds. Examples of class I hybrids include the intercalated clays and layered silicates discussed in the introduction and the SDA embedded OMS materials prior to extraction or calcinations. The most common class II hybrid materials are silicas covalently grafted with organics through silane chemistry. Class II hybrids are especially promising for applications as they are less prone to leaching. The hybrids developed in this dissertation belong to the Class II classification.

1.4.2 Grafting Approaches

Following the development of OMS materials in 1990s, a high level of interest was placed upon developing methods for modifying them with simple organic

molecules. These studies focused mainly on the attachment of single functional groups, some directly and others indirectly. The foundation for this work was performed by Sanchez and coworkers who studied the formation of organic hybridized sol-gels.³⁷

In these materials, organic groups are usually introduced *via* an organotrialkoxysiloxane, $R-Si(OR')_3$, where R contains the desired functional group and R' is the alkyl group of the alkoxide. Mono- or di-alkoxysiloxane may be preferable in some instances as they are less likely to self-condense; these, however, are also less reactive with surface silanols without the addition of an acid catalyst.

The two principal approaches for hybridizing OMS are *co-condensation* and *post-synthetic grafting*. The co-condensation route involves adding the organotrialkoxysiloxane *in-situ* to the synthesis mixture of the OMS and is incorporated “directly” into the structure. The post-synthetic route involves first synthesizing the OMS then reacting the organotrialkoxysiloxane with the surface silanols, “indirectly” incorporating it into the solid. Additionally, ordered mesoporous hybrids may be synthesized using bisilylated organics with SDA, which form a separate class of materials that will not be discussed here called periodic mesoporous oxides (PMOs). A recent review by Hoffmann outlines these approaches.³⁸ An example of post-synthetic grafting is shown in Scheme 1.5.

Andreas Stein's group at Minnesota.⁴³⁻⁴⁵ A review by Moller and Bein summarizes the work in this area up to 1998.³⁶ As the chemistry is the same, these functionalization methods studied for MCM-41 also apply to SBA-15 and other OMS.

The synthesis of highly functional well-ordered hybrid materials has been the subject of more recent work. The areas of focus of these studies have been: 1) spatially arranging functional groups; 2) synthesizing hybrids with multiple functional groups; and 3) uniformly incorporating high densities of functional groups. There have been some successful attempts at dealing with these issues in the last decade. For example, the Jones group at Georgia Tech developed a method for spatially arranging primary amines at relatively high densities on SBA-15 using tritylimine to set the distance between the incorporated groups and then hydrolyzing them to produce primary amines.⁴⁶ Mark Davis' group at Cal Tech also developed spatially arranged thiol groups on SBA-15.⁴⁷ Davis' group has also synthesized spatially arranged bifunctional materials for cooperative catalysis.⁴⁸ Though not on OMS, Alex Katz's group at Berkeley has investigated local environment effects on the catalytic properties of imprinted amines on silica, which are highly relevant to work on OMS.^{49,50} His group has also synthesized imprinted silica functionalized with isolated and patterned amines and thiols for catalysis.⁵¹ Lin's group at Iowa State has also shown some progress in directly incorporating multiple functional groups in OMS.⁵²⁻⁵⁴ Reviews by Davis (2002) and Shantz (2005) cover some of these more recent developments.^{31,36}

Also recently, increasing emphasis has been placed on incorporating larger chemical moieties into OMS by further functionalization of smaller functional groups,

such as amines, thiols, alkyl halides and alkenes. These hybrids include organometallic catalysts,^{31,55} dendrimers,⁵⁶⁻⁵⁸ and enzymes.⁵⁵ Work incorporating melamine-based dendrimers in OMS-hybrid design was the subject of my Master's work;⁵⁹ further studies have been done by others in the Shantz and Simanek groups at Texas A&M.^{56,58,60} In a related report, OMS - PAMAM dendrimer hybrids have been studied by Alper and Sayari's labs at the University of Ottawa.⁶¹ Work grafting polymers into OMS will be discussed below.

Motivated in part by previous investigations in our laboratory¹¹⁻¹⁴ and by the unique properties of polypeptides, this dissertation focuses on designing polypeptide-OMS hybrids. As polypeptides are a polymer and hybrid synthesis employs a surface-initiated polymerization, an understanding of polymer synthesis and grafting is highly valuable. A modified version of an overview of polymer synthesis developed in connection with my dissertation work follows in Sublevel 1.5.

1.5 Polymer Synthesis

Though some natural polymers have been used in limited ways for many centuries (e.g. galvanization of latex in Mesoamerica, circa 1600 BCE, and paper development in China, circa 100 CE), the first completely synthetic polymers were developed in the early 20th century in phenol-formaldehyde resins (1910 CE) and methyl rubber produced in Germany during World War I using 2, 3-dimethyl butadiene as a poor substitute for natural rubber.⁶² The work of Hermann Staudinger (1953 Nobel Prize in Chemistry) in the 1920s and Wallace Carothers at DuPont in the 1930s, among

others, led to widespread interest and research in polymer science in the 30s and 40s, resulting in a very large number and variety of polymers being developed (e.g. polymethylmethacrylate, poly(vinyl acetate), Nylon 66, polystyrene, polyethylene, polybutadiene, etc.). Many of these polymers found their way into almost immediate industrial use, finding use in many different applications.

Polymers can be synthesized using various techniques which are typically classified by reaction mechanism. The two principal mechanistic classifications generally used are step polymerizations and chain polymerizations. A *step polymerization* is one in which the polymerization “involves successive reactions between pairs of mutually-reactive functional groups which initially are provided by the monomer(s)” (Young & Lovell p. 17). *Chain polymerizations* are those in which a chain propagates through the reaction of a free monomer with the reactive end of the chain. It is often convenient to describe the mechanism of chain-growth polymerizations by the steps initiation, propagation, termination, and sometimes chain transfer. Chain polymerizations generally require an *initiator* which activates the first monomer in the chain (*Initiation*). *Propagation* is the continual reaction of the initiated species with other monomer and ends in *termination*. The transfer of the propagating species to another part of the polymer, contaminant, etc. is called *chain transfer*.

Allcock and Lampe⁶³ mention two distinct differences between step and chain polymerizations: 1) In step-growth, any two molecules can react with each other, whereas in chain-growth, reactions only occur at the end of a few initiated chains; and 2) Because of (1), step polymerizations use up the monomer fast and lead to large

molecular weight distributions, whereas in chain polymerizations, the monomer is steadily consumed over time leading to only monomer and high polymer in solution at any given time. Because these two classifications are rather broad it is convenient to break them down further into condensation and non-condensation for step polymerizations and ionic, ring-opening, free radical, and metal-coordinated for chain polymerizations.

1.5.1 Step-growth Polymerizations

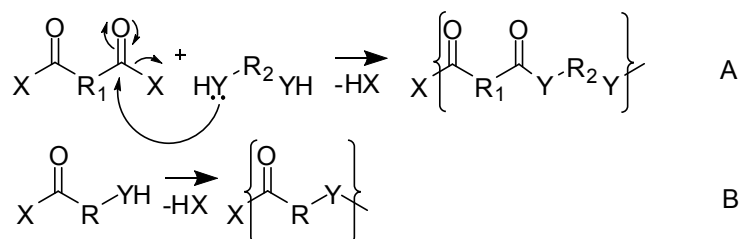
1.5.1.1 Polycondensation

Condensation is an example of a step polymerization in which small molecules are concurrently lost (e.g. Water, HCl) with the consumption of each monomer. Polyamides, polyesters, polycarbonates, and polyimides are just a few examples of polycondensation constructed polymers. The general mechanistic schemes for polycondensation – specifically, polyamides and polyesters – reactions are shown in Scheme 1.6. Scheme 1.6A shows the two monomer scenario, while 1.6B shows the mechanism for a single monomer. A specific example of a polymer made in this fashion is Nylon-66, which is synthesized using hexylmethylenediamine and adipic acid.

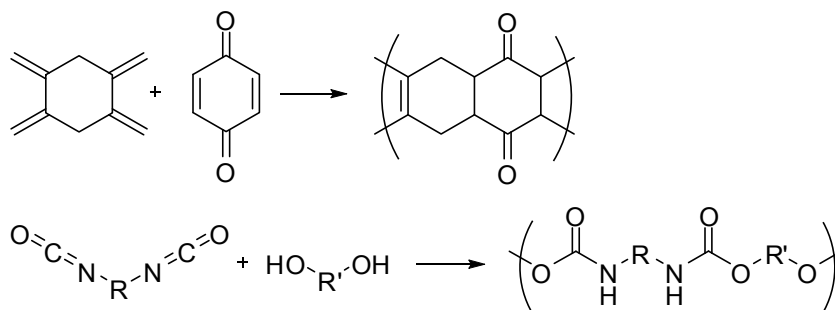
1.5.1.2 Other Step-growth Polymers

It is important to note that not all step-growth polymerizations follow polycondensation. Polymers constructed through step-wise through addition rather than substitution mechanisms fit into this category. Two notable examples are polymers

produced by Diels-Alder chemistry and polyurethanes synthesized by reacting diisocyanates and diols (Scheme 1.7).



Scheme 1.6 General mechanisms for polycondensation reactions for polyamides.



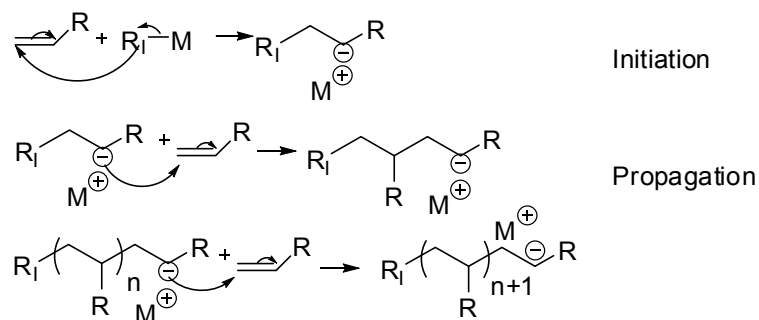
Scheme 1.7 A Diels-Alder constructed polymer (top) and polyurethane (bottom).

1.5.2 Carbanionic Polymerizations

Ionic polymerizations, proceed through chain-growth and usually employ an olefinic monomer ($\text{H}_2\text{C}=\text{CR}_1\text{R}_2$). Ionic polymerizations propagate through either a cation or an anion (or with metal coordination). Whether the monomer can follow an anionic or cationic path depends on the electronic configuration of the monomer. If the monomer has an electron-withdrawing group adjacent to the charge, the anion of the

monomer is stabilized. Similarly, if the adjacent group is electron donating, the cation is stabilized. Free-radical polymerizations have no such dependence on the electron-donating or withdrawing ability of the substituent (See Table 1.1).

Anionic polymerization is a chain-growth polymerization that propagates through a negative charge. As stated above and shown in Table 1.1, olefinic monomers with electron withdrawing groups are the most suitable for anionic polymerizations (e.g. styrene, methyl methacrylate, acrylonitrile, etc.). A general mechanism for anionic polymerizations is shown below (Scheme 1.8).



Scheme 1.8 General anionic polymerization mechanism.

Table 1.1 Susceptibility of various types of monomers to free-radical, cationic and anionic polymerization. Y, susceptible; (Y), expected susceptibility thwarted by side reactions; N, not susceptible. Reproduced from Young and Lovell, p. 69.⁶²

Monomer	Structure	Free-radical	Cationic	Anionic
Ethylene	$\text{CH}_2=\text{CH}_2$	Y	Y	N
1-Alkyl Olefins	$\text{CH}_2=\text{CHR}_1$	(Y)	(Y)	N
1,1-Dialkyl Olefins	$\text{CH}_2=\text{CHR}_1\text{R}_2$	(Y)	Y	N
1,3-Dienes	$\text{CH}_2=\text{CH}-\text{CR}=\text{CH}_2$	Y	Y	Y
Styrene, α -methyl styrene	$\text{CH}_2=\text{CRPh}$	Y	Y	Y
Vinyl halides	$\text{CH}_2=\text{CHX}$	Y	N	(Y)
Vinyl esters	$\text{CH}_2=\text{CHOCOR}_1$	Y	N	(Y)
Vinyl ethers	$\text{CH}_2=\text{CHOR}_1$	(Y)	Y	N
Acrylates, methacrylates	$\text{CH}_2=\text{CRCOOR}_1$	Y	N	Y

1.5.2.1 *Initial Carbanionic Polymerizations*

Initial attempts to anionically polymerize olefins, specifically styrene, were conducted with potassium amide (KNH_3) in liquid ammonia.⁶² This approach, however, resulted in termination through the chain transfer of the anion to ammonia.

1.5.2.2 *Living Carbanionic Polymerizations*

In the mid-1950's, Michael Szwarc discovered chain transfer/termination could be prevented for all practical purposes for the polymerization of styrene by means of electron transfer from sodium naphthalenide in THF; and monomer could continue to be added while maintaining very low polydispersities^{64,65} This became the first example of what are now termed "living" or controlled polymerizations. A simplistic definition

of a living polymerization is one that propagates without observable chain transfer or termination within the time frame of a given polymerization. Anionic polymerizations do not have a formal termination step, as seen above in Scheme 1.8, nor are they plagued by chain transfer like its cationic counterpart.

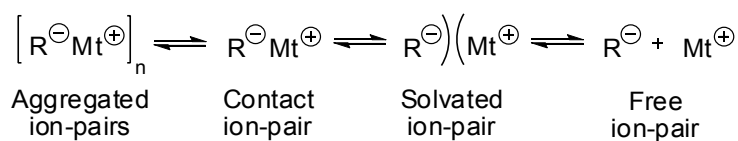
1) *Initial Work*

Following Szwarc's discovery, there were numerous attempts to apply electron transfer initiators to other monomers and systems.^{66,67} The resulting conclusion was that electron transfer initiators work very well in polar solvents, but poorly in non-polar solvents that do not solvate the ion-pair. Studies looking at styrene in non-polar solvents and other hydrocarbon monomers did not prove as successful, especially in the case of acrylic monomers and methyl methacrylate in particular.

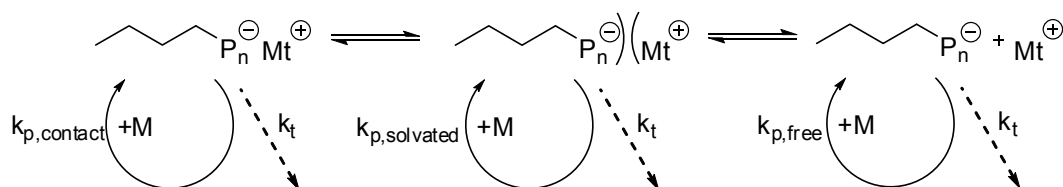
Using alkyllithium reagents as initiators was proposed by Zeigler in the late 1920s.⁶⁸⁻⁷⁰ Alkyllithium initiators showed significant promise as they are efficient for hydrocarbon monomers even in nonpolar solvents⁷¹ and were able to show living polymerizations under certain conditions. However, it was found that these systems are highly complex due to aggregation of the alkyllithium and the reactivity of the propagating carbanion strongly correlates with the size of the alkyl group and aggregate.⁷² The results on these two fronts led to the hypothesis – that was later proved correct – that the living character of the polymerization depended upon the nature of the propagating ion-pair, that is to say, the relationship between the ion and counterion.

2) *Ion-pairing*

A simplified model (Fuoss-Winstein^{73,74}) expresses anion-counterion pairing as an equilibrium between four types: aggregated, contact, solvated and free (Scheme 1.9). It was found that the rate of propagation depends upon how tightly bound the counterion is to the anion: a more tightly bound contact ion will react very slowly with monomer or not at all, while a solvated or free anion readily reacts (Scheme 1.10).^{75,76} It was eventually realized that it was the equilibrium between these ion pair types that brought control to the polymerization; increased propagation rates could be obtained in non-polar solvents and side reactions could be prevented in acrylic monomers by intelligently choosing the counterion to shift the equilibrium to the solvated ion-pair.



Scheme 1.9 Fuoss-Winstein anion-pair model for polar solvents.



Scheme 1.10 Model mechanism for the ion-pairing effect in carbanionic polymerizations

where $k_{p,\text{free}} > k_{p,\text{solvated}} \gg k_{p,\text{contact}}$.

3) *Ligated counterions*

Not long after the discovery of the living carbanionic polymerization and these initial experiments, it was shown that the addition of Lewis bases (σ -ligands) and Lewis bases (μ -ligands) could be used to increase and decrease the polymerization rate of styrene in non-polar solvents. One of the first of these experiments showed that small amounts of THF (a σ -ligand) dramatically increased the apparent propagation rate of styrene in benzene using an alkyllithium initiator.^{77,78} The highest rate was obtained with one equivalent of THF (initiator basis). This result is due to electron donation from the THF ether causing the lithium ion to be less tightly bound to the propagating chain ion. Other σ -ligands, such as tertiary amines and high electron density non-polar ligands, increase the polymerization of styrene at low concentrations, but decrease the rate at higher concentrations.⁷²

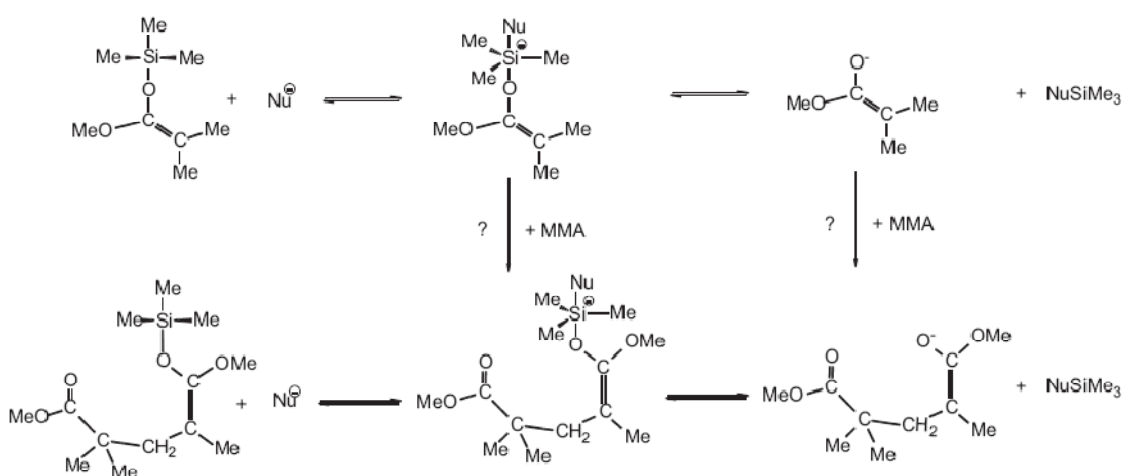
Lewis acids (μ -ligands), such as lithium alkoxides and metal alkyls, also dramatically affect anionic polymerizations, though in the opposite fashion as Lewis bases.⁷⁹⁻⁸² They act as electron acceptors and cause the lithium or metal cation to become more positive, interacting more with the propagating anion resulting in retardation. Retarded anionic polymerizations impart a large degree of control, such that polymerizations can be undertaken in bulk and high temperatures.^{79,80}

In the case of acrylic monomers, such as methyl methacrylate, σ ⁸³⁻⁸⁸ and μ ⁸⁹⁻⁹⁵ ligands can also be used to strongly influence control over the polymerization and they serve a dual purpose, not only to control the polymerization rate, but prevent side reactions such as back-biting that plague MMA anionic polymerizations under normal

conditions. σ , μ -type ligands, compounds that contain both a electron donor and acceptor, have been shown to greatly increase the rate of MMA polymerization while maintaining living conditions and preventing side reactions.⁹⁶⁻⁹⁹

1.5.2.3 Group-transfer

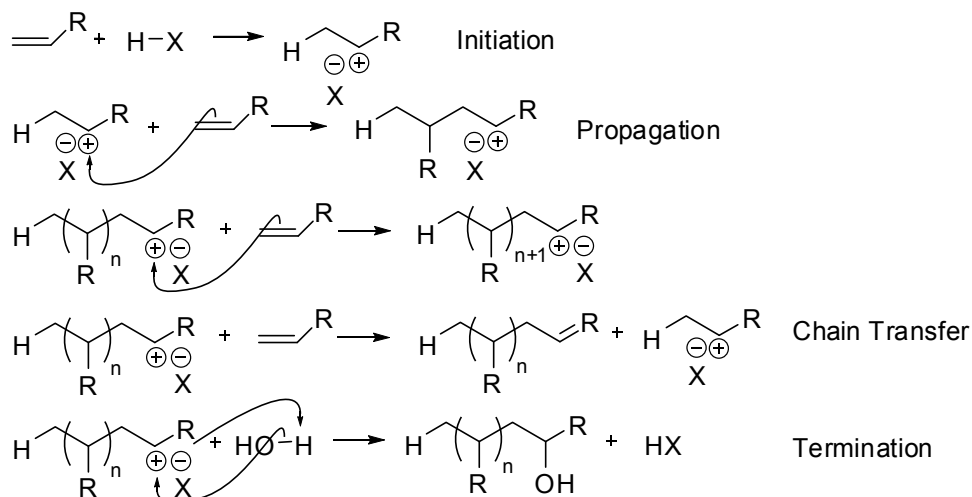
Though group-transfer polymerization (GTP) does not propagate through an anion (it follows a Michael Addition-type mechanism), the chemistry follows the same electron flow and thus deserves mention here. GTP was discovered by researchers at DuPont Co.¹⁰⁰ Sogah et al. at DuPont demonstrated that GTP could be used successfully to controllably polymerize a number of acrylic monomers: alkyl acrylates, *N,N*-dimethylacrylamide, acrylonitrile, and 2-methacrylonitrile. They were also able to prepare block copolymers with controlled MW of a series of alkyl methacrylates. GTP can follow either an associate or dissociative mechanism that likely depends on the nucleophilic catalyst. These mechanisms are shown in Scheme 1.11.



Scheme 1.11 Associative and dissociative GTP mechanisms for MMA.⁷²

1.5.3 Carbocationic Polymerization

Cationic polymerization propagates through a positive charge on the end of the reactive chain. Polymers which can be synthesized through this mechanism are poly(vinyl ethers), poly(α -methyl styrene), isobutylene, polyaldehydes, among others. Because cationic polymerization is chain-growth, the mechanism can be classified in terms of initiation, propagation, chain transfer and termination. A general reaction mechanism for cationic polymerization is shown in Scheme 1.12.



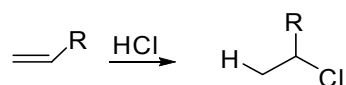
Scheme 1.12 General mechanism for cationic polymerizations.

1.5.3.1 Conventional Carbocationic Polymerization

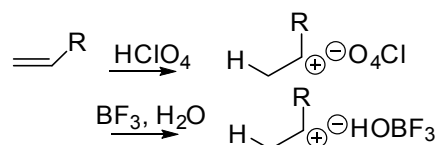
1) Initiation

In the same manner that carbanionic initiators introduce anions into the system, initiators for cationic polymerizations introduce a positive charge. This can be done by

two groups of compounds: strong protic acids and Lewis acids. The most common protic acids are sulfuric (H_2SO_4) and perchloric, (HClO_4) acids. Young and Lovell advise against the use of hydrogen halides because the halide counter ion rapidly reacts across the double bond to form a stable covalent bond, as shown below (Scheme 1.13).⁶² Lewis acids are the most important cationic initiators but require small amounts of a “co-initiator” such as water, organic halide, or even some acids (Scheme 1.14).



Scheme 1.13 Hydrogen halides react across the double bond and for that reason are poor initiators for cationic polymerization.



Scheme 1.14 Protic Acids (other than hydrogen halides) and Lewis acids are good cationic polymerization initiators.

2) Propagation, Chain Transfer and Termination

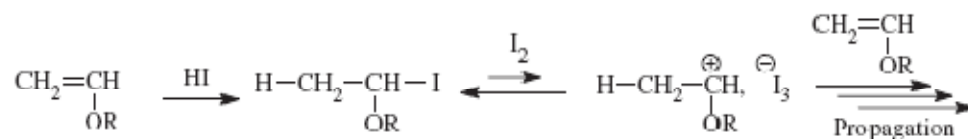
Propagation can occur by two possible modes: where the substituent groups are on adjacent carbons, termed head-to-head; or head-to-tail where the substituent groups are $\text{A}^1, 3$ (i.e. separated by a non-substituted carbon). Head-to-tail configuration is preferred because it places the carbocation on the more stable substituted carbon.

Cations are particularly susceptible to chain transfer, isomerization and termination as carbenium ions are extremely reactive. Protons can be eliminated from the growing chain by migrating to a monomer species or reforming the initiating species -- both having the same basic effect: lower MW and broad MW dispersion. Both these processes cause the polymer terminate with an alkene. Hydride abstraction from contaminants and other growing chains is also common, the latter leading to branching. Chain termination can also occur from minute quantities of water present in the reaction solution terminating the polymer with a hydroxyl group. Due to these effects, carbocationic polymerizations are generally conducted at very low temperatures in the attempt to promote propagation.

1.5.3.2 Controlled Carbocationic Polymerization

It was initially thought that it was impossible to control carbocationic polymerizations as in the carbanionic system due to the chain-transfer and termination prone cations, as noted above. The first example of living carbocationic polymerizations was not published until 1984 when Higashimura, Sawamoto et al. showed that vinyl ethers could be controllably polymerized when initiated by a combination of hydrogen iodide and iodine.¹⁰¹ In the beginning, it was thought that the polymerization mechanism followed a concerted approach involving a covalently bonded I_3 , rather than having a true cation as the active species. The following year it was realized that the polymerization in fact has a cation as the active species and the mechanism involved a

rapid exchange between a dormant (covalently bonded) species and an active cation in the form of an ion-pair (Scheme 1.15).¹⁰²



Scheme 1.15 Mechanism of living vinyl ether polymerization with HI/I₂.¹⁰²

Later reports followed the more general approach described by the mechanism in Scheme 1.16. As can be seen, the initiating system has generally either two or three components: the counterion of the strong acid initiator (X), a Lewis acid (MtX_n), and an accompanying nucleophile to stabilize the Lewis acid cation coordination (Nu). The accompanying nucleophile is generally necessary when the Lewis acid is too strong and thus binds too tightly to the cation (Recall a similar case above in living anionic polymerization). Table 1.2 shows some of the initiating systems known for vinyl ethers and isobutene.



Scheme 1.16: General mechanistic approach for living carbocationic polymerizations.¹⁰³

shown, can take place through propagation of either a cation or anion. Being thus, the initiating species that can be used are generally the same as those for anionic and cationic polymerizations. An important difference between ring opening and ionic polymerizations is that the driving force for the former is based in the relief of ring strain, whereas in the latter case it is the enthalpy of breaking the double bond of the olefin. Another interesting feature is that ring-opening polymerizations, in addition to many new monomers that cannot be polymerized by means of those mechanisms shown above, can be used to make many polycondensation polymers through a chain-growth mechanism. Some examples are polyamides, polyesters and polyethers.

1.5.4.2 *Controlled Ring-opening Polymerization*

In general, controlled ROP takes into consideration the same points as carbanionic or carbocationic polymerizations mentioned above.¹¹⁹ For this reason, we will only speak of these approaches in brief. We will then focus more specifically on a special anionic ROP, that of amino acid *N*-carboxyanhydrides, as it is the polymerization used in this dissertation.

1) *Anionic Ring-opening Polymerizations*

Initiators for anionic ROP depend upon the cyclic compound. For example, carboxylates, alkoxides, thiolates and silanolates are generally used for β -lactones, higher lactones, sulfides and siloxanes, respectively. As in the case of carbanionic polymerization, side reactions and propagation control can be obtained by carefully

selecting the counterion and other complexing agents. In general, the same counterion selection rules apply as for carbanionic polymerizations. For example, bulky Al Lewis acids dramatically improve control over propylene oxide polymerization.

2) *Cationic Ring-opening Polymerizations*

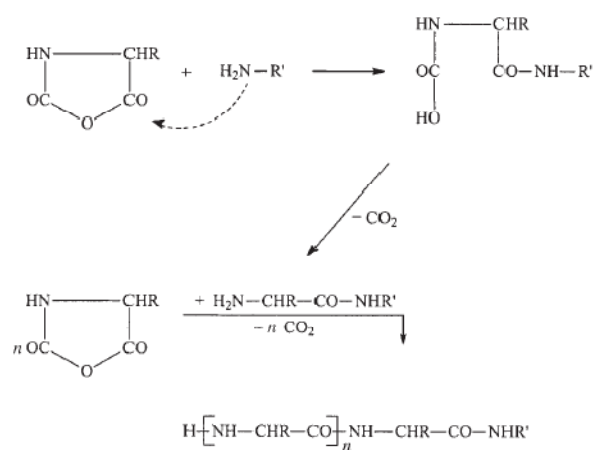
Living cationic ROP has proved more troublesome. The only sufficiently studied system is that of THF cationic polymerization. A good initiator for cationic THF polymerization is triflic acid or its derivatives.

3) *N-carboxyanhydride Polymerization*

A special case of ROP is the polymerization of amino acid *N*-carboxyanhydrides (NCAs) that are used to prepare polypeptides (Scheme 1.18). Monomers are prepared from α -amino acids by reaction with phosgene or triphosgene to form the cyclic anhydride. Classical initiators for NCAs are primary alcohols, amines and other mild bases and nucleophiles.¹²⁰ Living conditions can exist for some amino acid NCAs in the case of primary amine initiated polymerizations when the system is ultra dry and free of any other impurities. For some monomers, however, like alkyl glutamates, side reactions such as back-biting can occur. It is also possible, in the case of amine-initiated systems for more basic amines to deprotonate the NCA monomer, thus undesirably activating it.

Extensive work to eliminate such side reactions by employing metal catalysts has been performed by Deming et al. Nickel (0) catalysts ligated with cyclooctadiene and

either dipyridyl or two phenylphosphines have proved to be the most successful NCA catalysts to date.^{121,122} Side reactions can be almost completely eliminated and very monodisperse polypeptides and coblock polypeptides can be constructed. There is still significant room for improvement as these catalysts, as well as the monomers are extremely water and oxygen sensitive. Hexamethyldisilazane and trimethylsilyl amines have also recently been shown to be less burdensome in initiating living NCA polymerizations.¹²³



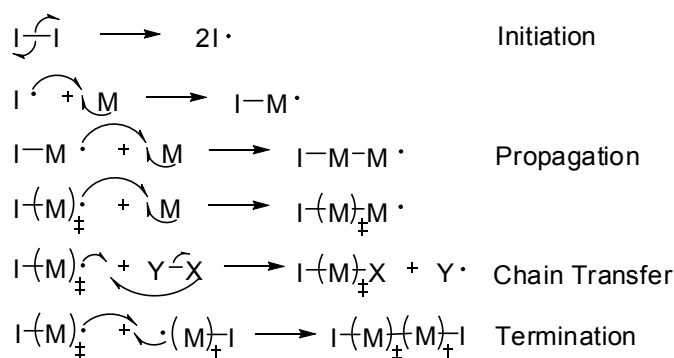
Scheme 1.18 General mechanism of amine-initiated NCA polymerizations.¹²⁰

1.5.5 Radical Polymerization

1.5.5.1 Conventional Radical Polymerization

Free-radical polymerizations are an example of chain-growth wherein – as the name suggests – the monomer is activated and propagated by free radicals. Some common examples of polymers which can be synthesized using the free-radical approach

are polystyrene, poly(vinyl chloride), polyethylene and poly(tetrafluoroethylene) (i.e. Teflon). Monomers are almost always olefins as they are very susceptible to free-radical addition taking the form $\text{H}_2\text{C}=\text{CR}_1\text{R}_2$ (R_2 is frequently hydrogen). A general mechanistic scheme for radical addition is shown in Scheme 1.19.



Scheme 1.19 General mechanism for free-radical polymerizations.

1) Initiation

Various radical initiators are available: thermolytic and redox. Thermal initiators are typically selected based on the desired reaction conditions; to avoid side reactions and limit chain transfer, they are generally restricted to those that cleave at lower temperatures such as organic peroxides, organic hydroperoxides, azo compounds, and metal alkyls (See Figure 1.11). Allcock and Lampe suggest as a thumb rule that thermal initiators have a rate constant of decomposition (k_{rxn}) between 10^{-7} and 10^{-6} mol-liter $^{-1}$ s $^{-1}$ in the desired temperature range for a 0.1M initiator concentration.⁶³ For example, benzoyl peroxide thermolytically cleaves between 60-80°C ($k_{\text{rxn}} = 1 \times 10^{14} e^{-29900/RT}$ s $^{-1}$)¹²⁴.

For lower temperature requirements, redox reactions can be used to produce initiating species. For example, the reaction between cumyl peroxide and the ferrous ion produces the cumyloxy radical at temperatures between 15-50°C, while thermolysis of cumyl peroxide occurs in the range of 85-105 °C. While in most cases an initiator is required, monomers such as styrene can be “self-initiated” in the presence of heat or light. In some cases, it is also possible to use ionizing radiation or initiate polymerization through photosensitization of the monomer (For more information, see Allcock & Lampe Chapter V). An example of radical initiation for vinyl chloride using di-*t*-butyl peroxide is shown in Scheme 1.20.

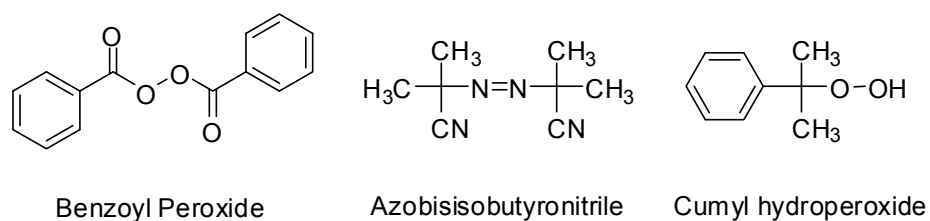
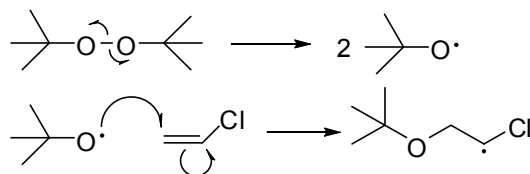


Figure 1.11 Some examples of free-radical initiators.



Scheme 1.20 The initiation of vinyl chloride by di-*t*-butyl peroxide.

2) *Propagation, Chain Transfer and Termination*

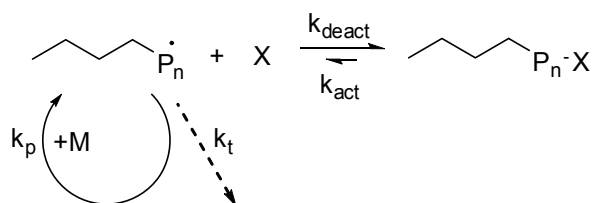
Propagation proceeds in the same way as in the ionic case except with a free radical as the reactive chain ending. Head-to-tail configuration is preferred because radicals, like carbocations, are more stable on more substituted carbons. Chain transfer occasionally occurs when the radical reacts with contaminants present in the reaction vessel or abstracts a proton from another part of a growing chain thus terminating itself and transferring the radical; it can normally be prevented in part by using a lower reaction temperature. Termination takes place when two propagating chains react together forming a covalent bond. Because propagation is preferentially head-to-tail, termination by *combination* usually results in a head-to-head linkage. A propagating chain can also be terminated by reacting with other radicals present in the reaction solution, called *disproportionation*.

1.5.5.2 *Controlled Radical Polymerization (CRP)*

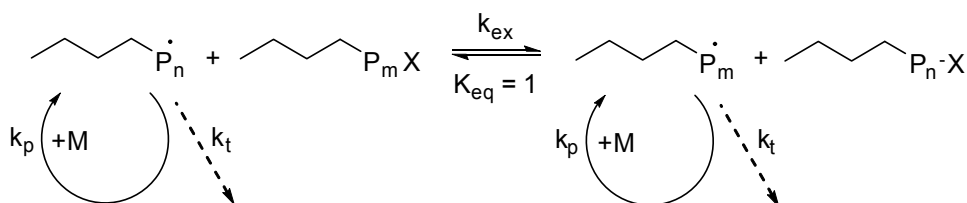
Free radical polymerizations have the broadest range of susceptible vinyl monomers, as the stability of the radical is not dependent upon the electron withdrawing or donating nature of the substituent. The classical free radical approach is also the most understood and industrialized polymerization technique. It is natural then -- of course -- that the scientific community has sought to bring control to it. Interestingly, however, of the classical polymerization approaches, the free radical polymerization was the last to have “living” conditions developed.

It was not until 1993 when M. K. Georges discovered that a narrow MW polydispersion could be obtained in the benzoyl peroxide-initiated polymerization of styrene when the radical scavenger TEMPO (2,2,6,6-tetramethyl-1-piperidynyl-*N*-oxy) was employed.¹²⁵ This became the first example of what is now called stable free radical polymerization (SFRP) and, more specifically, the first example of nitroxide mediated polymerization (NMP). This discovery led to extensive studies in developing other CRP methods.

A common feature in the approaches that have been developed to date is an interconversion between an active and dormant species – as we have seen in the carbanionic and carbocationic approaches – that slows the overall propagation rate, thus controlling the polymerization. The lifetime of a growing chain in classical RP is on the order of one second, whereas growing chains in CRP have a much longer duration, lasting more than an hour.¹²⁶ Of these methods, there are two general mechanistic approaches. The first approach relies on the persistent radical effect (PRE): the growing chain is trapped in equilibrium between an active and dormant. The second approach utilizes degenerative transfer (DT) in which the radical of a growing chain is reversibly transferred in a continuous fashion between chains, leaving one chain “reversibly” terminated while the other is free to propagate. General mechanisms for these approaches are outlined below in Schemes 1.21 and 1.22.



Scheme 1.21 General mechanism of PRE approach.



Scheme 1.22 General mechanism of DT approach.

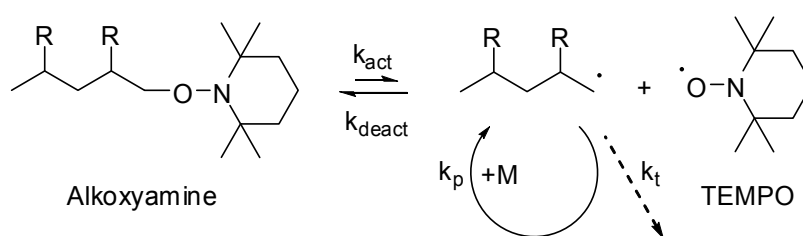
1) *PRE-based techniques*

The following techniques take advantage of the persistent radical effect: nitroxide mediated polymerization (NMP); cobalt mediated radical polymerization (CMRP); and atom transfer radical polymerization (ATRP). The first two are referred to as stable free radical radical polymerizations (SFRP) as they utilize stable free radicals. The later is somewhat different in that it employs metal complexes as catalysts for the reversible transfer of halides.

a) *SFRP: NMP and CMRP*

As mentioned above, the first example of SFRP and NMP was demonstrated by Georges et al. in 1993.¹²⁵ The basic principle behind NMP is that nitroxides form

reversible covalent bonds with propagating radicals. The equilibrium is heavily shifted toward the covalent bond (dormant species) drastically reducing the propagation rate and adding significant control to the polymerization. Polydispersities less than 1.3 were obtained for the polymerization of styrene. The approach used by Georges is shown in Scheme 1.4.18.



Scheme 1.23 TEMPO mediated free radical polymerization (R = Ph).

Though, TEMPO and its derivatives are very useful for the control in the synthesis of polystyrene, they are unable to provide the same control over the polymerization of other monomers. A number of other very useful nitroxides have been reported; DEPN, TIPNO and TEMPO-TMS are especially effective and commonly used (Figure 1.12).¹²⁷⁻¹²⁹ It has been shown that steric effects have a very strong impact on the utility of various nitroxide mediators: the larger the nitroxide, the more loosely bound the nitroxide becomes (i.e. lower disassociation energy).^{130,131} In many cases, this is highly desirable; however, in others, if the transfer group is too large, control is significantly disrupted. One must then balance carefully such factors when selecting a mediator for a desired monomer/application.

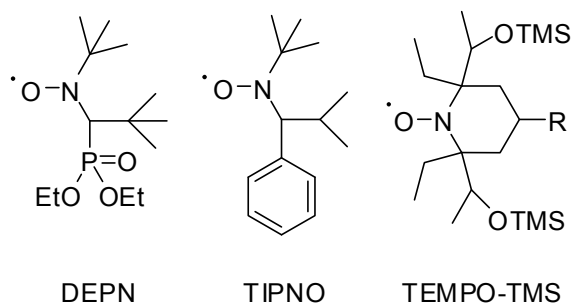


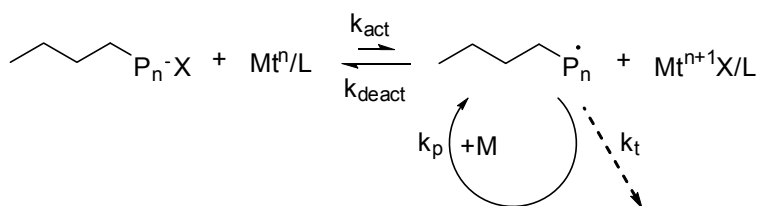
Figure 1.12 Persistent radicals used in NMP.

NMP can either be initiated through conventional radical initiator in the presence of persistent radicals or through unimolecular initiators. Unimolecular initiators have been developed, though sometimes their synthesis is tedious.¹³²⁻¹³⁴ These unimolecular initiators, in this case alkoxyamines, are the nitroxide adducts of the monomer or another active vinylic compound. SFRP can also be mediated by metal complexes,^{135,136} most notably of cobalt.¹³⁷⁻¹⁴⁰ Cobalt porphyrins have been shown to successfully mediate the polymerization of methacrylates; this is a point where the nitroxide mediators are severely lacking.

b) ATRP

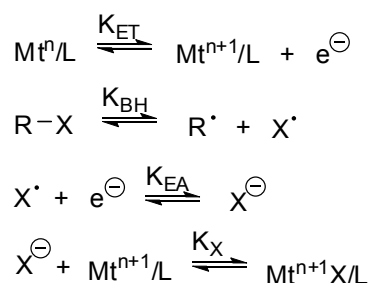
Originating from the common organic synthesis reaction known as atom transfer radical addition (ATRA)^{141,142}, ATRP, as in the methods above, takes advantage of a rapid equilibrium between an active radical species and a dormant inactive species. In this catalytic process, atom transfer from an organic halide to a reductive transition metal complex activates the radical species, while the reverse transfer deactivates it. The use

of a catalyst to activate the radical is a fundamental difference between ATRP and SFRP.¹²⁶ As a result of catalyst use, the reaction rate in ATRP depends not only on the persistent radical ($Mt^{n+1}X/L$), as in SFRP, but also on the activator (Mt^n/L). The mechanism of ATRP is shown in Scheme 1.24.



Scheme 1.24 A general mechanism for ATRP.

The overall reaction rate depends upon the equilibrium between activation and deactivation. In ATRP, the equilibrium constant can be expressed as $K_{\text{ATRP}} = k_{\text{act}}/k_{\text{deact}} = K_{\text{ET}}K_{\text{BH}}K_{\text{EA}}K_{\text{X}}$.¹⁴³ K_{ET} , K_{BH} , K_{EA} , and K_{X} represent the equilibrium constants for the four major steps of activation and deactivation, namely, oxidation of the metal complex (electron transfer), halide bond homolysis, reduction of the halogen to a halide ion (electron affinity), and halide association to the metal complex, respectively (Scheme 1.25). Being thus, it is important to carefully select the transition metal/ligands with respect to the desired monomer in order to tune the reaction rate.



Scheme 1.25 Sub-equilibria in K_{ATRP}^{143} .

i) Transition Metal/Ligands

The metal complex in ATRP consists of three components: a transition metal (Mt^n) with the capability to reversibly expand its coordination sphere (i.e. oxide), an appropriate ligand (L), and a counterion that reversibly binds to the metal center and exchanges with the propagating chain end (X^{\cdot}).^{144,145} Though most of the standard catalytically active transition metals have been successfully used in ATRP, Cu complexes have been shown to be the most efficient under diverse conditions and with a variety of monomers. Two of the more active ligands for copper complexes in ATRP are Me_6TREN and DMCBCy (Figure 1.13).¹⁴⁶ Rather simple ligands such as bipyridine can also be used.¹⁴⁷ Bromine and chlorine are the most common halogens employed as they are both easily homolyzed and form stable covalent bonds, in contrast to the unstable iodine and very tightly bound fluorine.

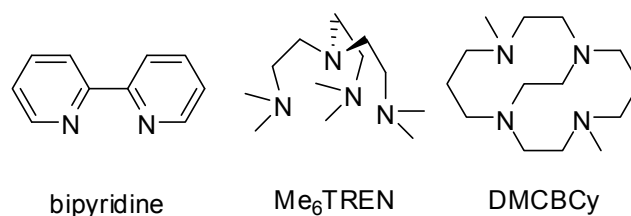


Figure 1.13 Examples of Cu ligands in ATRP.

ii) *Monomers*

ATRP can successfully polymerize a large variety of monomers, a key advantage over the previous SFRP methods discussed above.¹²⁶ ATRP can effectively polymerize ethylene, vinyl halides, vinyl ethers, methacrylates, dienes, etc. The monomer plays a significant role in the reaction rate of ATRP because it is dependent upon the energy of halide bond homolysis (K_{BH}). An interesting example of the dramatic effect of K_{BH} on the reaction rate was described by Gillies et al.¹⁴⁸ All things being equal (i.e. the same catalyst, monomer/initiator ratio, solvent, temperature, etc.), if it takes 1 hour to reach 90% conversion in the polymerization of methyl acrylate, it would take styrene and vinyl acetate 11 hours and 15 years, respectively, to obtain the same conversion (Figure 1.14). This example demonstrates the necessity for careful consideration of the catalyst and reaction conditions for a given polymerization (i.e. a more efficient catalyst is required for a monomer with a more tightly bound halide and vice versa to maintain control).

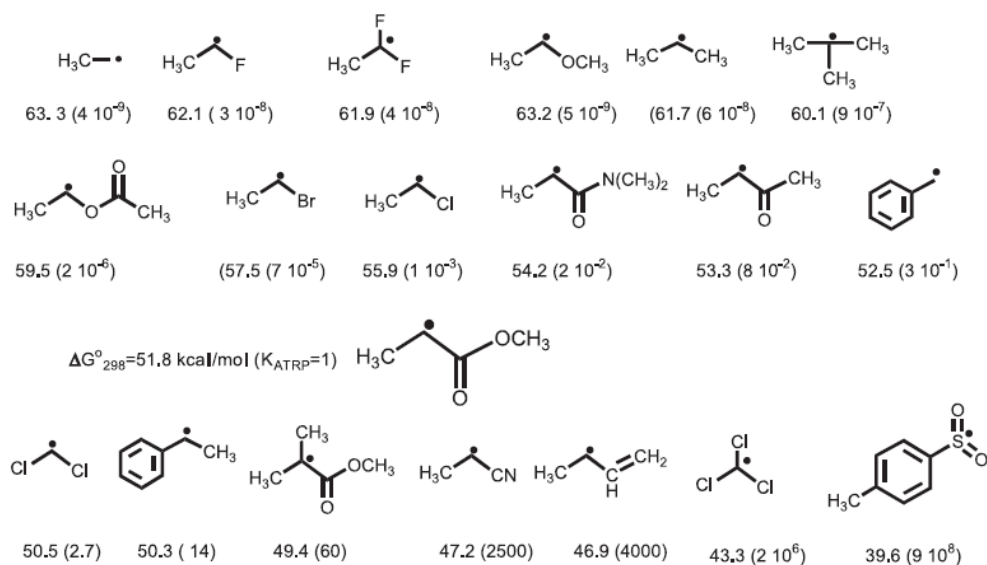


Figure 1.14 Free energy change (ΔG_o^{298}) and relative values of K_{ATRP} for homolytic bond cleavage of alkyl bromides deduced from DFT calculations at 25°C relative to methyl 2-bromopropionate ($K_{\text{ATRP}}=1$).¹⁴⁸

iii) Initiators

Effective initiators in ATRP are conjugated halides such as α -substituted methyl propionate or nitriles. Like other controlled polymerizations, the rate of initiation must be much faster than that of propagation, necessitating very active initiators. Tang et al.¹⁴⁷ through a series of studies demonstrated that three chemical characteristics have influence over the activation rate of the polymerization: 1) degree of substitution of the halide, 2) the type of halide (Cl, Br, or I) and 3) the stabilizing group. As might be expected, higher substitution, creating more stable radicals, leads to higher activation rates. Similar increases in the activation rate are observed for the more weakly bound halide and the better radical stabilizing group.

iv) *Other considerations*

Though ATRP provides extraordinary control over a wide range of monomers and enables scientists to construct a plethora of advanced materials, its use in industry is limited due to a number of obstacles, namely, 1) ATRP catalysts are extremely sensitive to oxidizers, 2) extensive post synthesis purification is required to purify the polymer from the high concentrations of catalyst needed, and 3) the mildly toxic catalysts can have environmental effects when disposed of in large quantities. Considerable work is underway to eliminate some of these issues so that industry can benefit from the wide range of new materials which can be constructed by ATRP.

2) *Degenerative Transfer*

Degenerative Transfer techniques follow a quite different approach than PRE. DT is much more similar to conventional RP and PRE-based techniques in that they are initiated by conventional initiators, reaction conditions are typical of conventional RP, as well as, the reaction kinetics.¹²⁶ Rather than employing a persistent radical that shifts the equilibrium between active and dormant species heavily toward the dormant one, DT utilizes a degenerative exchange of the capping group in the dormant species to an active radical. Because the transfer is between two equally reactive groups the equilibrium constant is one.

DT can proceed through either atom/group transfer or by addition-fragmentation chemistry. The simplest example of DT is the iodide transfer that occurs when conventional RP initiators are used in the presence of alkyl iodides.^{149,150} This method,

1.5.6 *Metal Coordinated Polymerization*

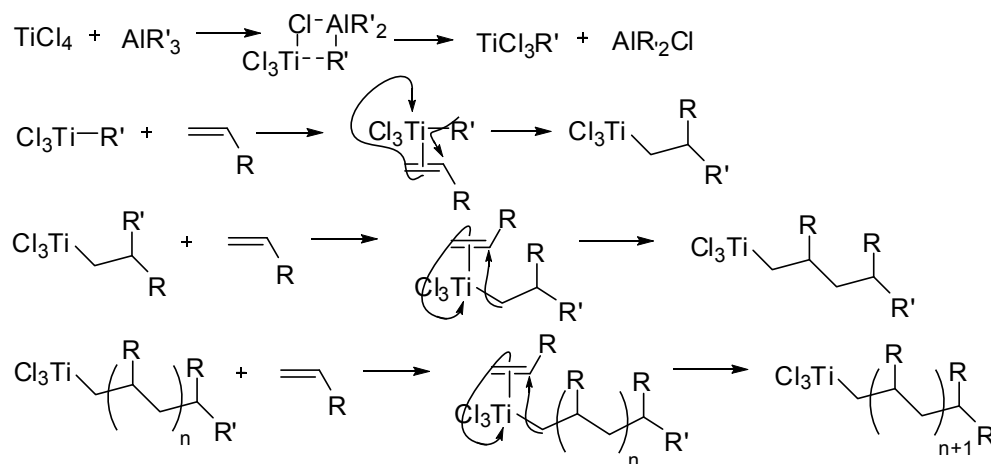
1.5.6.1 *Ziegler-Natta*

The first instances of the use of metal-coordination in polymer chemistry take place in what is now known as Ziegler-Natta coordination polymerization. The use of aluminum alkyl compounds with transition metal halides to synthesize polyethylene was first shown by Karl Ziegler in 1953.^{62,63} Ziegler's work was exploited by Giulio Natta to synthesize the first stereoregular polymers. The use of metal-coordination enables the polymerization of many non-polar monomers that cannot be synthesized by the above ionic approaches while avoiding the many side reactions inherent in conventional radical polymerizations. Ziegler and Natta shared the 1963 Nobel Prize in Chemistry for their work in metal coordination polymerizations.

1) *Mechanism*

The mechanism behind traditional Ziegler-Natta polymerization is very complicated and is still not well understood. There have been numerous proposed mechanisms. A very simplified mechanism presented by Clayden et al. is shown in Scheme 1.27.¹⁵⁹ The mechanism first involves ligand exchange between TiCl_4 and AlR_3 resulting in the formation of the Ti σ -complex responsible for catalyzing the polymerization. This Ti σ -complex then forms a π -complex with the alkene of the first monomer. The R group is inserted through carbo-titanation of the olefin. This process is repeated to begin the polymerization. The π -complex creates close interaction

between the side chains of the growing polymer and the inserted monomer. This steric interaction creates the tacticity in the resulting polymer.



Scheme 1.27 Simplified mechanism in Ziegler-Natta polymerization.

2) Catalysts

A variety of slightly different transition metal “cocktails” can be used in Ziegler-Natta polymerizations; however, almost all of them include a titanium complex (though some use V in its place).⁶² The majority of the more successful mixtures also include an Al complex like the one shown above. There are cases where Li, Na and Zn can be used in place of Al successfully. Changes in the catalyst mixture greatly affect the stereoregularity of the polymerization as well as the final yield and polydispersity. A big disadvantage to traditional Ziegler-Natta catalysts is that they are ill-defined and frequently insoluble in the reaction mixture. Current work in this area involves developing more well-defined defined catalysts to better understand their impact and

control their activity. We will see how this same problem also affected early attempts in ring-opening metathesis in the next section.

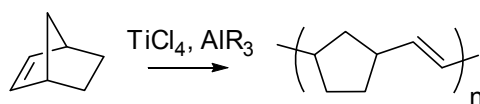
1.5.6.2 *Ring-opening Metathesis Polymerization (ROMP)*

1) *Initial Studies*

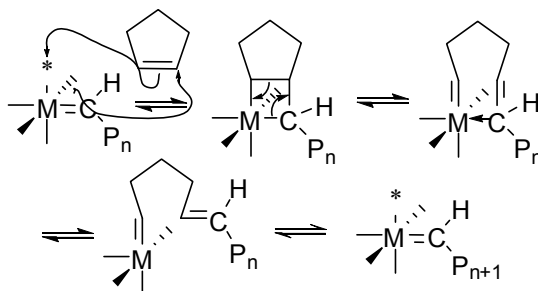
A new reaction was discovered by mistake during the failed Ziegler-Natta type polymerization of norbornene with TiCl_4 and AlR_3 by Truett *et al.* in 1960 (Scheme 1.28).¹⁶⁰ What they had actually prepared, was the first recorded ring-opening metathesis polymerization (ROMP). This was a rather extraordinary discovery as it opened the door for the direct synthesis of unsaturated polymers; this is not readily feasible through the addition approaches we have shown above. It was found by Truett *et al.* and by Natta *et al.* independently that heterogeneous catalysts of Ti, W, or Mo halides with Al co-catalysts successfully polymerized norbornene. The work of Calderon in the 1960s demonstrated that it was possible to polymerize ROMP reproducibly using a homogeneous catalyst mixture of WCl_6 and Et_2AlCl in ethanol.¹⁶¹ Though throughout these initial reports the mechanism of metathesis was not known, Chauvin *et al.* proposed the mechanism in 1971 that was eventually accepted.¹⁶² A general mechanism for ROMP, a special case of metathesis is shown in Scheme 1.29.

These discoveries demonstrated the potential of ROMP. The problem remained, however, how to develop it into a tunable and controllable reaction; to this point none of the preparations exhibited living conditions and the developed catalysts were very sensitive to water & air and side reaction prone. Part of the problem was that these

initial systems used very ill-defined catalysts, what R. H. Grubbs terms “black box catalysts” because the exact role of the catalyst and its influencing factors were unknown due to the complexity of the system. This obstacle led to intensive research by a number of groups, though primarily by those of Richard R. Schrock and Robert H. Grubbs, to develop very well-defined catalysts which could be well understood and tuned.



Scheme 1.28 Polynorbornene synthesis by Ziegler catalyst as performed by Truett et al.



Scheme 1.29 ROMP mechanism for polycyclopentene.

2) *Living ROMP*

The catalyst is the main controlling factor in ROMP. The main goal of groups involved in ROMP research was not only to develop well-defined catalysts that could perform ROMP in a living fashion, but also to be able to polymerize a wide variety of cyclic olefins. In these investigations, several factors seem to play the most important

roles: 1) create highly active catalysts; 2) moderate this reactivity to chemoselectively react with olefins as opposed to impurities (i.e. prevent side reactions); and 3) prevent catalyst chain transfer.¹⁶³ The progression in chemoselectivity of various transition metals used in ROMP is shown in Table 1.3.

Table 1.3 Reactivity of transition metals investigated in ROMP with respect to olefins.¹⁶³

Ti / Ta	W	Mo	Ru
acids	acids	acids	olefins
alcohols	alcohols	alcohols	acids
aldehydes	aldehydes	aldehydes	alcohols
ketones	ketones	olefins	aldehydes
esters/amides	olefins	ketones	ketones
olefins	esters/amides	esters/amides	esters/amides

↑ increasing reactivity

The first investigations focused primarily on Ti and Ta catalysts. These catalysts, though they exhibited many properties of living polymerizations, such as low polydispersities, etc., had fairly low activities and were very sensitive to impurities. Investigations then shifted to tungsten and later to molybdenum and ruthenium. This progression occurred as a result of the factors listed above: an effort to balance overall reactivity with chemoselectivity for olefins. Unfortunately, there is not space to discuss these interesting developments, nor is it within the scope of this general review of polymer synthesis. A major breakthrough took place with the introduction of the metal

alkylidene discovered by the Schrock group using what are now attributed Schrock carbenes. The most successful catalysts developed through this process are shown in Figure 1.16. The catalysts to the left were developed by the group of Richard Schrock¹⁶⁴⁻¹⁷³ and those to the right were developed by Robert Grubbs¹⁷⁴⁻¹⁷⁸. For their contributions in metathesis chemistry they were awarded the Nobel Prize in Chemistry along with Yves Chauvin who first understood the metathesis mechanism. Both sets of catalysts can perform ROMP on a number of monomers such as norbornenes, cyclopentenes, cyclobutenes, etc. and even in some cases cyclohexene. The molybdenum Schrock catalyst holds the current title for the catalyst with the highest activity, while the Grubbs catalysts are the most chemoselective and can be employed in less rigorous conditions; modified Grubbs catalysts have even been used to polymerize cyclic olefins in water.^{179,180} Part of the beauty of these two systems is that the ligands can be tuned to specifically meet the demands of the respective monomer and reaction conditions.

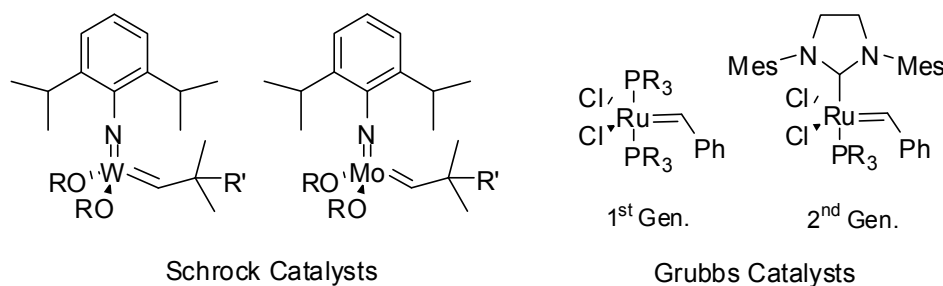


Figure 1.16 The most common ROMP catalysts.

1.6 Surface Grafting

1.6.1 General Remarks

Not only are polymers extremely useful materials on their own, but by combining polymers with other materials through the process of grafting we can enhance the properties of both components. Polymer grafting can be used to modify surfaces of other polymers and inorganic materials to create an almost endless number of new and interesting materials. These new materials can have a broad range of applications in the synthesis of designer films/coatings, stabilization of colloidal particles, lubrication and adhesion effects, rheology and even uses in biological implants, etc. As one might expect, there are many types of polymer grafts. Initially, for simplicity, we will focus on planar inorganic surfaces and will mention general methods for preparing these composites. This general description will be followed by an overview of literature relevant to this dissertation including polymer grafts on OMS.

Polymer grafting offers a unique set of problems in terms of our ability to construct them uniformly, with tunable length and spacing and with the properties we desire. Grafting can be performed either by chemical attachment to the surface or through physical adsorption. Covalent attachment allows the polymer to have a fixed end and be irreversibly bound to the surface. For this reason, it is preferred when trying to make highly uniform films. A graphic schematic of adsorbed vs. covalently attached polymers can be seen in Figure 1.17 below.¹⁸¹

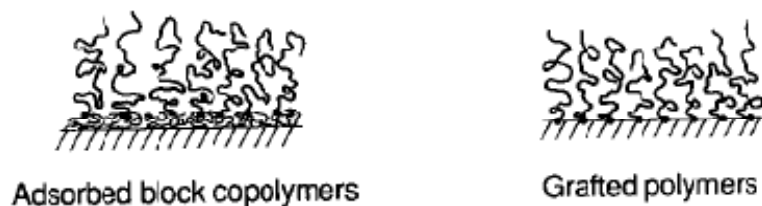


Figure 1.17 Graphic depiction of adsorbed vs. covalently attached polymers.

1.6.2 Polymer Brushes

1.6.2.1 Definition

Sufficiently dense covalently bound grafts (i.e. number of chains per surface area) that force polymer chains to become stretched and nearly linear due to crowding effects from other polymers are commonly referred to as *polymer brushes*. The study of polymer brushes not only allow us to create new and interesting materials, but also facilitate the study the way polymers behave in other tethered architectures such as micelles, vesicles and polymer bilayers that are not readily characterized.

1.6.2.2 “Graft to” vs. “Graft from”

Within covalently grafted polymer systems, there are two principle methods of construction: the *graft to* and *graft from* approaches. The *grafting to* approach involves a solution phase polymerization followed by attachment to the surface. The *grafting from* approach uses a direct polymerization from the surface by previously attached initiators such as those described above modified with the appropriate surface linking group.¹⁸²⁻¹⁸⁶

Figure 1.18 illustrates the difference between the two approaches.

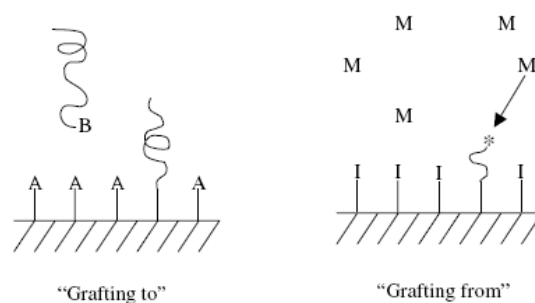


Figure 1.18 Pictorial representation of surface grafting approaches.¹⁸⁷

Both approaches have inherent advantages and disadvantages. While in the *grafting to* approach one can use solution-based synthesis wherein it is much easier to control the MW using approaches outlined above and then graft those very well-defined and characterized polymers to a surface, they invariably lead to lower grafting densities due to entropic effects. On the other hand, though it is more difficult to control and characterize surface-initiated polymerizations, they can usually lead to very high surface densities and thicker layers than are possible by the *grafting to* method.

1.6.2.3 Literature

A variety of different polymerizations have been used to synthesize polymer brushes. As they allow maximum control over polymer brush synthesis, polymerizations with living characteristics have been extensively used. Many of the polymerization types discussed above have been used in the literature, including RAFT, ATRP, NMP and controlled anionic, cationic and ring opening polymerizations and are the subject to

various review articles.^{188,189} Some examples of surface bound initiators used in the formation of polymer brushes are shown in Figure 1.19.

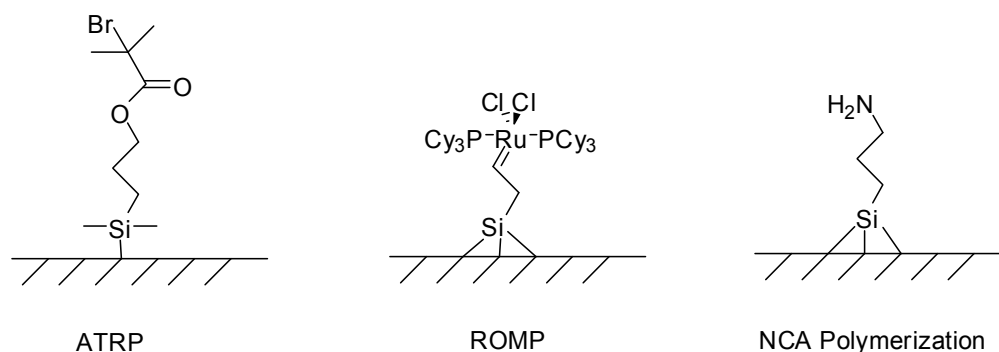


Figure 1.19 Examples of surface bound initiators for the *grafting from* approach.

1.6.3 Polypeptide Brushes

Surface-tethered polypeptide brushes (most notably poly-(L-glutamates)) have been grown off amine-functionalized planar surfaces using NCAs by a number of groups.¹⁹⁰⁻¹⁹⁹ The original work published by Whitesell and Chang showed that L-alanine NCAs could be polymerized off of amine “tripods” on gold surfaces.²⁰⁰ L-phenylalanine, a much larger monomer, could only be polymerized by pushing the amine initiators farther apart using a tripod double layer.

On silicon and glass planar surfaces, the most active groups have been those of Curtis Frank and his student Ying-Chih Chang^{190,191,195-197,201,202} and A.J. Schouten.^{194,198,199,203-207} These works have used primary amines as initiators with the majority focusing exclusively on poly-(γ -benzyl-L-glutamate). A variety of different methods

have been used to prepare these grafts, including solution chemistry^{194,198,203}, solvent-free melt polymerization²⁰⁶ and vapor deposition^{191,195,196}. While the vapor deposition studies show thick brushes over 100nm can be produced, the solution chemistry approach yields layers around 15nm and is highly sensitive to impurities. An early work by Chang and Frank compare solution *graft to* and *graft from* approaches, concluding that the *graft from* method does not produce high density brushes.¹⁹⁰ Successful grafts form α -helices and prefer an orientation perpendicular to the substrate in solvents such as chloroform.²⁰¹ The one work reporting the synthesis of poly-L-lysine tethered to surfaces indicates that it is both helical and also orients perpendicular to the surface.¹⁹⁶ However, this system has not been as thoroughly studied as the poly-(L-glutamates).

There have also been several works on amorphous and colloidal silica. Work by Schouten's group shows that the poly-(L-glutamates) and poly-(L-aspartates) could be grafted efficiently to microparticulate silica (Aerosil A200V, d~12nm).²⁰⁴ In contrast to the planar surfaces, no observable solution polymer was formed. There have been reports in the literature grafting polypeptides from colloidal particles, specifically by Paul Russo's group at LSU. They successfully synthesized poly-(γ -benzyl-L-glutamate) and poly-Z-L-lysine grafted colloidal particles using amine initiators.^{192,193} Other works in the literature investigate polypeptides grafted onto silica/alumina as chiral stationary phases^{208,209} and on colloidal silica crystals for use as membranes.²¹⁰ However, to our knowledge, there have been no reported works of polypeptide grafting to OMS through NCA chemistry.

1.6.4 Polymer Grafting to OMS

Many reports investigating other polymers in OMS, predominantly through radical polymerization, however, can be found in the literature. For example, atom transfer radical polymerization (ATRP) has been used by Kruk et al. to graft polyacrylonitrile, poly(2-(dimethylamino)ethyl methacrylate) and polystyrene to FDU-1 and SBA-15.²¹¹ Audioun et al.²¹² and Moreno et al.²¹³ similarly reported polymerizations using methyl methacrylate (MMA) and its derivatives in SBA-15 by ATRP. Polymers have also been incorporated into MCM-41 by radical polymerizations: Lenarda et al. used nitroxide-mediated polymerization (NMP) to graft polystyrene²¹⁴ and Moller et al.²¹⁵ performed a free radical polymerization to graft PMMA. Free radical polymerization has also been used to incorporate polystyrene in the cubic MCM-48 by He et al. Polymers “threaded” through the pores of OMS, such as the conductive polyaniline, have also been reported.²¹⁶⁻²¹⁹ Additionally, there have been studies functionalizing OMS with polyethyleneimine (PEI) through the ring-opening polymerization of aziridine.²²⁰⁻²²²

1.7 Research Hypothesis and Objectives

Given the chemical variety and physical characteristics of polypeptides noted above and the model characteristics of an ordered mesoporous silica support, we believe novel hybrid materials with unique properties can be developed through the incorporation of polypeptides into OMS. The principal goal of the following work is to

understand how to develop such hybrids and manipulate their properties through synthetic variables. To this end, several objectives were developed:

- 1) Demonstrate NCA polymerization is an effective approach to graft polypeptides to planar silicon, colloidal silica, and OMS (Chapters III & IV)
- 2) Understand the effects of OMS pore size and topology, surface initiator loading and monomer identity on such hybrids through rigorous characterization (Chapter IV)
- 3) Develop the ability to selectively graft polypeptides to inner and outer surfaces of OMS as this extends our control over hybrid design (Chapter V)
- 4) Synthesize novel hybrids by grafting polypeptides to monodisperse mesoporous silica spheres (Chapter VI)

CHAPTER II

EXPERIMENTAL METHODS

2.1 Introduction

This chapter describes the general synthesis procedures used for the polypeptide-silica hybrids and the major analytical techniques used in their characterization. The first section will cover synthetic procedures. The second section will cover characterization methods. Powder X-ray diffraction (XRD) and porosimetry will be briefly described. The bulk of the discussion will then move to infrared spectroscopy (IR) and x-ray photoelectron spectroscopy (XPS) as these are the two most important methods for characterizing the hybrid material following polypeptide grafting.

2.2 Synthetic Procedures

2.2.1 *Synthesis of Polypeptide Brush – OMS Hybrids (Chapter IV)*

2.2.1.1 *Materials*

Sodium silicate (PQ Brand N, SiO₂ 28.7%, SiO₂/Na₂O = 3.22), cetyltrimethylammonium bromide (CTAB, Fisher Chemical, high purity grade), H₂SO₄ (Sigma-Aldrich, 95-98% ACS reagent), sodium hydroxide (NaOH, Mallinckrodt Chemicals, pellet), tetraethoxysilane (TEOS, Fluka, >99%), Pluronic P123 (EO₂₀PO₇₀EO₂₀, MW = 5800, BASF), ethanol (Sigma-Aldrich, 99.9%, ACS reagent), *n*-butanol (EMD, 99%) and HCl (Sigma-Aldrich, reagent grade, 37%) were used in the OMS synthesis as received. 3-aminopropyltrimethoxysilane (APTMS, Aldrich, 97%)

was used for post-synthetic grafting and distilled prior to use. Triphosgene (TCI America, 98%), H-Lys(Z)-OH (Novabiochem, 98%), and L-alanine (Aldrich, 99%) were used for *N*-carboxyanhydride synthesis. *n*-Hexane (Sigma-Aldrich, >95%, ACS reagent grade), tetrahydrofuran (THF, Sigma-Aldrich, >99.9%, Chromasolv HPLC) and toluene (Sigma-Aldrich >99.5%, ACS reagent grade) were used in the post-synthetic grafting, NCA synthesis and polymer grafting steps and were dried and deoxygenated using an MBRAUN MB SPS solvent purification system. Nitromethane (ACROS, 98%), nitrobenzaldehyde (Fluka, >99%, HPLC), and deuterated chloroform (Cambridge Isotope, 99.8% D, 1% V/V TMS) were used as received for the Henry reaction. Hydrofluoric acid (Sigma-Aldrich, 48wt% in water) and 1,1,1,3,3,3-hexafluoroisopropanol (Aldrich, >99%) were used in the silica framework dissolution.

2.2.1.2 MCM-41

MCM-41 was synthesized using the reported procedure of Edler and White.²²³ 7.9 g of sodium silicate solution were mixed with 45.4 mL deionized water. 0.27 g of NaOH were added to the solution, followed by 7.8 mL of 1 M H₂SO₄. 7.29 g of CTAB were dissolved in the solution and stirred for 15 minutes at room temperature. The mixture was then placed in an oven at 100 °C for 24 h under static conditions. After 24 hours the sample was removed from the oven, allowed to cool sufficiently that it could be easily handled and titrated to a pH of approximately 10 using 1 M H₂SO₄. The sample was then placed back in the oven at 100 °C. The titration step was performed two additional times at regular 24 hour intervals. The total heating period was 96 hours.

The solid products were filtered, washed with deionized water, and air-dried overnight. The solid products were calcined to remove CTAB. The calcination procedure was as follows: the air-dried samples were heated from room temperature to 100 °C at a rate of 1 °C/min; held at 100 °C for 2 h; increased from 100 to 500 °C at a rate of 1 °C/min; and then held at 500 °C for 5 h.

2.2.1.3 *SBA-15*

SBA-15 samples were synthesized using a method similar to that reported by Zhao and coworkers.³⁰ 4.0 g of Pluronic P123 were dissolved in 60 mL of 4 M HCl and 85 mL of deionized water by stirring for 5 h at room temperature. Then, 8.5 g of TEOS were added to that solution and stirred for 24 h at 35 °C. The mixture was then aged at 80°C for 24 h without stirring. After filtering, the solid product was calcined for 5 hours at 550 °C in a similar manner to the MCM-41 procedure described above.

2.2.1.4 *KIT-6*

KIT-6 was synthesized according to the method reported by Kleitz et al.³² 6g of Pluronic P123 were dissolved in 217g of DI water and 11.8g of concentrated HCl (35%). After warming to 35°C and while stirring, 6g of butanol were added. After 1 hour stirring, 12.9g of TEOS were added and the mixture was subsequently stirred at 35°C for 24 hours. Immediately following, the mixture was heated to 100°C for an addition 24 hours under static conditions. The solid product was filtered while still hot and the

Pluronic removed by extraction in a mixture of HCl and ethanol. After drying at room temperature, the solid product was calcined at 500°C.

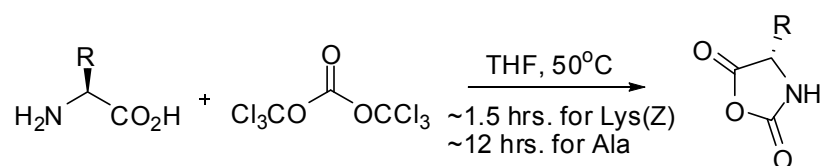
2.2.1.5 *Amine-functionalization*

Amine-functionalized OMS was prepared using post-synthetic grafting. All reagents and OMS were handled under an inert atmosphere. In a typical grafting, one gram of OMS was heated and dried under vacuum overnight (< 0.1 mbar, ~100°C). 50ml of dry toluene were added, followed by 0.25mmol, 0.5mmol, or 0.75mmol of distilled APTMS depending upon the desired degree of functionalization. The reaction proceeded at RT for 24 hours. The solid product was centrifuged, washed in toluene (1x), methanol (1x), methanol/water (1x), methanol (1x), and dried overnight in a 40°C oven.

2.2.1.6 *N-carboxyanhydride Monomer Synthesis*

The *N*_ε-Z-L-Lysine (L-Lys(Z)) NCA was synthesized in dry THF using triphosgene as described by Daly and Poche²²⁴ (Scheme 2.1). Standard Schlenk line techniques were employed in the NCA monomer synthesis and polymer grafting steps. Typically, 4.6g of L-Lys(Z) (16.4mmol) and 2.2g of triphosgene (7.4mmol) were dried under vacuum for a minimum of 20 minutes in separate Schlenk flasks. 75ml and 50ml of dry THF were added to the L-Lys(Z) and triphosgene, respectively, directly from the solvent drying system. The triphosgene solution was added via cannula transfer to a rapidly mixing L-Lys(Z) slurry. The reaction flask was capped and placed in a 50°C

water bath. After ~1.5 hours of stirring at 50°C under argon, the solution became transparent indicating the completion of the reaction. The NCA was recrystallized in 400ml of dry n-hexane overnight in a standard freezer twice and, subsequently, filtered and dried under vacuum for immediate use (~5g or >95% yield). L-Alanine NCA was prepared in a similar fashion with two notable differences: 8.1mmol of triphosgene and NCA synthesis took place overnight. The yield of L-Ala NCA was 64%.

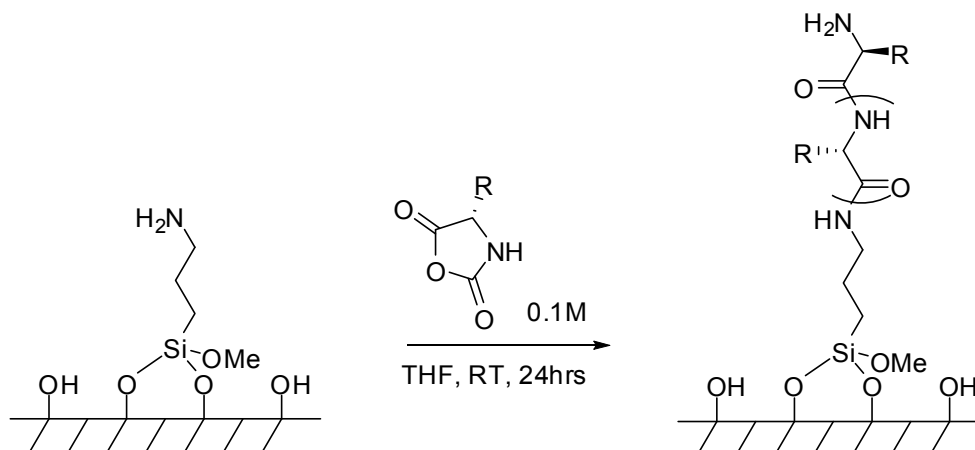


Scheme 2.1 *N*-Carboxyanhydride Synthesis: R= -CH₃ for L-Ala and -CH₂CH₂CH₂CH₂NHCbz for L-Lys(Z).

2.2.1.7 *N*-carboxyanhydride Polymerization

The NCA was polymerized in a *graft from* approach using the amines on the OMS surface as initiators (Scheme 2.2). In a typical procedure, 0.5g of amine-functionalized OMS were heated and dried overnight under vacuum. A 0.1M NCA solution was prepared in dry THF and 50ml were transferred to the dried OMS via cannula (40:1 monomer/initiator for the 0.25mmol APTMS/g SiO₂, 20:1 and 13:1 for the 0.5 and 0.75mmol APTMS/g SiO₂ substrates, respectively). The powder and solution were vigorously stirred at room temperature for 24 hours. After completion the powder

was centrifuged and rinsed in 50ml of THF (2x), DMF (2x) and chloroform (2x). The composite was dried in a 40°C oven and stored.



Scheme 2.2 Peptide grafting to silica surface: R= $-\text{CH}_3$ for L-Ala and $-\text{CH}_2\text{CH}_2\text{CH}_2\text{CH}_2\text{NHCbz}$ for L-Lys(Z). Note: The number of silane bonds to the surface is not necessarily as depicted.

2.2.1.8 *Deprotection*

The Cbz-protected peptides were deprotected using a 33wt% solution of HBr in acetic acid. For example, 200mg of composite material were stirred for 30 minutes in 2ml of HBr solution. The composite was filtered and rinsed multiple times with toluene and acetone. The sample was neutralized by stirring in a 1 mM NaOH solution overnight then filtered and rinsed with water and methanol.

2.2.1.9 *Catalytic Testing*

The nitroaldol reaction (Henry reaction) was used to test the catalytic activity of the peptide-OMS composites in the manner performed by Bass and coworkers.⁴⁹ For each test, 0.38 g of 4-nitrobenzaldehyde (2.5 mmol) were added to a 10mL Schlenk flask with 10-25mg pre-dried deprotected peptide-OMS composite (0.025mmol on amine basis; calculated from TGA results). The composite and 4-nitrobenzaldehyde were dried under vacuum for one hour, followed by the addition of 1.35 mL of nitromethane (25 mmol). The mixture was stirred at 40° C under argon for 7 hours. 50 μ L aliquots were removed every 30 minutes for the first 2 hours and then again at 7 hours. The aliquots were analyzed by ¹H NMR in *d*-chloroform. The conversion and yields were calculated by integrating the peaks for the β -hydroxyl (¹H δ 5.6 ppm) and α,β -unsaturated (¹H δ 7.72-7.75 ppm) products with respect to that of 4-nitrobenzaldehyde (¹H δ 10.1 ppm).

2.2.1.10 *Analytical*

Powder X-ray diffraction (PXRD) measurements on MCM-41 were performed using a Bruker-AXS D8 powder diffractometer with Cu K α radiation. X-ray diffraction measurements were performed on SBA-15 and KIT-6 samples using a Bruker-AXS Rotating-Anode NANO-STAR Small Angle X-ray Scattering Instrument with Cu K α radiation. Infrared spectroscopy was performed on the composites using a Nexus 670 FT-IR Spectrometer from Thermo Nicolet. Thermal gravimetric analyses (TGA) were performed using a TG 209C Iris Instrument from Netzsch over a temperature range

of 100 to 550 °C using oxygen and nitrogen purges (1:1, 10ml/min) and a temperature ramping rate of 1°C min⁻¹. Nitrogen adsorption experiments were performed on a Micromeritics ASAP 2010 micropore system. The samples were degassed under vacuum at 100°C overnight prior to analysis. The surface areas and mesopore volumes were determined using the α_s -method. The mesopore size distributions were calculated from the adsorption branch of the isotherm using the Barret-Joyner-Halenda (BJH) method with a modified equation for the statistical film thickness.⁴⁰ ¹³C{¹H} CP-MAS were performed at 100.61 MHz using a 4 mm probe with ZrO₂ rotors and a spinning rate of 9 kHz, a 2 ms contact time, a ¹H 90° pulse length of 2.5 μ s, and a 5 s recycle delay. Chemical shifts were referenced to tetramethylsilane. X-ray photoelectron spectroscopy (XPS) was performed on a Kratos Axis Ultra Imaging XPS using a monochromatic Al K α source. Solution ¹H NMR spectra were measured on a 300 MHz Varian Mercury spectrometer. The ¹H 90° pulse length was 6 μ s, the recycle delay was 6 s, and 16 FIDs were recorded per spectrum. Chemical shifts were reference to TMS. Mass spectra were acquired using matrix-assisted laser desorption/ionization time of flight (MALDI-TOF) on an Applied Biosystems Voyager-DE STR Biospectrometry Workstation. Positive ion mode and a 2,4,6-trihydroxyacetophenone (THAP) matrix were used. Samples were prepared for MALDI-TOF MS by dissolving approximately 20mg of composite in 2 ml of a 1:1 solution of 48wt% aqueous HF and 1,1,1,3,3,3-hexafluoroisopropanol. Elemental analysis was performed by Galbraith laboratories.

2.2.2 Surface Selective Grafting of Poly-L-lysine from SBA-15 (Chapter V)

2.2.2.1 Materials

Tetraethoxysilane (TEOS, Fluka, >99%), Pluronic P123 (EO₂₀PO₇₀EO₂₀, MW = 5800, BASF), ethanol (Sigma-Aldrich, 99.9%, ACS reagent), and HCl (Sigma-Aldrich, reagent grade, 37%) were used in the OMS synthesis as received. 3-aminopropyltrimethoxysilane (APTMS, Aldrich, 97%) and 3-mercaptopropyltrimethoxysilane (MPTMS, Aldrich, 97%) were used for post-synthetic grafting and distilled prior to use. Triphosgene (TCI America, 98%) and H-Lys(Z)-OH (Novabiochem, 98%) were used for *N*-carboxyanhydride synthesis. *n*-Hexane (Sigma-Aldrich, >95%, ACS reagent grade), tetrahydrofuran (THF, Sigma-Aldrich, >99.9%, Chromasolv HPLC) and toluene (Sigma-Aldrich >99.5%, ACS reagent grade) were used in the NCA synthesis and polymer grafting steps and were dried and deoxygenated using an MBRAUN MB SPS solvent purification system. *N,N*-Diisopropylethylamine (DIPEA, 98%) was purchased from Fluka. The NHS-Fluorescein (>90%) and TS-link BODIPY-TMR C5 thiosulfate were purchased from Pierce and Invitrogen, respectively.

2.2.2.2 Amine-functionalized SBA-15 for Poly-L-lysine Only Samples (X1/I1)

SBA-15 was synthesized as described above in Sublevel 2.2.1.3. The solid product, however, was not calcined but rather filtered without washing and dried at 40°C until used. The as-made SBA-15 was divided into two 1 g batches; both were vacuum-dried overnight. All reagents and OMS were handled under an inert atmosphere. One batch was functionalized with 2ml of 3-aminopropyltrimethoxysilane

(APTMS) in 50 ml dry toluene (**X1**), while the other was capped with hexamethyldisilazane (HMDS) (2 ml HMDS/50 ml toluene).

The Pluronic template in both samples was extracted using refluxing ethanol and HCl. The solid products were rinsed in ethanol and dried at 40°C overnight. 0.5 g of the HMDS-capped sample was vacuum-dried overnight and further functionalized with 0.25mmol APTMS in 25ml of dry toluene (0.5mmol/g APTMS) (**I1**).

2.2.2.3 *Amine/thiol-functionalized SBA-15 for Polylysine/thiol Samples (X2/I2)*

SBA-15 was synthesized as described above in Sublevel 2.2.1.3. The solid product, however, was not calcined but rather filtered without washing and dried at 40°C until used. 10 ml of the distilled APTMS or MPTMS was added to 1.2 g of as-made SBA-15 in a Teflon-capped 35ml glass tube. The slurry was stirred rapidly while irradiating with 300 W of 2.54 GHz microwaves for 15minutes in a CEM Discovery Microwave Reactor. A cooling fan was used in order to keep the temperature of the slurry around 50°C. The vessel was cooled and the powder filtered and rinsed in toluene and ethanol.

The powder was then placed back in another clean glass tube with 20ml of 1:1 hexanes and ethanol. The slurry was stirred rapidly while irradiating with microwaves (100 W, 2.54 GHz) for three cycles of 2 minutes, with a cooling fan applied during irradiation and for 2 minutes between each cycle. The vessel was cooled and the powder filtered and rinsed in ethanol. This microwave-aided extraction procedure was repeated twice with 25ml ethanol.

Internal functionalization was performed using a traditional post-synthetic grafting procedure. In a typical grafting, 0.5 g of OMS was dried under vacuum overnight (< 0.1 mbar). 25ml of dry toluene were added, followed by 0.25mmol, of distilled APTMS or MPTMS depending upon the desired organosilane. For APTMS, the reaction proceeded at RT for 24 hours. For MPTMS, 100 μ l of water was added and the mixture was refluxed for 24 hours. The solid product was centrifuged, washed in toluene (1x), methanol (1x), methanol/water (1x), methanol (1x), and dried overnight in a 40°C oven.

2.2.2.4 *Fluorescent Labeling*

Labeling was performed as recommended by the suppliers. ~ 1 mg of each sample was dispersed in 1 ml 0.1M phosphate buffer (pH = 7.5) followed by the addition of 100 μ l of a 1 mg/ml solution TS-link BODIPY-TMR C5 thiosulfate in water. The samples were shaken for 3 hours. The powder was centrifuged and rinsed repeatedly in water and ethanol. The dyed powder was redispersed in a 0.2M sodium borate buffer (pH = 8.5) followed by the addition of 100 μ l of a 5 mg/ml solution of NHS-Fluorescein in DMF. The samples were again shaken for 3 hours. The solid was centrifuged and rinsed repeatedly in DMF and ethanol.

2.2.2.5 *NCA Monomer Synthesis and Polymerization*

L-Lys(Z)-NCA was prepared as described for the peptide brush — OMS hybrids (Sublevel 2.2.1). Polymerization was also performed in a similar manner. In a typical

procedure, 0.25g of functionalized silica were dried overnight under vacuum. A 0.1M NCA solution was prepared in dry THF and 12.5ml (5mmol/g FS) or 25ml (10mmol/g FS) were transferred to the dried OMS via cannula. The powder and solution were vigorously stirred at room temperature for 24 hours. After completion, the powder was centrifuged and rinsed in 50ml of THF (2x), DMF (2x) and ethanol (2x). The composite was dried in a 40°C oven and stored.

2.2.2.6 *Deprotection and Neutralization*

The Cbz-protected peptides were deprotected using a 33wt% solution of HBr in acetic acid. For example, 200mg of composite material were stirred for 30 minutes in 2ml of HBr solution. The composite was filtered and rinsed multiple times with toluene and acetone. The sample was neutralized by stirring in a 40:1 solution of ethanol and DIPEA for ~2hrs, centrifuged, and rinsed with ethanol.

2.2.2.7 *Analytical*

X-ray diffraction measurements were performed on SBA-15 using a Bruker-AXS Rotating-Anode NANO-STAR Small Angle X-ray Scattering Instrument with Cu K α radiation. Infrared spectroscopy was performed on the composites using a Nexus 670 FT-IR Spectrometer from Thermo Nicolet. Thermal gravimetric analyses (TGA) were performed using a TG 209C Iris Instrument from Netzsch over a temperature range of 100 to 900 °C using oxygen and nitrogen purges (1:1, 10ml/min) and a temperature ramping rate of 5°C min⁻¹. Nitrogen adsorption experiments were performed on a

Micromeritics ASAP 2010 micropore system. The samples were degassed under vacuum at 100°C overnight prior to analysis. The surface areas and mesopore volumes were determined using the α_s -method. The mesopore size distributions were calculated from the adsorption branch of the isotherm using the Barret-Joyner-Halenda (BJH) method with a modified equation for the statistical film thickness.⁴⁰ X-ray photoelectron spectroscopy (XPS) was performed on a Kratos Axis Ultra Imaging XPS using a monochromatic Al K α source. Confocal microscopy was performed using a Leica TCS SP5 microscope. The images were obtained using a pinhole diameter of 100nm, a 63X oil objective, and Ar 488nm and HeNe 543nm lasers for excitation. SEM images were obtained with a JOEL JSM 7500F field emission scanning electron microscope. Samples were prepared by dispersing the powders in THF and depositing on a copper grid. A working distance of 6 mm was used and a 5.0kV voltage.

2.2.3 Polypeptide Grafting from Monodisperse OMS Spheres (Chapter VI)

2.2.3.1 Materials

Tetramethoxysilane (TMOS, Fluka, >99%), cetyltrimethylammonium chloride (CTACl, Aldrich, >98%), methanol (Sigma-Aldrich, 99.8%, ACS reagent), and NaOH (Sigma-Aldrich, reagent grade, >98%) were used in the OMS spheres synthesis as received. 3-aminopropyltrimethoxysilane (APTMS, Aldrich, 97%) and 3-mercaptopropyltrimethoxysilane (MPTMS, Aldrich, 97%) were used for post-synthetic grafting and distilled prior to use. Triphosgene (TCI America, 98%) and H-Lys(Z)-OH (Novabiochem, 98%) were used for *N*-carboxyanhydride synthesis. *n*-Hexane (Sigma-

Aldrich, >95%, ACS reagent grade), tetrahydrofuran (THF, Sigma-Aldrich, >99.9%, Chromasolv HPLC) and toluene (Sigma-Aldrich >99.5%, ACS reagent grade) were used in the NCA synthesis and polymer grafting steps and were dried and deoxygenated using an MBRAUN MB SPS solvent purification system. *N,N*-Diisopropylethylamine (DIPEA, 98%) was purchased from Fluka.

2.2.3.2 *OMS Sphere Synthesis*

OMS Spheres with a thiol functionalized core were synthesized according to Yano's procedure with a core/shell silane ratio of 2 to 1. Typically, 7.04 g of CTACl (cetyltrimethylammonium chloride) were dissolved in 1600 g of 49:51 (w/w) methanol/water (784 g/816 g), followed by the addition of 6.84 g 1 M NaOH. After mixing for ~5minutes and while stirring rapidly, 34.7 mmol of a 9:1 (mol/mol) TMOS/MPTMS mixture (4.75g/0.68g) were added. After a period of ~15 seconds, the clear solution turned opaque. After waiting an additional 30 minutes, 3.42 g of 1 M NaOH solution and 17.35 mmol TMOS (2.64g) were added to the solution. The mixture was continually stirred for 8 hours and aged without stirring overnight. The resulting solid powder was filtered without washing and dried in an 45°C oven for three days. The synthesis yielded about 5.7 grams of OMS spheres prior to extraction.

2.2.3.3 *Amine-functionalization, Monomer Synthesis and Polymerization*

1 g (as-made) was dried under vacuum for 24hrs. ~50mL of dry toluene was added, followed by 2ml of distilled APTMS. The solution was stirred for 1 hour,

followed by filtration, and washing in ethanol. Extraction of the CTACl template was performed by refluxing in a 1:100 (v/v) HCl/EtOH for at least 3 hours.

L-Lys(Z)-NCA and L-Glu(Bz)-NCA were synthesized according to the standard approach described in Sublevel 2.2.1. Three batches of 250mg amine-functionalized OMS spheres were dried overnight under vacuum. ~10ml of dry THF were added to each flask. The OMS spheres were dispersed in the THF through sonication and rapid stirring. To each flask, 15ml of NCA were added while stirring rapidly: Flask 1 was entirely L-Lys(Z)-NCA; Flask 2, entirely L-Glu(Bz)-NCA; and Flask 3, a 1:1 (mol/mol) mixture.. The polymerization proceeded at RT for 24 hours. Deprotection and neutralization were performed as described in Sublevel 2.2.2.6.

2.2.3.4 *Fluorescent Labeling*

Labeling was performed by adding 100 μ l of a BODIPY-TMR solution in DMF (1mg/ 100 μ l) to ~ 1 mg of each sample and shaking on a shakeplate. After 1 hour, 100 μ l of a NHS-Fluorescein solution in DMF (1mg/ 100 μ l) was added, followed by an additional hour of shaking. The samples were centrifuged and repeatedly rinsed in DMF and methanol.

2.2.3.5 *Analytical*

The analytical details are the same as above in Sublevel 2.2.2.7.

2.2.4 Initial Work on Planar Silicon, Colloidal Silica and OMS (Chapter III)

2.2.4.1 Materials

Double-side polished silicon wafers were obtained from the International Wafer Service. Tetraethoxysilane (TEOS, Fluka, >99%), ethanol (Sigma-Aldrich, 99.9%, ACS reagent), and ammonium hydroxide (EMD, reagent grade, 28-30% in water) were used in the colloidal silica synthesis as received. 3-aminopropyltrimethoxysilane (APTMS, Aldrich, 97%) was used for the amine-functionalization and distilled prior to use. Fmoc-OSu (>99%) was obtained from NovaBiochem and used as received. Triphosgene (TCI America, 98%) and H-Lys(Z)-OH (Novabiochem, 98%) were used for *N*-carboxyanhydride synthesis. *n*-Hexane (Sigma-Aldrich, >95%, ACS reagent grade), tetrahydrofuran (THF, Sigma-Aldrich, >99.9%, Chromasolv HPLC) and toluene (Sigma-Aldrich >99.5%, ACS reagent grade) were used in the NCA synthesis and polymer grafting steps and were dried and distilled over calcium hydride (for hexane) or sodium metal (for THF and toluene).

2.2.4.2 Polymerization from Silicon Wafers (w/o Fmoc-spacing)

Silicon wafers were cut into 1" x 0.5" slices using a dicing saw. Immediately prior to use wafers were cleaned in a piranha solution at RT for 2 hours (7:3, sulfuric acid / hydrogen peroxide (30%)). The cleaned wafers were copiously rinsed in water and acetone.

Precleaned wafers were placed in Schlenk flasks and were evacuated for ~30 minutes. 15 ml of dry toluene was added followed by 400 μ l of APTMS. The flask was

capped and placed in an oven at 100°C where it was left for 24 hours under static conditions. After the reaction, the wafers were cleaned repeatedly in methanol, water and acetone. Monomer synthesis was carried out as described above. Amine-functionalized wafers were evacuated in Schlenk flasks for ~30 minutes, followed by the addition of 10ml of 0.1M NCA solution. The reaction was carried out at 40°C for 24 hours under argon on a shake plate. The wafers were removed and cleaned repeatedly in chloroform.

2.2.4.3 *Polymerization from Silicon Wafers (w/ Fmoc-spacing)*

Fmoc-APTMS was prepared in a similar manner to that used by Cheng et al.²²⁵ Typically, 10.0 mmol of distilled APTMS was mixed with 50 ml of dry methylene chloride under argon in a Schlenck flask and cooled in an ice bath. In a separate Schlenk flask, 10.2 mmol Fmoc-OSu was dissolved in 10 ml dry methylene chloride under argon. This solution was transferred to the APTMS flask *via* cannula wire. The mixture was stirred for 2 hours, followed by solvent removal using a u-connector and a liquid nitrogen-cooled Schlenck flask under vacuum. The unpurified product was dissolved in 50 ml of dry toluene.

Precleaned wafers were placed in Schlenk flasks and were evacuated for ~30 minutes. 15ml of dry toluene was added followed by 1ml of the Fmoc-APTMS solution. The flask was capped and placed in an oven at 100°C where it was left for 24 hours under static conditions. After the reaction, the wafers were cleaned repeatedly in methanol, water and acetone. The Fmoc protecting group was cleaved in a 20% solution

(v/v) of piperidine in DMF for 20 minutes, followed by rinsing in chloroform.

Monomer synthesis was carried out as described above. Amine-functionalized wafers were evacuated in Schlenk flasks for ~30 minutes, followed by the addition of 10ml of 0.1M NCA solution. The reaction was carried out at 40°C for 24 hours under argon on a shake plate. The wafers were removed and cleaned repeatedly in chloroform.

2.2.4.4 *Polymerization from Colloidal Silica*

Colloidal silica was synthesized using the Stober method.¹⁸ A solution was prepared containing 500ml ethanol, 57 ml DI water and 30 ml concentrated ammonium hydroxide (28-30wt%). While stirring vigorously, 15 ml of distilled TEOS was added quickly and the flask was covered. After approximately 5 minutes, the solution became opaque. The solution continued to be stirred for 2 hours. The cover of the flask was removed and the solution was stirred until ammonia could no longer be smelled through wafting. The particles were then collected by centrifugation and dried in air. Amine-functionalization, polymerization, and neutralization were performed in a manner similar to the OMS spheres (Sublevel 2.2.3.2).

2.2.4.5 *Polymerization from OMS*

MCM-41 was synthesized and the subsequent amine-functionalization and polymerizations were performed in a manner similar to that in Sublevel 2.2.1.

2.2.4.6 *Analytical*

X-ray photoelectron spectroscopy (XPS) was performed on a Kratos Axis Ultra Imaging XPS using a monochromatic Al K α source. Infrared spectroscopy was performed using a Nexus 670 FT-IR Spectrometer from Thermo Nicolet. Circular dichroism measurements were performed on an AVIV 62DS spectropolarimeter over a wavelength range of 190-250 nm. A 0.1 nm data point interval was used and the resulting data was averaged over at least three scans. For these measurements, the silicon wafers were placed in a cuvette leaning at an angle of approximately 60° and the polymerized colloidal silica particles were dispersed in chloroform. A Brookhaven ZetaPALS instrument was used for the dynamic light scattering measurements on the bare, amine-functionalized and polymerized colloidal particles.

2.3 **Analytical Methods**

2.3.1 *X-ray Diffraction*

X-ray diffraction is important for characterizing the nanostructure in OMS. These materials are powders ($\sim 1\mu\text{m}$), so single-crystal diffraction methods are not applicable. In powder X-ray diffraction (PXRD), in contrast to single-crystal methods, the particles are randomly oriented such that all the crystal planes face the X-ray beam. Though OMS are not crystalline, the mesopores possess long range order which give rise to Bragg peaks.

2.3.1.1 *Basic Theory and Instrument Configuration*

The X-rays used are typically from bombarding either copper (Cu) or molybdenum (Mo) with high energy electrons, though in principle almost any metal could be used. The emitted X-rays are then filtered or passed through a monochromator to produce $K\alpha$ radiation from the respective metal. $CuK\alpha$ possesses a wavelength of 1.541 Å and $MoK\alpha$ possesses a wavelength of 0.709 Å. Once the X-rays impinge on the sample, they diffract off of each of the exposed planes and a detector rotates around the sample recording the intensities of diffraction at each angle. There are other instrument geometries, however, this arrangement is the one used here. The diffraction peak intensities are plotted as a function of 2θ , where θ is the angle of diffraction. The angles at which the peaks are observed can be used to determine the interplanar spacing of atoms (periodicity) or d -spacing for each crystal plane using Bragg's Law (See Figure 2.1). For OMS, these values can be used to estimate the unit cell dimensions of the pore arrangements. Bragg's Law can be expressed as the following:

Error! Bookmark not defined.
$$n\lambda = 2d \sin(\theta)$$

(2.1)

where

λ = the wavelength of the monochromatic X-ray beam, [L]

n = some integer 1, 2, 3...

θ = the angle of incidence, [radians]

d = the interplaner spacing of atoms, [L]

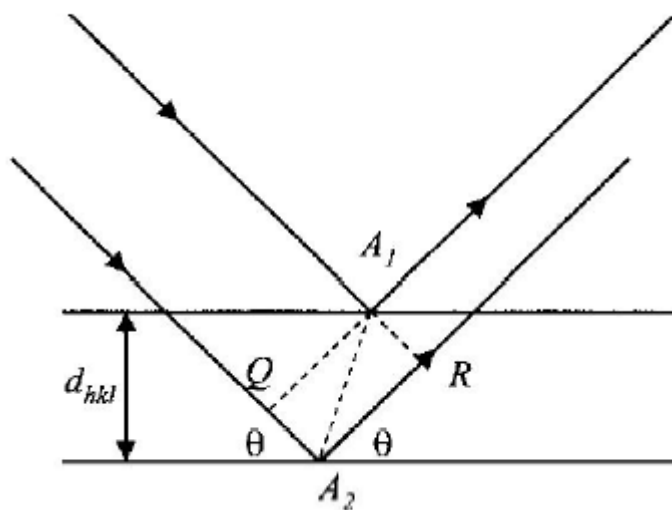


Figure 2.1 A visual representation of Bragg's Law.²²⁶

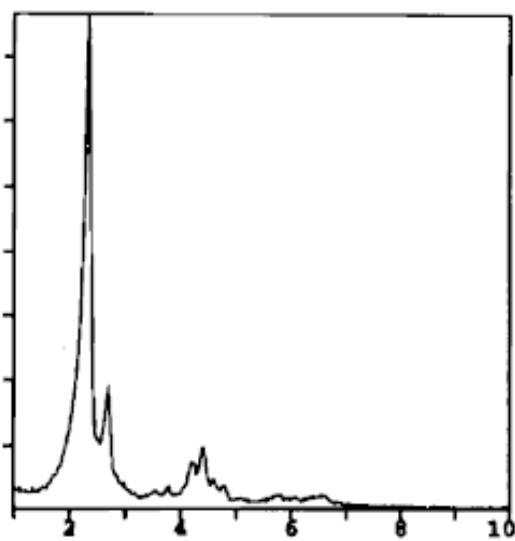


Figure 2.2 The XRD pattern of MCM-48.²⁷

By comparing the positions of the peaks versus 2θ and knowing the pore topology/symmetry, one can assign Miller indices – which are related to a plane of reflection – to a peak and derive the unit cell parameters. The unit cell parameters for OMS are related to the distance between the repeating arrangement of the pores (i.e. hexagonal, cubic, etc.). For well-studied OMS, such as MCM-41 (Figure 2.2) or SBA-15, a comparison between peak values gathered during experiment and known relationships between peaks obtained in the literature is all that one must do to identify the structure.

2.3.2 Adsorption (Porosimetry)

Nitrogen physisorption is one of the most common methods used to determine the pore size distribution, surface area, and pore volume in porous materials and is the method used here to characterize OMS and OMS hybrids.

2.3.2.1 Basic Theory

Physisorption differs from chemisorption in that it is adsorption due to van der Waals forces rather than chemical bonding, it is reversible, and can form multiple layers whereas chemisorption is inherently restricted to a monolayer.²²⁷ These differences make physisorption a good method for probing the internal structure of porous materials. Such measurements are usually done at the triple point of the analysis gas (77 K for nitrogen). There are six classifications of physisorption isotherms as shown in Figure 2.3.²²⁷ A Type I isotherm is indicative of a microporous structure. Type II is the

isotherm of a non-porous solid. Type IV is a mesoporous solid and is the isotherm type with which the analyses in this thesis shall deal. Types III, V and VI are uncommon and will not be discussed.

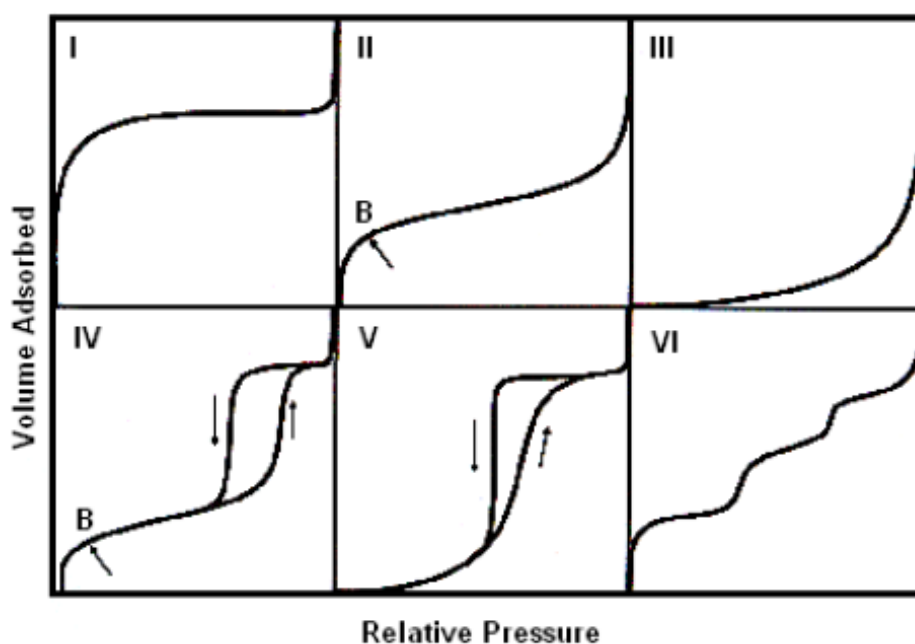


Figure 2.3 The six IUPAC adsorption isotherm classifications.²²⁷

2.3.2.2 α_s Analysis

α_s analysis is a method which can be used to extract information about the pore volume and surface area from an adsorption isotherm. The key assumption in this method is that the surface chemistry of the reference material is the same as the analyzed sample. In the α_s approach, the isotherm is non-dimensionalized the isotherm (volume adsorbed versus relative pressure, p/p_0) by dividing the volume adsorbed (v_{exp})

at each relative pressure by the volume adsorbed at $p/p_0 = 0.4$ and redefining this value as α_s .

$$\alpha_s = \frac{v_{\text{exp}}}{v_{\text{exp}, p/p_0=0.4}} \quad (2.2)$$

An equation for this isotherm, $\alpha_s(p/p_0)$ can be fitted to the data by employing common curve fitting techniques. Using this equation, one can construct a plot of the volume of probe gas adsorbed versus α_s . A sample which is nonporous would exhibit a straight line. Conversely, areas of nonlinearity indicate porosity. It is from these sections that data can be obtained concerning pore volume and surface area.

The pore volume information is determined by drawing tangent lines to each nonlinear section of the isotherm and extrapolating them back to the y-axis.²²⁷ The intercept of the tangent line to the first section is the micropore volume. For an OMS such as SBA-15 which has micropore and mesopores, the next section's tangent line will have the total pore volume as its intercept. The mesopore volume can be determined by subtracting these two values. The surface area can be determined by knowing the slope from the origin to the point at a relative pressure of 0.4 and substituting it into the equation:

$$S = \frac{S_{\text{ref}} \eta}{v_{p/p_0=0.4}} \quad (2.3)$$

where

- S = the surface area
 v = the volume adsorbed
 η = the slope

2.3.2.3 BJH Analysis

The Barret-Joyner-Halenda (BJH) analysis²²⁸, which is derived from the Kelvin equation, is commonly used to determine the pore size distribution in mesoporous solids. Assuming cylindrical pores, which is the case for most OMS, and using parameters developed in 1997 by Jaroniec *et al.*²²⁹ the pore size distribution can be estimated with the expression:

$$r(p/p_0) = \frac{\gamma V_L}{RT \ln(p/p_0)} + t(p/p_0) + 0.3 \quad (2.4)$$

$$t(p/p_0) = 0.1 \left[\frac{60.65}{0.03071 - \log(p/p_0)} \right]^{0.3968} \quad (2.5)$$

where

- V_L = the molar volume of liquid adsorbate
 γ = the surface tension of the liquid adsorbate
 t = the liquid film thickness

2.3.3 *Fourier Transform Infrared Spectroscopy (FT-IR)*

FT-IR is a commonly used vibrational spectroscopy technique in chemistry which relates the absorption of infrared radiation to chemical bond information. Here, IR spectroscopy is principally used to confirm the grafting of polypeptides from the silica matrices and the success of the subsequent deprotection step for protected polypeptide grafts by HBr.

2.3.3.1 *Instrument Configuration*

IR spectroscopy is performed by passing infrared light (typically $30\mu\text{m}$ - $2.5\mu\text{m}$ or 4000 - 400cm^{-1} in wavenumbers for mid-IR) through a sample (solid, liquid or gaseous) and observing the degree of absorbance compared to a reference scan. Chemical information is obtained in this manner as light frequencies associated with specific molecular bond vibrations are selectively absorbed while others are transmitted. As collecting data at each wavelength using a monochromator is time consuming, modern FT-IR employs data collected from a broadband light source which is subsequently separated into individual wavelengths by means of an interferometer and Fourier transform processing. Figure 2.4 shows the typical instrument configuration consisting of the light source, sample, and detector. The reference scan is usually run in the sample chamber before the sample is inserted and not in a separate cell as shown.

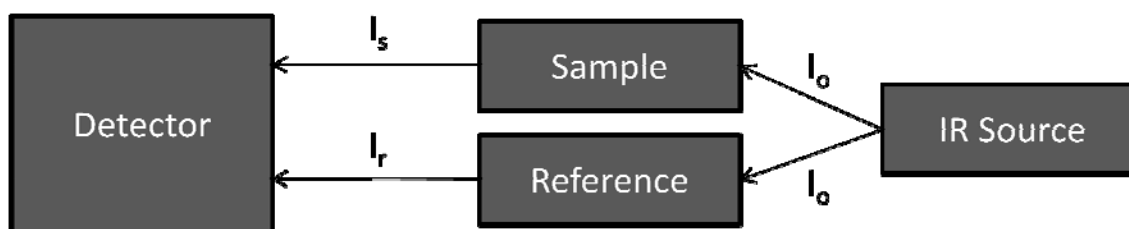


Figure 2.4 Typical FT-IR spectrometer instrument configuration.

As in other absorption spectroscopic techniques, absorbance (A) can be described in IR by the Beer-Lambert Law (2.6) where ϵ is the extinction coefficient, c is the concentration of the absorbing species, and l is the path length of the beam through the sample. Absorption can be calculated from the experimentally observed ratio of the transmitted sample (I_s) and reference light intensities (I_r), or transmittance (T), through equation 2.8. Resulting spectra can be displayed in either terms; absorbance will be used here.

$$(2.6)$$

$$- \quad - \quad (2.7)$$

2.3.3.2 Dipole Moments

In order to explain how and why IR radiation is absorbed, the concept of the dipole moment must first be introduced. A *dipole moment* is the magnitude of the directionally biased distribution of electrons (charge) within a molecule. Permanent dipoles exist in polar molecules such as water or fluoromethane (Figure 2.5) that, with

few exceptions, do not have a center of inversion. A permanent dipole moment (μ) is defined mathematically as a separation of charge (e) over a distance (r).

$$\mu = er \quad (2.8)$$

This concept is extremely important as the electric field component of light can only be absorbed completely by dipoles that are oscillating at the same frequency; in other words, dipoles are required for absorption in IR spectroscopy. The dipole need not be permanent, however, and can result from asymmetrical vibration modes as will be shown below.

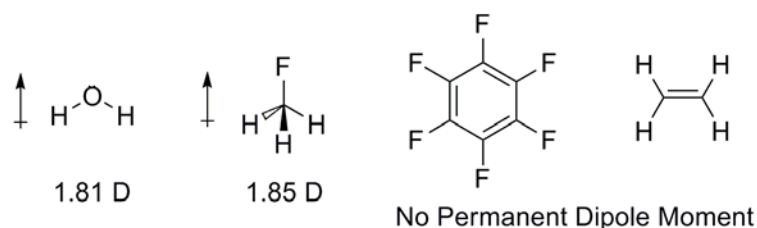


Figure 2.5 Examples of molecules with and without permanent dipole moments.²³⁰

2.3.3.3 *Vibration Energy Levels*

According to quantum mechanics, vibration energies are quantized and occur at discrete energy levels or frequencies. Two models that exist for estimating the vibrational frequencies assume diatomic molecules behave as either harmonic or anharmonic oscillators. The potential well for a harmonic oscillator can be described by the behavior of two atoms connected by a spring obeys Hooke's law (Figure 2.6). Though Morse potential is more accurate as it allows for the disassociation of the bond

at high energies, the harmonic case is sufficient for the current discussion. Equation 2.9 a-c show Hooke's law, the potential curve derived from it and the associated solution to the two particle Schrödinger equation, respectively:

$$f = -k(r - r_e) \quad (2.9a)$$

$$V = \frac{1}{2}k(r - r_e)^2 \quad (2.9b)$$

$$E_v = h\omega(v + \frac{1}{2}) \quad (2.9c)$$

where

f = the restoring force associated with the spring

k = the force constant

r = the length of the spring

r_e = the equilibrium length, $f(r_e) = 0$

V = the potential energy

E_v = the vibrational energy

v = the vibrational quantum number ($v = 1, 2, 3 \dots n$)

ω = $\frac{1}{2\pi} \sqrt{\frac{k}{\mu}}$

μ = the reduced mass

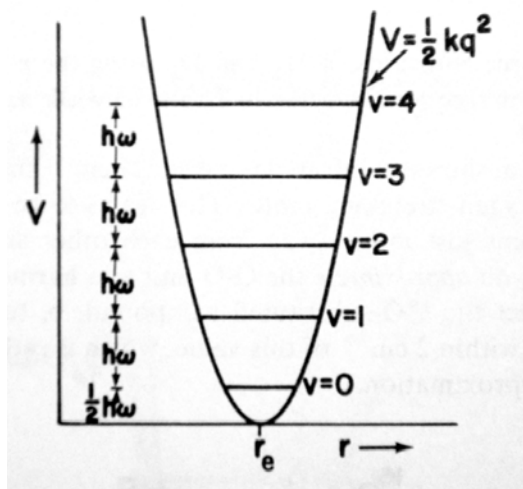


Figure 2.6 Potential well for the harmonic oscillator.²³⁰

For most molecules, the only transition observed is the fundamental transition, $v = 0 \rightarrow v = 1$, as usually only the zero point energy level ($E_v = \frac{1}{2} h\omega$) is occupied at room temperature. For example, the fundamental transitions for HBr and CO are 2559.2 cm^{-1} and 2143.3 cm^{-1} , respectively.²³⁰ Subsequent transitions, $v = 0 \rightarrow v = n$, are called overtones. Though already noted implicitly through the above equations, it should be mentioned that frequency required to reach the first and subsequent transitions is proportional to the strength of the bond, especially when comparing like compounds. It would follow then that the observed frequency for stretching along the principal bond in an alkene ($\text{C}=\text{C}$) is lower than that of an alkyne ($\text{C}\equiv\text{C}$), as is the case.

2.3.3.4 Modes of Vibration for Polyatomic Molecules

In polyatomic molecules, vibrations occur in sets of vibrations called *modes of vibration* rather than strictly for individual bonds. Based on degrees of freedom, polyatomic molecules, in general, have $3N-6$ normal modes of vibration and $3N-5$ if they are linear, where N is the number of atoms. These *normal modes of vibration* are the basis set for all other vibrations and form an irreducible representation of the molecule's point group (i.e. they are intimately tied with the molecule's symmetry elements). By knowing the point group and respective symmetry elements, these modes can be derived.

Combinations of symmetry elements will give rise to symmetrical and asymmetric modes. Recall that it was said above that a change in the dipole moment with vibration is required for IR activity. If there is no mode that exists that a) is an oscillating dipole and b) vibrates at the frequency of the incident light, the photon cannot be absorbed. For molecules with no permanent dipole, such as CO_2 , asymmetrical modes of vibration that do not have an inversion center form temporary dipoles making them IR active (ν_3 and ν_2 in Figure 2.7). Modes which fail to create a dipole are inactive (ν_1 in Figure 2.7).

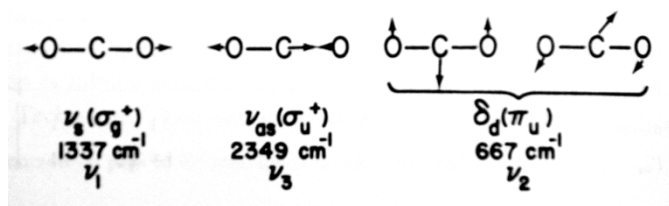


Figure 2.7 Normal modes of vibration for carbon dioxide.²³⁰

2.3.3.5 Spectral Analysis

Though it can be extremely helpful for a detailed study of a molecule's IR spectra, point group analysis can be very complex for large molecules. It is usually sufficient to look at "types" of vibrations related to a chemical functional group. It is prudent, however, to keep in mind those modes which may be IR inactive and probe them, if necessary, with Raman spectroscopy, a complementary technique that uses polarizability as its basis rather than the dipole moment. Figure 2.8 shows the possible vibration types for the methylene group: symmetric & asymmetric stretching, bending, wagging and twisting. These are fairly universal types and occur in many functional groups. Vibrations which do not directly stretch the bond, such as bending and rocking, typically occur at lower frequencies (wavenumbers). Numerous tabulated frequency ranges exist for generalized functional groups, some of which specify the types of vibration (Figure 2.9). Such tools combined with a general understanding of the discussion described above and literature reports aid in spectral analysis; this approach is used here.

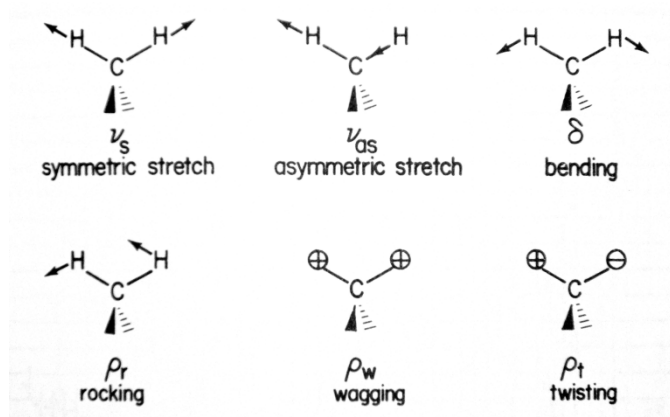


Figure 2.8 Types of vibration for a methylene group.²³⁰

Bond	Type of Compound	Frequency (cm^{-1})	Intensity
C-H	alkane	2800-3000	strong
=C-H	alkene or arene	3000-3100	medium
\equiv C-H	alkyne	3300	strong
C=C	alkene	1620-1680	variable
C \equiv C	alkyne	2100-2260	variable
C \equiv N	nitrile	2200-2300	variable
C=O	ketones, aldehydes acids, esters	1700-1750	strong
O-H	alcohols	3590-3650	variable, sharp
	H-bonded alcohols	3200-3400	strong, broad
	H-bonded acids	2500-3000	variable, broad
N-H	amines	3300-3500	medium

Figure 2.9 Tabulated IR absorption band ranges by functional group.²³⁰

2.3.4 X-ray Photoelectron Spectroscopy (XPS)

X-ray photoelectron spectroscopy is an electronic spectroscopy technique for determining surface elemental and chemical compositions of solids and is thus a very useful method for observing the external compositions of the polypeptide—OMS composites described herein.

2.3.4.1 Instrument Configuration

In XPS, monochromatic X-ray radiation that is emitted from a source hits the sample (usually a solid) causing core electrons to be ejected. A detector measures the kinetic energies of these electrons that can subsequently be related to the binding energy of core electrons as will be discussed below. Like X-ray diffraction, X-rays are generated by the bombardment of a metal with high energy electrons. For XPS, these

metals are generally either magnesium or aluminum as their $K\alpha$ radiation is sufficient to eject the core electrons of most atoms. The photon energies of magnesium and aluminum $K\alpha$ radiation 1253.6 eV ($\lambda = 9.89 \text{ \AA}$) and 1486.6 eV ($\lambda = 8.3386 \text{ \AA}$), respectively. It is essential that monochromatic radiation is used to prevent undesirable satellite peaks in the spectrum. A general schematic of the XPS instrumentation is shown in Figure 2.10. Unlike XRD, ultra high vacuum conditions (UHV) are required in order to avoid a) peaks resulting from the gas phase and adsorbed molecules and b) inelastic collisions of electrons causing the loss of their characteristic kinetic energy.

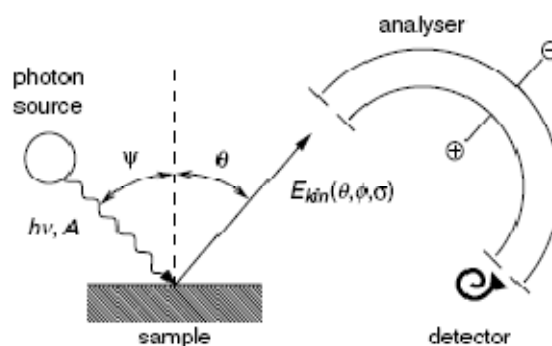


Figure 2.10 Simplified schematic of photoemission spectroscopy.²³¹

2.3.4.2 Basic Theory

The basis for XPS is the *photoelectric effect*, first observed by Heinrich Hertz and later explained by Einstein (1921 Nobel Prize in Physics). The photoelectric effect occurs when a photon of sufficient energy interacts with an electron bound to an atom of lower energy and results in its ejection; such an electron is termed a *photoelectron*.

Einstein first formulated the relationship between the frequency of light and kinetic energy of the emitted photoelectrons in 1905. This relationship can be represented as

$$E_k = h\nu - E_b \quad (2.10)$$

where

h = Planck's constant

ν = the frequency of the light source

E_k = the kinetic energy of the emitted photoelectron

E_b = the binding energy or work function, φ

The *binding energy*, here, is defined as the minimum energy required to displace an electron from an atomic orbital to the vacuum level (i.e. beyond interactions with the nucleus or solid surface). Thus, in an ideal scenario, the energy of the photon, $h\nu$, not used in the initial electron displacement is converted to kinetic energy. The detector records the intensity (usually, counts per second, CPS) at each kinetic energy. As both the initial light frequency and kinetic energies are known, a plot can be constructed relating the associated intensities and binding energies. A general schematic of the photoemission process for XPS is shown in Figure 2.11.

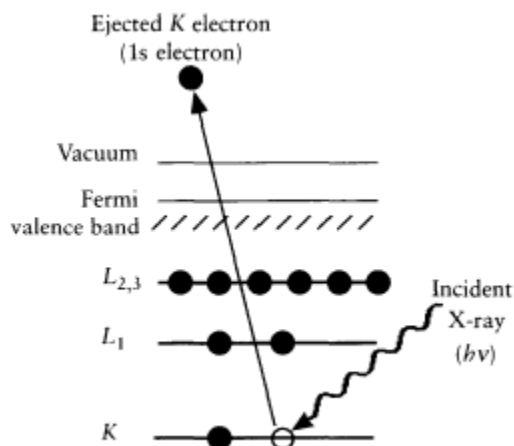


Figure 2.11 Schematic of the photoemission process for XPS. K, L₁ and L_{2,3} are X-ray notation for 1s, 2s and 2p orbitals, respectively.²³²

A key consequence of equation 2.10 is that only electrons with binding energies lower than the incident photon energy will be observed in the spectrum. Valence electrons may be ejected at frequencies of UV light while core electrons closer to the nucleus require much higher frequencies in the X-ray region. This broad range of frequencies results in two principal types of photoemission spectroscopy: ultraviolet photoemission spectroscopy (UPS) and X-ray photoelectron spectroscopy (XPS). As UPS deals with valence electrons, which are involved in molecular bonding, it provides molecular information rather than strictly elemental. XPS on the other hand deals with core electron emissions which are elemental in character as they are not involved in bonding.

As core electrons interact closely with the nucleus, they ‘feel’ the difference in nuclear charge that distinguishes atoms and consequently give rise to distinct peaks

when ejected. Subtle differences in these peaks due to the bonding environment are also present. Koopman's theorem states that the observed binding energy in photoemission is equal to the orbital energy calculated from the Schrödinger equation. This, however, is only an approximation as it does not account for energy differences in initial and post-ejection states due to relaxation effects. Similarly, Koopman's theorem fails in its prediction that electrons in the same orbital with different spins have the same binding energy. The spin of the electron (m_s), however, adds ($+1/2$) or subtracts ($-1/2$) to the angular momentum of the orbital (m_l) leading to splitting. Figure 2.12 shows an example of the splitting of the 3d and 3p orbital electron peaks in the spectrum of Sn.

Another interesting aspect of XPS (and photoelectron spectroscopy in general) is its surface selectivity for solids. Though X-rays easily pass through most solid materials, ejected electrons undergo inelastic scattering upon collision with other atoms, especially at high energies. As a result, the number of observed electrons exponentially decays with surface depth and is Z-dependent. In most cases, ~10nm is a reasonable estimate of the observable depth. In addition to the sample's properties, the observable depth is a function of the X-ray source (frequency) and the incident angle. Non-destructive depth profiling is thus possible by performing angle-resolved measurements or using multiple source frequencies (e.g. dual anode or synchrotron radiation).

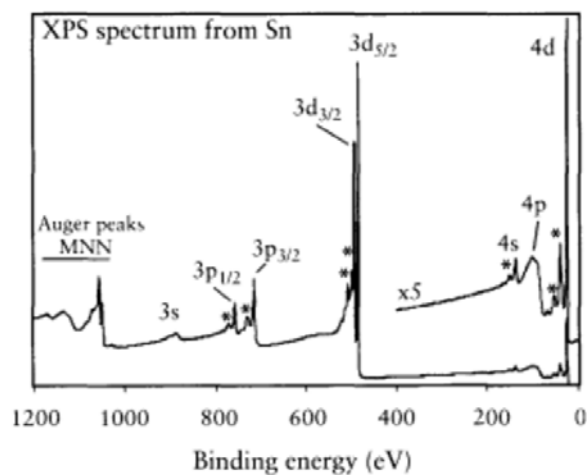


Figure 2.12 XPS spectrum of Sn.²³²

2.3.4.3 *Spectral Interpretation*

Tabulated binding energies for almost every element, including various bonding environments, are readily available from the National Institute of Standards and Technology on its website (<http://srdata.nist.gov/xps>). There are similarly numerous other binding energy databases and books available. Though this is true, there are some fairly obvious trends in the binding energies that are worth noting. One of these is that for a given orbital, say 1s, as the atomic number increases so does the binding energy of the emitted electron. This trend holds for core electrons (but not valence shell electrons) because the attraction force from the nucleus becomes stronger with an increase in the number of protons. More obvious is the fact that higher level orbitals yield electrons with lower binding energies (See Figure 2.12 as an example).

In addition to photoelectron emissions, there is another related phenomenon which can sometimes complicate spectral analysis: the presence of Auger peaks.

Though in Auger spectroscopy an electron beam is used as the source, Auger electrons can be ejected as a result of photoemission in XPS. After a core electron is ejected an outer orbital electron must drop in order to take its place which can result in either a photon being emitted (X-ray fluorescence) or another outer orbital electron. Such electrons have fixed kinetic energies and are observed along with photoelectrons. As the kinetic energy is the characteristic feature of Auger electrons rather than the binding energy, by changing the source (if possible) Auger peaks will shift proportionally enabling proper spectral assignment.

A number of satellite features can also occur. These features are due to 'shake up' and 'shake off' relaxations and surface plasmons. The first two of these are due to two types of relaxations which 'push' the ejected electron away adding to its kinetic energy. These types are rare in occurrence and do not show up in any spectra described here. Surface plasmons result from electrical fluctuations at the surface of conductive metal samples and appear as oscillations at higher binding energies to the source element. These occur here only in the work performed on silicon wafers for the Si 2s and Si 2p peaks.

2.3.4.4 *Quantitative Analysis*

Peaks in XPS can be analyzed quantitatively as the relative sensitivities to photoemission for most elements and orbitals have been experimentally determined. These relative sensitivity factors are normalized to the F 1s peak which has a sensitivity of unity. By integrating the peak areas (A_j) and dividing by the sensitivity factors (F_j),

atomic compositions (x_j) can be calculated for the analyzed layer as shown below in equation 2.11.

$$x_i = \frac{A_i/F_i}{\sum_j A_j/F_j} \quad (2.11)$$

CHAPTER III

INITIAL WORK

3.1 Introduction

As mentioned in the introduction, there has been significant interest in the synthesis and investigation of polypeptide brushes — typically poly-(L-glutamates) — on metal oxide and gold surfaces.^{194-196,198,200,206} The motivation behind such studies are that polypeptide brushes should serve as model systems for studying how binding more complex macromolecules to surfaces might affect such physical properties as the effect of various external stimuli on their folding/conformation and preferred orientation. Similarly, planar surfaces facilitate characterization of the polymer layer by techniques like XPS, attenuated total reflectance FTIR (ATR-FTIR, a surface sensitive IR technique), and atomic force microscopy (AFM). Though some groups have used solution methods to graft the polypeptide layer, the most popular technique has been vapor deposition.

Initially, the principal theme of this dissertation was synthesizing polypeptides brushes on silicon wafers through solution chemistry and studying their properties for the reasons described above. We were particularly interested in amino acids that had not received much attention, most notably L-lysine. Though these attempts proved rather unsuccessful, the results are worth noting, especially in regard to the eventual progression toward polypeptide-OMS hybrids.

3.2 Experimental

These samples were prepared according to the procedure outlined in detail in Chapter II (Sublevel 2.2.4). Briefly, silicon wafers were cleaned using a piranha solution for two hours, rinsed in copious amounts of water followed by acetone, and then amine functionalized in dry toluene (400 μ L silane in 15mL toluene) with distilled 3-aminopropyltrimethoxysilane (APTMS). 10ml of a 0.1M solution of purified NCA in dry THF was added to the flask containing the dried amine-functionalized wafer. The wafers were reacted at 40°C under static conditions for 24 hours. Schlenk techniques were employed in each step of the synthesis to maintain a dry atmosphere. Using this approach, we have attempted grafting four different polypeptides from amine-functionalized silicon: caboxybenzyl-L-lysine; benxyl-L-glutamate; L-alanine; and glycine. Similar procedures were used for the colloidal particle and ordered mesoporous silica grafting and are likewise found in Sublevel 2.2.4.

3.3 Results

3.3.1 Silicon Wafers

3.3.1.1 Z-L-Lysine

Our primary focus was on poly-L-lysine and its derivatives, particularly the protected Z-lysine. XPS analysis on the poly-Z-L-lysine grafted samples showed almost no increase in organic content (Figure 3.1). However, one can notice a small amount of peak splitting in the C 1s scan indicative of a carbon with a high oxidative state that is

not apparent in the APTMS C 1s peak. This result lends credence to the fact that there is a small amount of polymerization occurring.

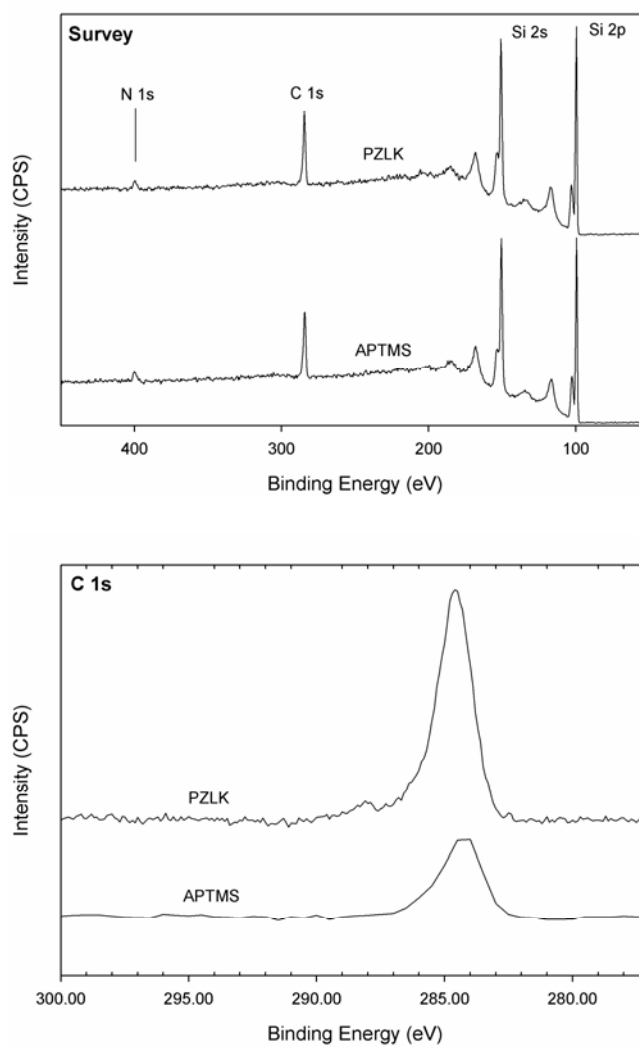


Figure 3.1 Survey (top) and C 1s (bottom) XPS scans of PZLK and APTMS grafted from silicon.

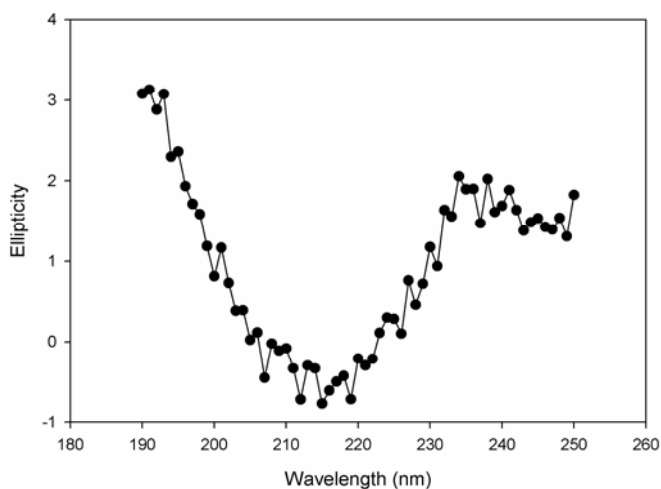


Figure 3.2 CD spectra of PZLK grafted from silicon.

Circular Dichroism was also performed which shows a broad peak between 210nm and 220nm. From Fasman's work on CD spectra of polypeptides,^{233,234} it appears that there is a predominant β -sheet conformation present; the broadening provides evidence for the existence of a small amount of α -helices as well (Figure 3.2). The low intensity of the signal, however, makes definitive conclusions about the conformation difficult. IR was also performed on these samples using an Attenuated Total Reflectance (ATR) attachment to look specifically at surfaces. Performing IR on these samples, as in the CD, proved extremely challenging, especially because of the extreme sensitivity to humidity changes and the long scan times required to obtain an acceptable signal to noise ratio at such low loadings.

3.3.1.2 *Other Amino Acids*

The three other amino acids used were glycine, L-alanine and benzyl-L-glutamate. These samples yielded similar results: a lack of significant increase in organic content by XPS and a broad peak between 220nm by CD. Similar difficulties were encountered when using IR.

3.3.1.3 *Fmoc-spacing of Amine Initiators*

To lessen steric crowding at the surface in an effort to enhance the polymerization, APTMS was protected with Fmoc prior to surface attachment²²⁵ and deprotected prior to NCA addition (Scheme 3.1). XPS data indicates increased polypeptide attachment; the C 1s and N 1s peak areas increase relative to that of silicon. Another notable feature in the XPS is the clear appearance, disappearance and reappearance of the splitting in the C 1s high resolution scan. This supports the attachment of the Fmoc-APTMS (Fmoc carbamate), the deprotection of the amine (no carbamate) and at least some polymer formation (Z carbamate). The splitting also appears more apparent than in the non-spaced sample. We are, however, still unable to observe the appearance of the amide I and benzyl carbamate peaks in the IR. The CD spectrum also looks nearly the same as those for the samples amine functionalized using conventional grafting. Thus, despite these increases in the relative XPS peak areas, these results do not seem to compare well with others reported in the literature.

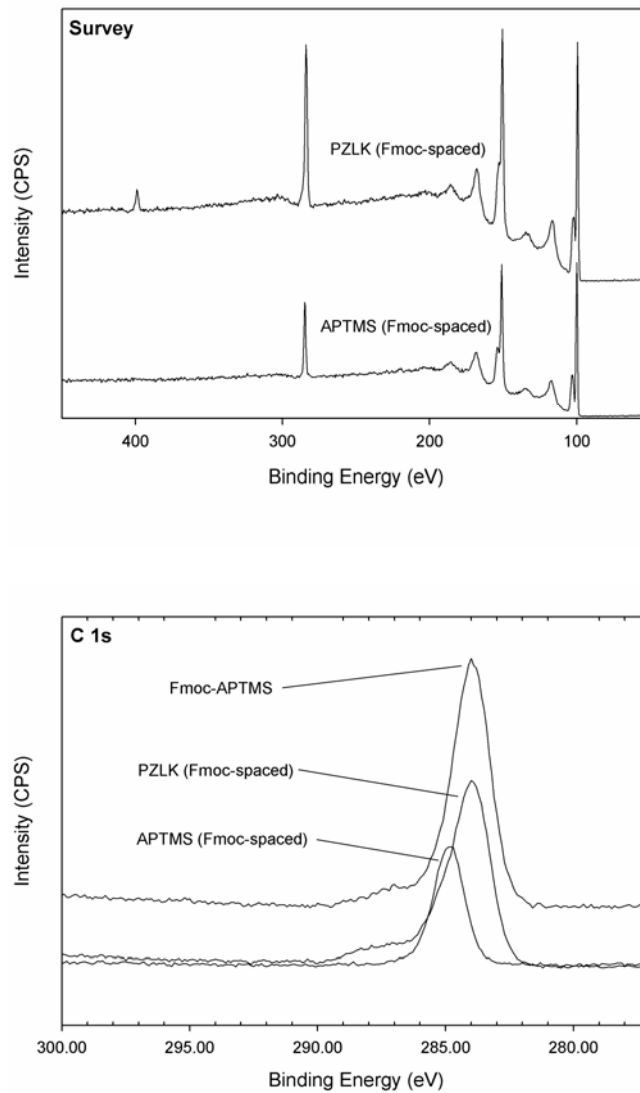
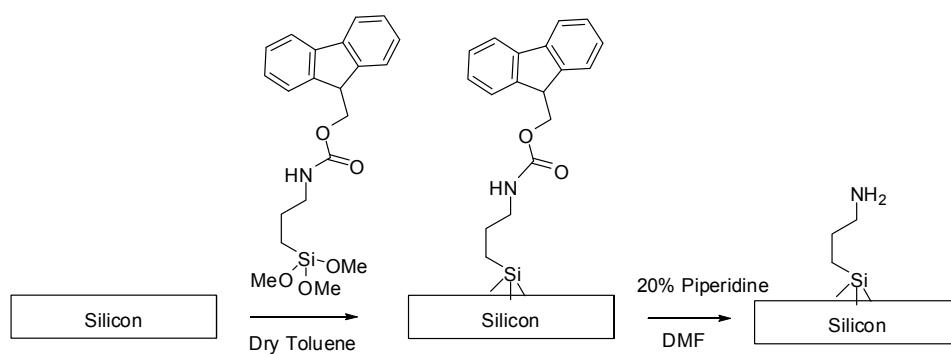


Figure 3.3 Survey (left) and C 1s (right) XPS scans of Fmoc-spaced PZLK and APTMS grafted from silicon. The C 1s scan also shows the Fmoc-APTMS grafted surface.



Scheme 3.1 Synthesis schematic of Fmoc-spaced surfaces.

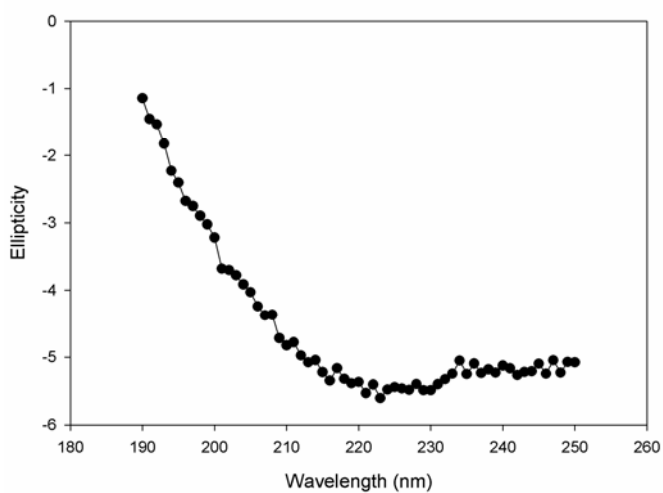


Figure 3.4 CD spectra of Fmoc-spaced PZLK on silicon.

3.3.2 Colloidal Silica

In order to obtain a preliminary understanding of another system, a polymerization of Z-Lysine-NCA were performed on amine-functionalized colloidal silica spheres in a similar manner to the studies of Fong & Russo.^{192,193} The silica spheres were synthesized according to the Stober Method, amine-functionalized using freshly distilled 3-aminopropyltrimethoxysilane (APTMS) in anhydrous toluene, and then poly-Z-L-lysine was grafted from the surface by reacting the functionalized particles with approximately 0.05M Z-Lysine NCA in rigorously dried THF for 24 hours. The resulting particles were characterized using IR, XPS, CD and Dynamic Light Scatter (DLS).

The transmission mode FT-IR spectrum shows the formation of the amide I and amide II peaks as well as the benzyl carbamate aromatic stretch in the polymerized sample, confirming successful polymerization. XPS analyses agree with the IR data showing a clear increase in the C 1s and N 1s peaks in the polymerized sample relative to the Si 2p and O 1s peaks when compared to the amine-functionalized sample and bare particles. CD performed on particles suspended in chloroform yielded a very broad peak between 230nm and 210nm indicative of an α -helix/ β -sheet mix. It is also worth noting that the intensity of the signal for the particles is much higher than for the planar films due to the increased surface area and possible increase in functionalization. The initial bare particles were approximately 109nm in diameter by DLS and monodisperse. DLS shows that the amine-functionalized particles are 505nm in diameter and the

polymerized particles are 925nm. These large increases, especially for the amine-functionalized samples indicate that aggregation is probably taking place.

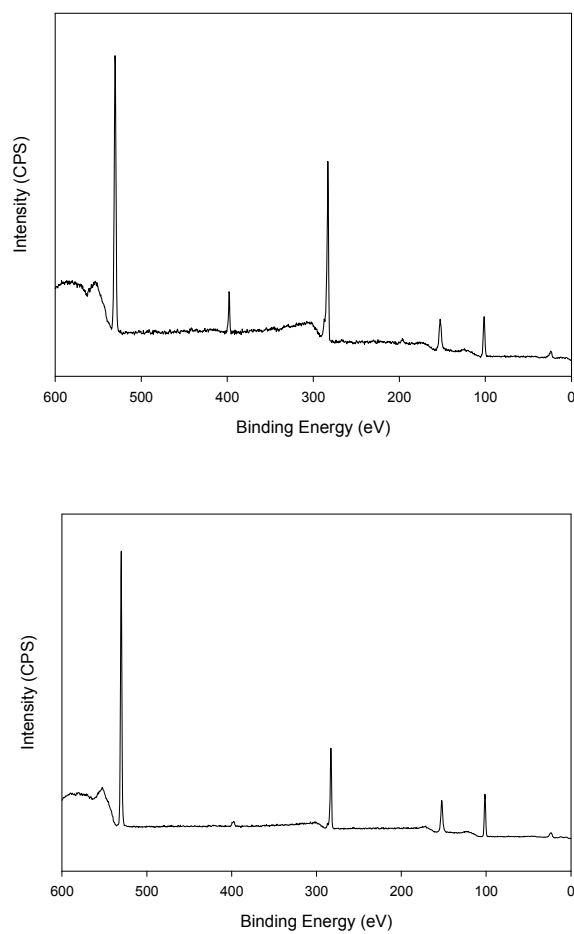


Figure 3.5 XPS survey scans of APTMS (bottom) and PZLK (top) on colloidal silica.

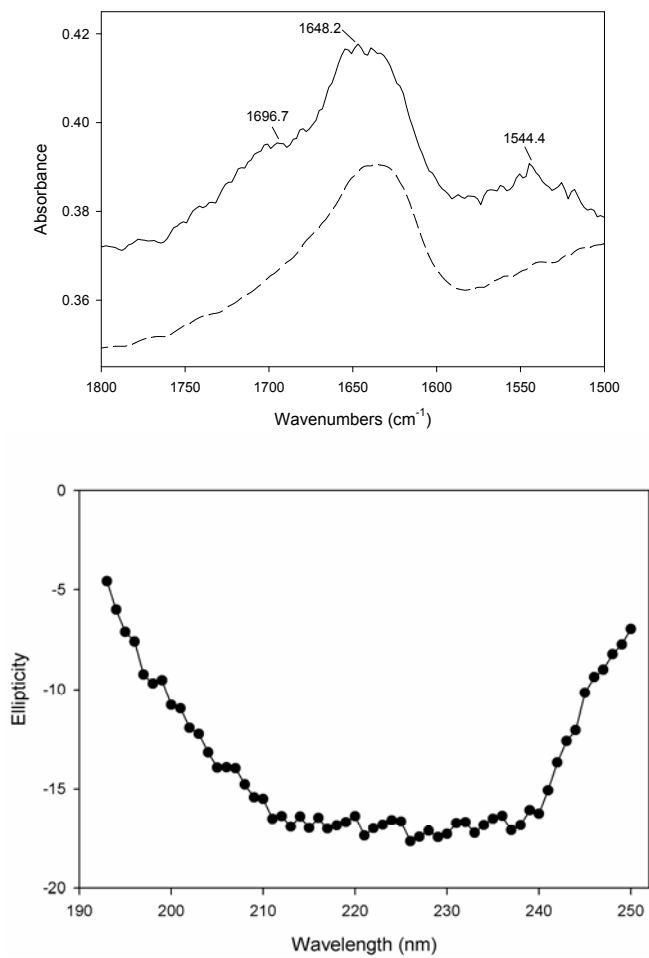


Figure 3.6 FT-IR (top) and CD (bottom) of the PZLK grafted from colloidal silica. APTMS functionalized particles (- - -) are also shown in the FT-IR for comparison.

3.3.3 Polymerizations on Ordered Mesoporous Silica (OMS)

In addition to the work on the silicon wafers and colloidal particles, preliminary studies were performed on the ability to graft polypeptides from amine initiators within the pore networks of ordered mesoporous silicas. In these preliminary studies only MCM-41 was used. These were synthesized in the same manner as the materials above where MCM-41 was first synthesized, amine functionalized, and polymerized in consecutive steps. Here, 0.5 grams of 0.5mmol APTMS/gram MCM-41 were used. Three different NCAs were tested: Z-L-lysine, glycine and alanine. The synthesized materials were analyzed primarily by IR. Nitrogen Adsorption was also used on the poly-Z-L-lysine sample. IR shows a large amount of polymer in all the samples that were prepared as seen by the amide peaks in Figure 3.7. N₂ adsorption on the poly-Z-L-lysine sample showed no porosity after functionalization.

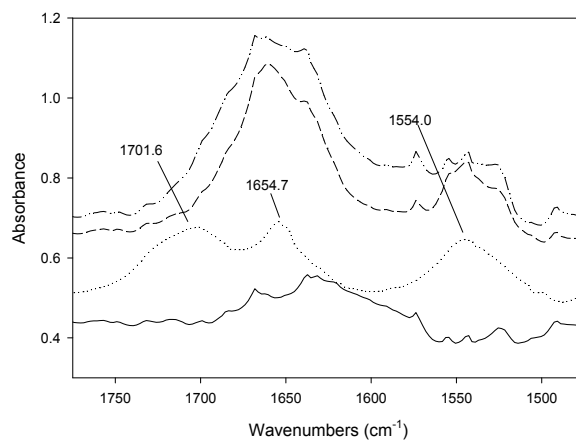


Figure 3.7 FT-IR of various polypeptides grafted to MCM-41: Polyglycine, Poly-L-alanine, PZLK, APTMS-MCM-41(from top to bottom).

3.4 Conclusions

From the above data, it appears that polymerizations on planar surfaces are not effective and only oligomers are formed as evidenced by the XPS and CD spectra shown above. The XPS shows negligible increases in organic content following polymerization and the CD shows prevalence of the β -sheet conformation indicative of oligomers 10 units or less in length in non-grafted peptides.²³⁵⁻²³⁸ It is possible, however, that some α -helices are present from the broadening in the CD peak. The rough surfaces in AFM images (not shown) also indicate that the polymerization is anything but uniform. Regardless, it is apparent that “living” polymerization has not taken place in these samples and only few, if any, form polymer chains. This result could be due to a number of reasons such as steric crowding at the surface, a decrease in THF wettability of the surface after oligomers are formed, or termination steps resulting in “dead” polymers unable to propagate. Work by Chang and Frank support such conclusions as they similarly found that solution-based methods unsuccessfully grafted significant amounts of polypeptide to planar silicon.¹⁹⁰

Preliminary results on grafting polypeptides to both colloidal silica and OMS, however, proved successful. Given the promising preliminary results on OMS, and the tunable properties of polypeptides and OMS noted in the introduction, peptides grafted from OMS could lead to some interesting materials and applications. As a result of this potential, the absence of NCA polymerizations on OMS in the literature, and our extensive previous work on OMS, the shift to polypeptide-OMS hybrids is a logical progression from the work on silicon wafers and colloidal silica.

CHAPTER IV

POLYPEPTIDE— OMS HYBRID MATERIALS*

4.1 Introduction

In this chapter, we describe our efforts to synthesize well-defined polypeptide grafts in ordered mesoporous silica. More specifically, we investigate the grafting of poly-Z-L-lysine (PZK) and poly-L-alanine (PA) in the OMS materials MCM-41, SBA-15 and KIT-6. The effects of pore size, pore topology, surface initiator loading and monomer identity are discussed based on the characterization of these materials by a battery of methods, including porosimetry, thermogravimetric analysis, infrared spectroscopy, X-ray photoelectron spectroscopy, solid state NMR and mass spectrometry.

4.2 Experimental

MCM-41, SBA-15, and KIT-6 were synthesized and calcined as described above. Amine-functionalized samples of each OMS were prepared using traditional toluene-based post-synthetic grafting. Three different loadings were used: 0.25, 0.5, and 0.75 mmol 3-aminopropyltrimethoxysilane (APTMS) per gram SiO₂. 0.5g of each were vacuum-dried and reacted with 50ml of 0.1M *N*-carboxyanhydride in THF for 24 hours (10mmol NCA/g NH₂-SiO₂, 20:1 monomer/initiator ratio). Z-L-lysine and L-alanine

* Reproduced with permission from Lunn, J.D.; Shantz, D.F. *Chemistry of Materials* **2009**, *21*, 3638-3648. Copyright 2009 American Chemical Society.

were used as monomers. Detailed synthesis procedures for these samples can be found in Chapter II (Sublevel 2.2.1).

4.3 Results

4.3.1 Parent Materials

The parent materials were characterized by porosimetry and PXRD to confirm synthesis of the desired mesophases and so we could accurately determine the effect of peptide grafting. Figure 4.1 shows representative PXRD results for the parent OMS materials and Figure 4.2 shows their nitrogen adsorption isotherms. For MCM-41, the $\langle 100 \rangle$, $\langle 110 \rangle$ and $\langle 210 \rangle$ reflections can be clearly seen in the PXRD pattern; though much more subtle, the $\langle 210 \rangle$ is also present at $6^\circ 2\theta$. The characteristic $\langle 100 \rangle$, $\langle 110 \rangle$ and $\langle 200 \rangle$ reflections are also observed for SBA-15 confirming the hexagonal pore arrangement. In the KIT-6 cubic pattern, the $\langle 211 \rangle$ peak at approximately $0.9^\circ 2\theta$ dwarfs the neighboring $\langle 220 \rangle$ reflection. Two broad peaks are also present between $1.4^\circ 2\theta$ and $2.0^\circ 2\theta$ which encompass the $\langle 321 \rangle$, $\langle 400 \rangle$, $\langle 420 \rangle$, $\langle 322 \rangle$, $\langle 422 \rangle$ and $\langle 431 \rangle$ reflections. The adsorption isotherms of each substrate are also indicative of successful mesophase synthesis. The tabulated analysis of the adsorption isotherms is shown below along with the composite adsorption data.

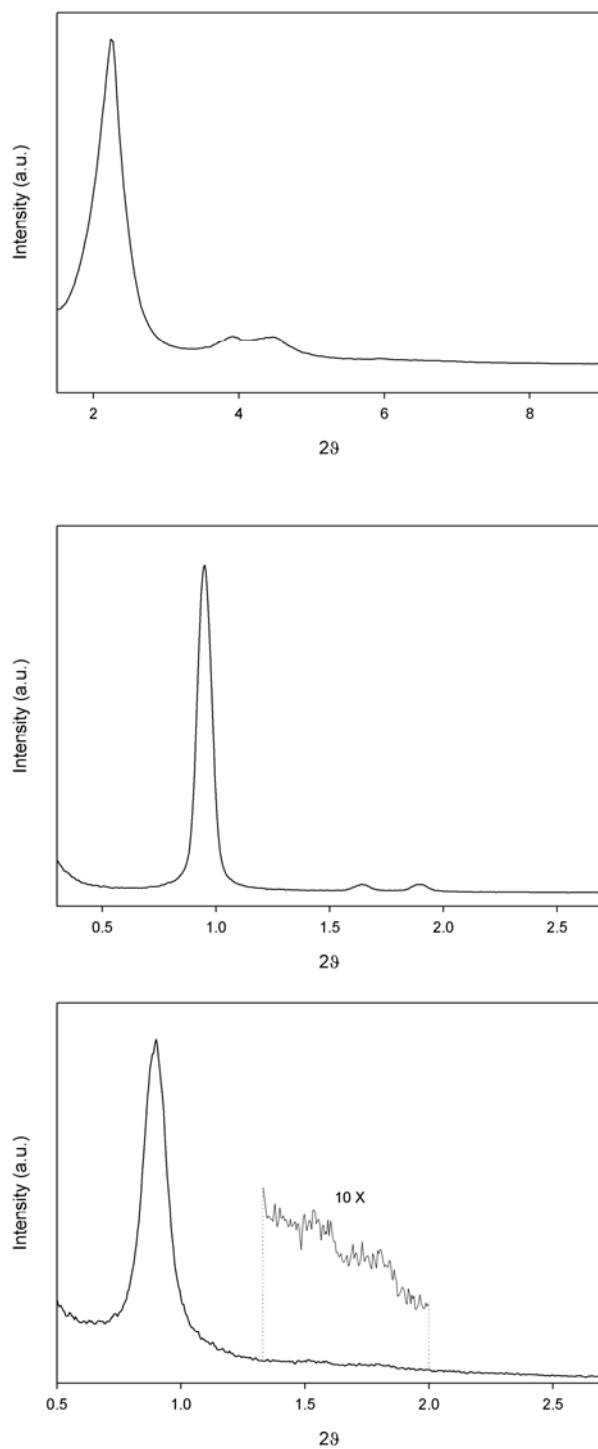


Figure 4.1 PXRD of MCM-41 (top), SBA-15 (middle), and KIT-6 (bottom).

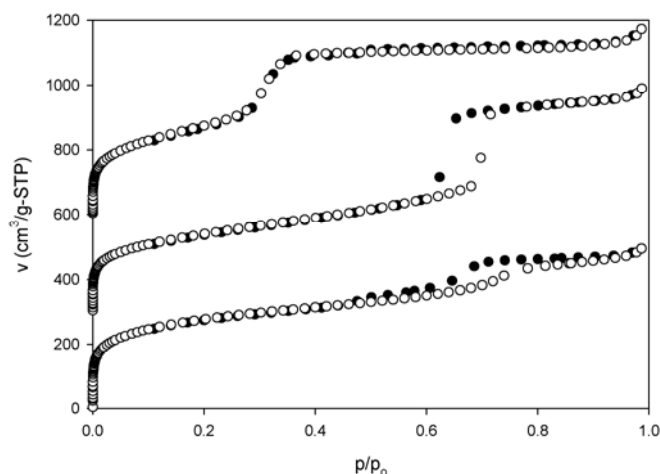


Figure 4.2 Adsorption isotherms of MCM-41 (top), SBA-15 (middle), and KIT-6 (bottom). The adsorption branch is represented by open circles; desorption by closed circles. The offset between isotherms is $300\text{cm}^3/\text{g-STP}$.

4.3.2 Poly-Z-L-lysine (PZK)—OMS Composites

4.3.2.1 N_2 Adsorption

Nitrogen adsorption was used to quantify the changes in porosity in the OMS resulting from peptide grafting. The α_s and BJH methods were used to calculate the surface area, pore volume and pore size distribution. These results are summarized in Table 4.1. In both the MCM-41 and SBA-15 composites of PZK the pore volumes and surface areas drop dramatically after polymerization. The low initiator loading samples maintain some porosity, while the two higher loadings exhibit little or none. The KIT-6 composites behave quite differently, despite the similar pore size and surface area of the parent material as compared to SBA-15; the pore volume, surface area, and pore

diameter decrease steadily with increasing initiator loading. Some porosity and surface area is maintained even at the highest initiator loading. The explanation for these results is likely related to the difference in pore topology/surface characteristics of KIT-6.

Table 4.1 Tabulated nitrogen adsorption results for the poly-Z-L-lysine—OMS composites.

Sample ID	$S(\alpha_s)$ [m ² /g]	V_{meso} [cm ³ /g]	$d_p(\text{BJH})$ [nm]
MCM-41	1083	0.72	2.8
PZK-0.25APTMS-MCM41	367	0.17	2.3
PZK-0.50APTMS-MCM41	70	~0	-
PZK-0.75APTMS-MCM41	38	~0	-
SBA-15	918	0.93	7.0
PZK-0.25APTMS-SBA15	102	0.06	6.3
PZK-0.50APTMS-SBA15	22	~0	-
PZK-0.75APTMS-SBA15	10	~0	-
KIT-6	1065	0.62	7.6
PZK-0.25APTMS-KIT6	591	0.25	6.6
PZK-0.50APTMS-KIT6	309	0.11	6.8
PZK-0.75APTMS-KIT6	105	0.07	5.9

4.3.2.2 *Thermogravimetric Analysis*

TGA was performed on the composite materials to determine the degree of organic functionalization. The MCM-41 based composites had weight losses of 41.8wt%, 42.3wt% and 31.2wt% for the 0.75, 0.50 and 0.25mmol APTMS/g MCM-41 peptide composites, respectively. The SBA-15 composites showed slightly higher

organic contents: 49.3wt%, 47.3wt% and 30.3wt% for the 0.75, 0.50 and 0.25mmol APTMS/g SBA-15 peptide composites, respectively. The KIT-6 composites showed a much lower degree of functionalization with 31.6wt%, 16.2wt% and 9.6% for 0.75, 0.50 and 0.25mmol/g initial amine loadings, respectively.

The highest two initial amine loadings for MCM-41 have high and essentially equal organic contents. This result is consistent with the adsorption data that show no porosity in these samples. It also provides substantial evidence that the pores are not merely blocked, but completely filled with organic material. This same conclusion is true for the highest two initial amine loadings for SBA-15, except the organic content is about 15% higher due to the increased pore volume (by 29%). The 0.25mmol APTMS/g SiO₂ composites for MCM-41 and SBA-15 show about a quarter reduction in their organic content compared to the higher initiator loadings. This result is again consistent with the porosimetry results that show larger mesopore volumes in these two samples with respect to the samples with higher initial amine loadings. With regards to the KIT-6 composites, TGA shows that there is much less organic grafted than might be expected based on the other OMS composites. Just as in the other OMS composites, the TGA data matches very nicely with the adsorption isotherms: less organic leads to more porosity. The results for the KIT-6 composites seem to indicate the ability to tune the porosity and organic content by changing the initiator loading.

4.3.2.3 *Elemental Analysis*

Table 4.2 Elemental composition. “TGA” denotes theoretical values calculated from the TGA results; “XPS”, from X-ray photoelectron spectroscopy; and “EA”, from elemental analysis. C/N and C/Si ratios are on a molar and weight basis, respectively.

Sample	C/N _{TGA}	C/N _{XPS}	C/N _{EA}	C/Si _{TGA}	C/Si _{EA}
PZK-0.75APTMS-MCM41	6.61	7.84	5.92	0.98	1.09
PZK-0.50APTMS-MCM41	6.82	6.88	5.91	1.02	1.05
PZK-0.25APTMS-MCM41	6.93	7.31	5.60	0.62	0.66
PZK-0.75APTMS-SBA15	6.70	6.72	6.52	1.33	1.40
PZK-0.50APTMS-SBA15	6.85	6.88	6.60	1.23	1.19
PZK-0.25APTMS-SBA15	6.92	8.09	6.36	0.60	0.67
PZK-0.75APTMS-KIT6	6.40	7.25	5.81	0.63	0.45
PZK-0.50APTMS-KIT6	6.33	7.50	5.30	0.26	0.24
PZK-0.25APTMS-KIT6	6.67	9.29	4.49	0.15	0.15

Elemental analysis was performed to verify our TGA results/calculations, as well as the spectroscopic methods that show peptide is formed in the composite. C/N ratios (on a molar basis) and C/Si (on a weight basis) from our TGA calculations (and XPS for C/N, *vide infra*) are compared with those from elemental analysis (Table 4.2). Complete EA results are available in the Supporting Information. The C/N ratio of a single monomer unit and aminosilane is 7 and 3, respectively. Because the majority of the

organic material is from the polymer, one would expect samples with more polymer to have C/N ratios close to 7 and those with greater influence from the silane to have slightly lower values. Elemental analysis and TGA calculations show this to be in fact, true. XPS similarly shows values very consistent with EA and TGA, though some numbers are slightly askew – probably due to residual carbon on the external surface or carbon tape used in the measurement. The C/Si ratios calculated from TGA match the EA very well.

4.3.2.4 *Infrared Spectroscopy*

Transmission FT-IR was used to verify the presence of the peptide brushes as manifested by the appearance of the amide I and II bands. Figure 4.3 shows the spectra obtained for the three initial amine loadings for the MCM-41 composites. The spectra for the SBA-15 and KIT-6 samples are in the Supporting Information. In all the samples – save the low amine loading composite for KIT-6 – the benzyl carbamate ($\sim 1700\text{ cm}^{-1}$), amide I ($\sim 1655\text{ cm}^{-1}$), amide II ($\sim 1545\text{ cm}^{-1}$, plus $\sim 3080\text{ cm}^{-1}$ overtone) and amide A ($\sim 3300\text{ cm}^{-1}$) bands are clearly present. Additionally, bands resulting from C-H stretching in the lysine side chain and organosilane can be observed between 2800 cm^{-1} and 3000 cm^{-1} . The silanol (Si-OH) and Si-O-Si bands from the parent materials are likewise observed at $\sim 3450\text{ cm}^{-1}$ (broad) and $\sim 1080\text{ cm}^{-1}$, respectively. The amide peaks are more intense relative to those corresponding to the parent material for the composites with higher initial amine loadings, indicating qualitatively higher peptide loadings for higher initial amine loadings, consistent with the TGA and porosimetry results.

Accurate determination of peptide conformation based on the amide I and II bands alone is difficult due to the broadness of the peaks and water adsorption in the same region; more in-depth studies are needed.

Accessibility to the side-chain amine groups is important for many applications and motivated our efforts to successfully remove the Cbz protecting group. Figure 4.4 shows the IR spectra for the deprotected and protected 0.75mmol APTMS/g MCM-41 composite. The absence of the benzyl carbamate peak and retention of the amide I and II peaks evidence effective deprotection of the side chain amines while avoiding amide hydrolysis. TGA on the resulting deprotected composites compares very well with our calculations. For example, the deprotected 0.25mmol APTMS/g MCM-41 composite showed an organic content of 19.8wt% compared to the calculated 18.6wt%.

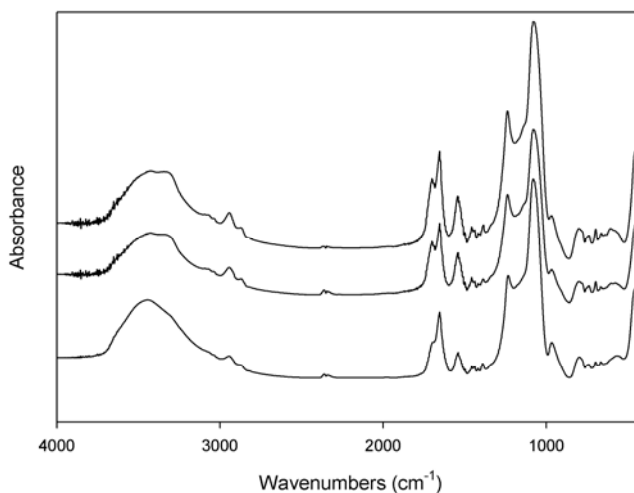


Figure 4.3 IR spectra of the Poly-Z- L-lysine—MCM-41 composites. From top to bottom 0.75, 0.50, and 0.25 mmol APTMS/g SiO₂.

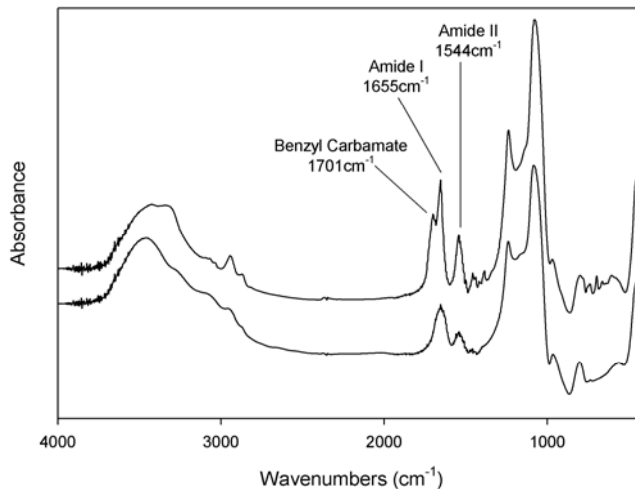


Figure 4.4 IR spectra of the protected (top) and deprotected (\bullet HBr) (bottom) 0.75mmol APTMS/g SiO₂ Poly-Z- L-lysine—MCM-41 composite.

4.3.2.5 $^{13}\text{C}\{^1\text{H}\}$ CP MAS NMR

Solid state NMR spectroscopy provides further evidence for peptide formation within the composite (Figure 4.5). $^{13}\text{C}\{^1\text{H}\}$ CP MAS NMR was performed on the protected and deprotected 0.75mmol APTMS/g MCM-41 Peptide—MCM-41 composite. The characteristic peaks due to the aliphatic lysine side chain carbons (α , β , γ , δ and ϵ) are present in the spectra for both materials between 20ppm and 60ppm.²³⁹ The amide carbon has a resonance of 173-175ppm and is similarly present in both spectra. The peaks between 60ppm and 170ppm are the aromatic carbons, the benzylic carbon and the carbamate carbon from the protecting group;²³⁹ they are significantly diminished after treatment with HBr. Two of the aminosilane carbons are obscured by the resonances for the lysine side chain; however, the α -carbon peak (with reference to the silicon) can be

seen at approximately 7ppm.²⁴⁰ The presence of the amide carbon peak in the protected composite confirms the IR data demonstrating peptides are indeed formed in the composite. Similarly, the fact that this peak is preserved following deprotection provides additional evidence of the peptide structure being retained upon treatment with HBr. Another interesting feature is the lack of any carboxylic acid carbon peak at approximately 180ppm. If peptide was formed in solution and merely adsorbed on the surface it seems likely this peak would be observed; however, it is not.

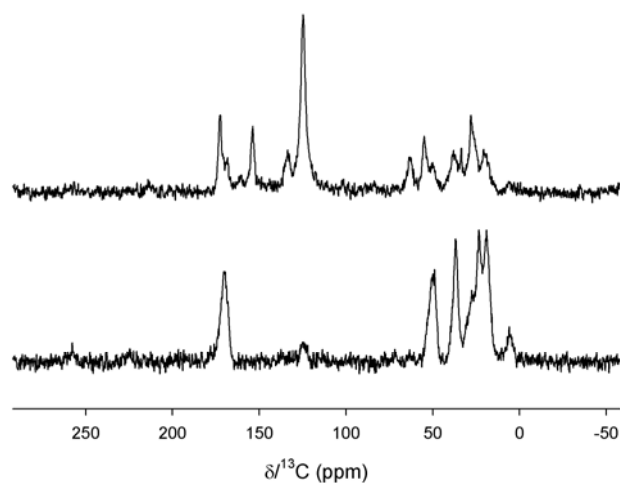


Figure 4.5 $^{13}\text{C}\{^1\text{H}\}$ CP MAS NMR of the side chain protected (top) and deprotected ($\bullet\text{HBr}$) (bottom) 0.75mmol APTMS/g MCM-41 Poly-Z- L-lysine composite.

4.3.2.6 *X-ray Photoelectron Spectroscopy*

XPS was used to investigate the elemental composition of the composites' surfaces. Figure 4.6 shows the XPS spectra for the side-chain protected MCM-41 composites; the spectra for the SBA-15 and KIT-6 are included in the Supporting Information. The XPS results indicate significant amounts of organic on the outer surface as indicated by the large N 1s (405 eV) and C 1s (284 eV) peaks compared to the Si 2p (100 eV). The KIT-6 composites on the other hand appear to show little outer surface functionalization. This result corroborates the above IR, porosimetry, and TGA data above which show little peptide is grafted to the KIT-6 composites, especially at low loadings of amine initiator. Also, just as in the IR, we see evidence for increased organic on the surface with increased amine loadings for three OMS materials.

The C/N ratios vary between 6.7 and 8.1 (Table 4.2); this compares closely to the expected value of 7 (C/N ratio for Lys(Z) monomer unit). As noted above, variance on the upper end can most likely be attributed to residual carbon on the OMS surface prior to functionalization or the carbon tape used in the measurement; variance on the lower end can be attributed to the influence of the aminopropylsilane initiator. The only sample that deviates from the above range is the 0.25mmol APTMS/g KIT-6 peptide composite, which has a C/N of 9.3. As the amount of organic on the surface is small compared to the others, the residual carbon has a much larger impact on the intensity of the C 1s peak. As additional evidence of peptide formation on the external surface, splitting can be seen in high resolution scans of the C 1s peak that occurs in the same manner as in poly-Z- L-lysine (Appendix A).

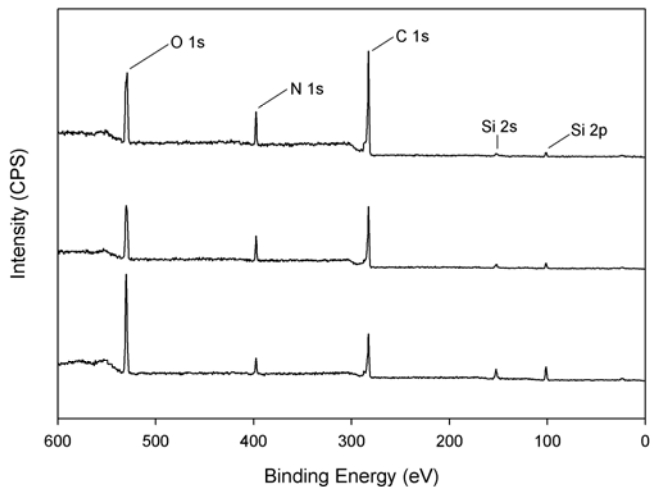


Figure 4.6 XPS of the Poly-Z-L-lysine—MCM-41 composites: 0.75mmol APTMS/g (top); 0.50mmol APTMS/g (middle); and 0.25mmol APTMS/g (bottom).

4.3.2.7 Mass Spectrometry

MALDI-TOF MS has been shown in the literature to be quite useful in determining molecular weight distributions of low molecular weight homopolymers, especially when the distribution is narrow,²⁴¹⁻²⁴⁵ this approach has also been used for polypeptides.¹²³ Wanting to obtain a better understanding of the influence of pore size, topology and initiator loading on the peptide MWs, MALDI-TOF MS was performed on peptide obtained from the three SBA-15 composites and the 0.5mmol APTMS/g OMS initiator loading of the MCM-41 and KIT-6 composites by dissolution of the silica framework. Figures 4.7-4.9 show the MALDI-TOF MS spectra for the three PZK-SBA-15 composites. Observed chemical species include the protected peptide with fluorinated silane and the protected polymer with fluorinated silane that is missing one Z

protecting group. The 0.25mmol APTMS/g SiO₂ SBA-15 composite shows a rather normal distribution of MWs centering on peptide lengths of 4 to 6. The results for the higher initiator loadings in SBA-15 show a less well-defined distribution that is shifted slightly toward lower chain lengths of 3 to 4. The 0.5 mmol APTMS/g SiO₂ loading of the MCM-41 and KIT-6 composites closely resemble these two samples with distributions centered on chain lengths of 3 to 4 (Appendix A). In the SBA-15 composites, the peptide length is limited to 8 monomer units or less. This limit is reasonable considering the pore size of SBA-15 is 8nm, the length of one monomer unit is about 3.5Å when elongated and the rather large side chain of L-Lys(Z).

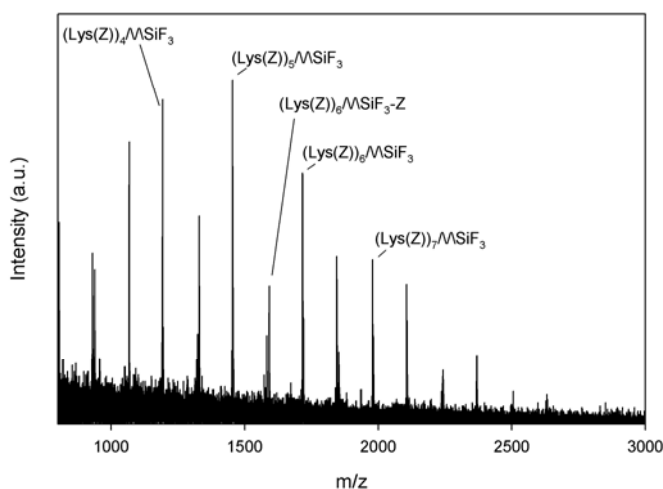


Figure 4.7 MALDI-TOF MS of peptide from the 0.25mmol APTMS/g SBA-15 Poly-Z-L-lysine composite. Note the spacing of peaks is equivalent to the mass difference of one monomer or the loss of a single Cbz protecting group. Only select peaks are labeled.

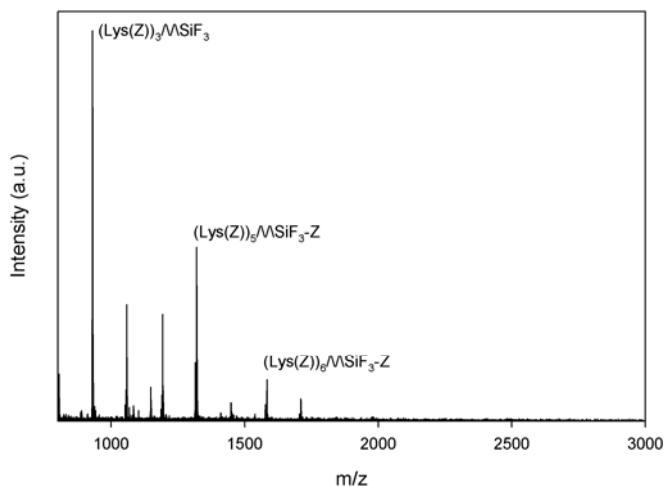


Figure 4.8 MALDI-TOF MS of peptide from the 0.50mmol APTMS/g SBA-15 Poly-Z-L-lysine composite. Note the spacing of peaks is equivalent to the mass difference of one monomer or the loss of a single Cbz protecting group. Only select peaks are labeled.

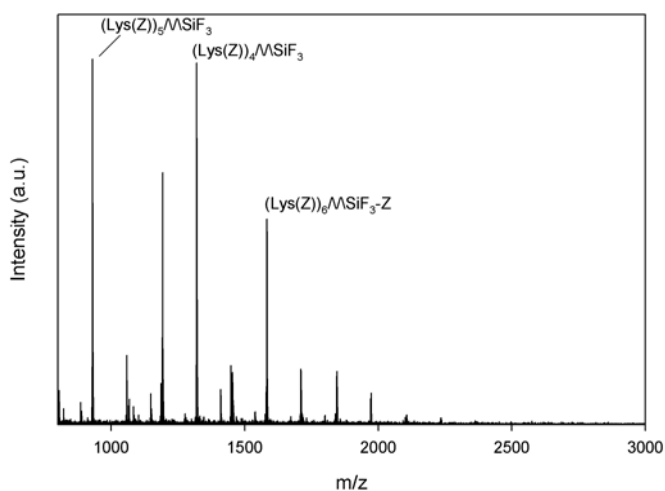


Figure 4.9 MALDI-TOF MS of peptide from the 0.75mmol APTMS/g SBA-15 Poly-Z-L-lysine composite. Note the spacing of peaks is equivalent to the mass difference of one monomer or the loss of a single Cbz protecting group. Only select peaks are labeled.

4.3.2.8 Catalytic Data (Henry Reaction)

To look at the accessibility of the side chain amines in the deprotected L-lysine composites, the nitroaldol (Henry) reaction between *p*-nitrobenzaldehyde and nitromethane was used as a probe. Catalytic testing was performed on the low initiator loading for MCM-41 and SBA-15 and the high initiator loading for all three OMS materials. These results are tabulated in Table 4.3. Conversions match closely with the with the porosimetry data, showing that higher conversions and turnover frequencies (TOF) are obtained for samples with higher porosity. The selectivity between the alcohol (A) and unsaturated product (B) is fairly constant in all samples where conversion was observed.

Table 4.3 Catalytic results for the nitroaldol reaction between *p*-nitrobenzaldehyde and nitromethane.

mmol APTMS /g SiO ₂	MCM-41			SBA-15			KIT-6		
	X (7hr)	A/B	TOF [h ⁻¹]	X (7hr)	A/B	TOF [h ⁻¹]	X (7hr)	A/B	TOF [h ⁻¹]
0.25	40%	1.1	5.7	37%	0.8	5.3	---	---	---
0.50	---	---	---	---	---	---	---	---	---
0.75	2%	0.8	0.3	~ 0	N/A	N/A	16%	1.3	2.3

4.3.3 Poly-*L*-alanine (PA)—OMS Composites

Composites were also synthesized using *L*-alanine NCA to contrast with the much larger *L*-lysine(Z) monomer. All three amine loadings were synthesized on SBA-15, while only the 0.5mmol APTMS/g SiO₂ was synthesized on MCM-41 and KIT-6. The same battery of characterization techniques was employed to analyze these samples.

4.3.3.1 N₂ Adsorption

Nitrogen porosimetry shows a similar trend to the poly-Z-*L*-lysine composites in that there is decreasing porosity with increased initial amine loading (Table 4.4). The lowest loading still maintains about half of its initial porosity, the mid loading with significantly less, and the high loading with essentially no porosity. The pore diameter also incrementally decreases with increasing initiator loading, akin to the KIT-6 composites of PZK. In the MCM-41 and KIT-6 composites, similar pore volumes and surface area decreases to the SBA-15 composites occur, however, BJH analysis indicates the pore diameters are much smaller. This makes sense for MCM-41, as its pore diameter is much smaller prior to any functionalization. The much more dramatic decrease in the KIT-6 pore diameter is probably due to its lower initial pore volume.

Table 4.4 Tabulated nitrogen adsorption results for the poly-L-alanine—OMS composites.

Sample	$S(\alpha_s)$ [m ² /g]	V_{meso} [cm ³ /g]	$d_p(\text{BJH})$ [nm]
MCM-41	1084	0.71	2.8
PA-0.50APTMS-MCM-41	360	0.13	< 1.5
SBA-15	918	0.93	7.0
PA-0.25APTMS-SBA15	662	0.39	5.6
PA-0.50APTMS-SBA15	233	0.10	4.8
PA-0.75APTMS-SBA15	143	0.05	< 1.5
KIT-6	1091	0.59	7.6
PA-0.50APTMS-KIT6	268	0.12	< 1.5

4.3.3.2 Thermogravimetric Analysis

TGA on the three poly-L-alanine composites on SBA-15 showed weight losses of 42.42wt%, 40.19wt% and 41.15wt% for the 0.75, 0.50 and 0.25mmol APTMS/g SBA-15 composites, respectively. For the MCM-41 and KIT-6 composites, similar results were obtained: 40.03wt% and 36.59wt%, respectively. This weight loss corresponds to a complete or near complete polymerization (i.e. 100% monomer conversion). This result is interesting in that porosity changes in the poly-Z-L-lysine composites were associated also with a difference in overall organic content; in contrast, here all three samples have essentially the same organic content by TGA. We speculate that this is a result of increased spacing of more or less equal length polymers inside the pores at low initial amine loadings with polymers of increased length on the external surface. This result indicates that porosity in the poly-L-alanine composites can be controlled purely by the

surface initiator loading. It is also noteworthy that the high organic content and low porosity of the KIT-6 composite contrast significantly with those in PZK KIT-6 composites that showed little peptide functionalization.

4.3.3.3 *Infrared Spectroscopy and X-ray Photoelectron Spectroscopy*

FT-IR spectra as in the poly-Z-L-lysine composites confirm the presence of poly-L-alanine. The amide I and II bands can be seen at about 1660 cm^{-1} and 1545 cm^{-1} , respectively (Figures 4.10 and 4.11). The amide A (3310 cm^{-1}) and C-H stretches ($2800\text{--}3000\text{ cm}^{-1}$) are also clearly observed. It is noteworthy that the intensities of the amide bands (I, II and A) are stronger relative to the silanol and Si-O-Si bands than in the PZK composites. This result is very reasonable when we take into account the high organic loadings (observed by TGA) and the much smaller side chain of alanine (compared to PZK). XPS analysis of the surface likewise shows a very large amount of polymer on the surface, as evidenced by the domination of the spectra by the N1s and C1s peaks; the Si2s and 2p peaks are almost non-existent (Figure 4.12).

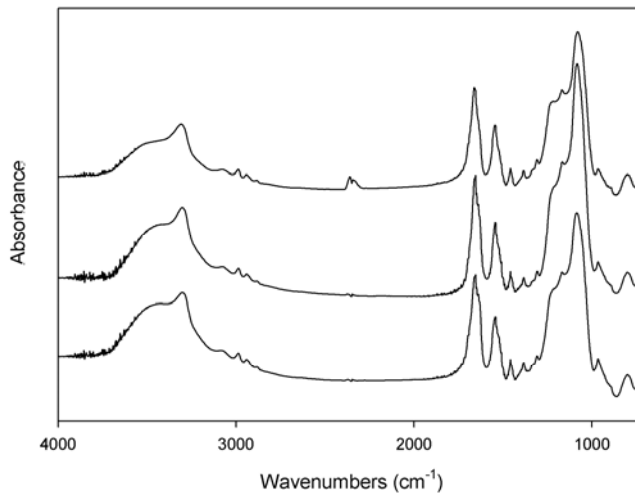


Figure 4.10 IR spectra of the Poly-L-alanine—SBA-15 composites: 0.75mmol APTMS/g (top); 0.50mmol APTMS/g (middle); and 0.25mmol APTMS/g (bottom)

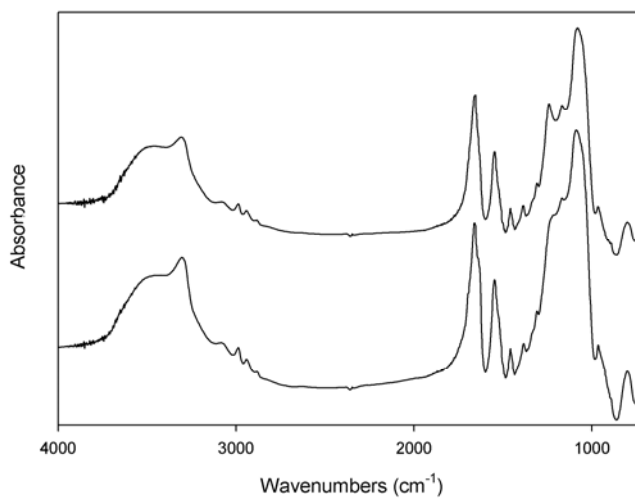


Figure 4.11 IR spectra of the Poly-L-alanine—MCM-41 (top) and KIT-6 (bottom) composites, both containing 0.5mmol ATPMS/g SiO₂.

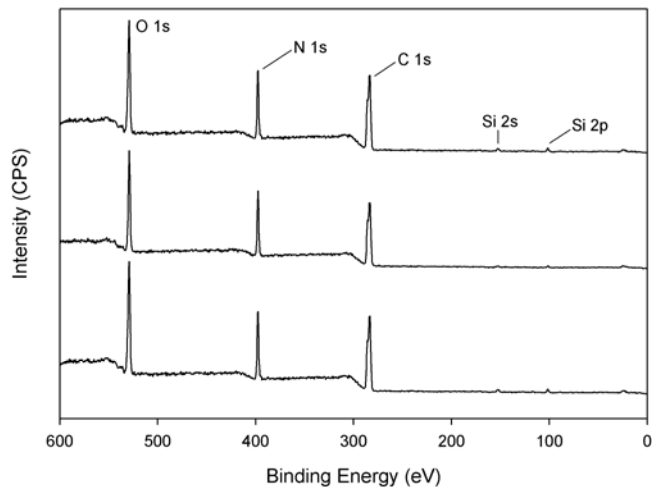


Figure 4.12 XPS of the Poly-L-alanine—SBA-15 composites: 0.75mmol APTMS/g (top); 0.50mmol APTMS/g (middle); and 0.25mmol APTMS/g (bottom).

4.3.3.4 Mass Spectrometry

MALDI-TOF MS was also performed on the poly-L-alanine—OMS composites. Results show polymers of much longer chain lengths than in the PZK composites with an upper bound of about 35 mer units in the SBA-15 composites. Observed chemical species include the peptide with fluorinated silane and the peptide without the silane. Figures 4.13-15 show the MALDI-TOF MS results for the poly-L-alanine—SBA-15 composites. In the low initiator loading in SBA-15 composite, as in the PZK—SBA-15 composite, the MW distribution looks almost Gaussian and is centered on chain lengths of 24 and 25. There is also a large peak corresponding to the 12 monomer unit. At the higher initiator loadings, the MW distribution becomes broader and almost bimodal at the highest loading. This phenomenon makes sense when we take into consideration the

monomer to initiator at the higher loadings is 20 and 13, lower than the average chain length observed for the low initiator loading composite. The MALDI-TOF MS results for the MCM-41 composite show a much smaller MW with a prevalence of much smaller chains (Figure 4.16). This result demonstrates the effect the confining effect the pore size has on peptide growth. Interestingly, this effect was not noticeable in the PZK composites. In the KIT-6 composite, the MW distribution is shifted to the left of that for SBA-15 composites, though not as dramatically as in MCM-41 (Figure 4.17).

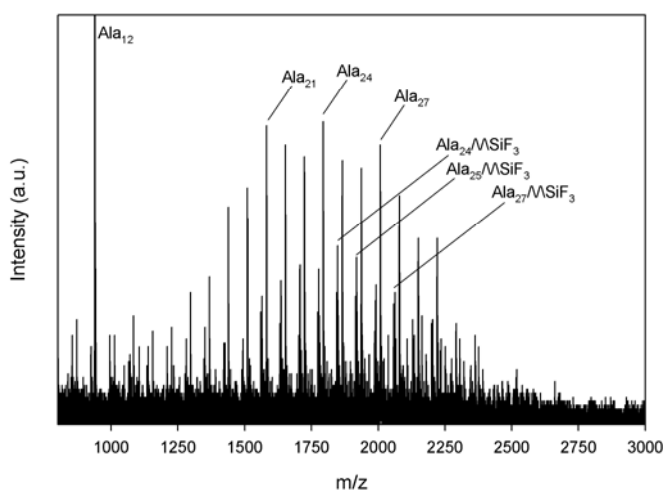


Figure 4.13 MALDI-TOF MS of peptide from the 0.25mmol APTMS/g SBA-15 Poly-L-alanine composite. Note the spacing of peaks is equivalent to the mass difference of one monomer. Only selected peaks are labeled.

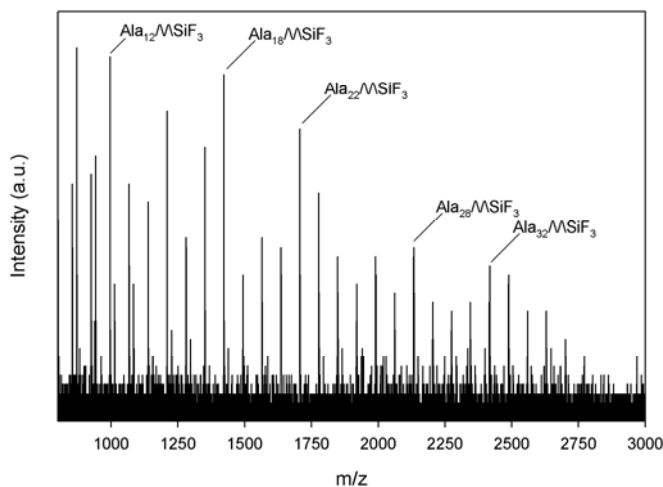


Figure 4.14 MALDI-TOF MS of peptide from the 0.50mmol APTMS/g SBA-15 Poly-L-alanine composite. Note the spacing of peaks is equivalent to the mass difference of one monomer. Only select peaks are labeled.

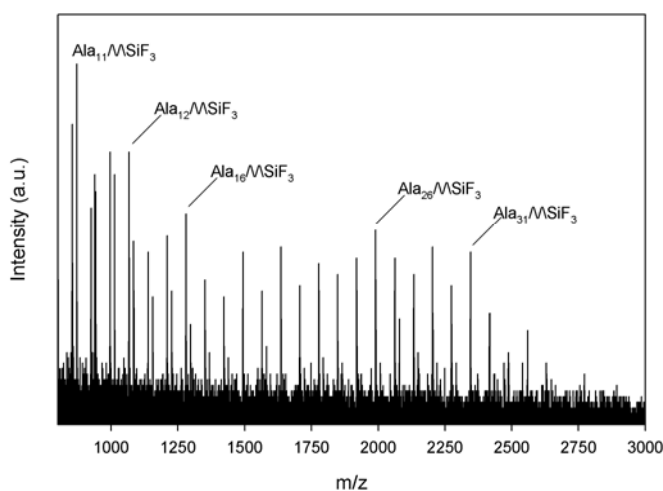


Figure 4.15 MALDI-TOF MS of peptide from the 0.75mmol APTMS/g SBA-15 Poly-L-alanine composite. Note the spacing of peaks is equivalent to the mass difference of one monomer. Only select peaks are labeled.

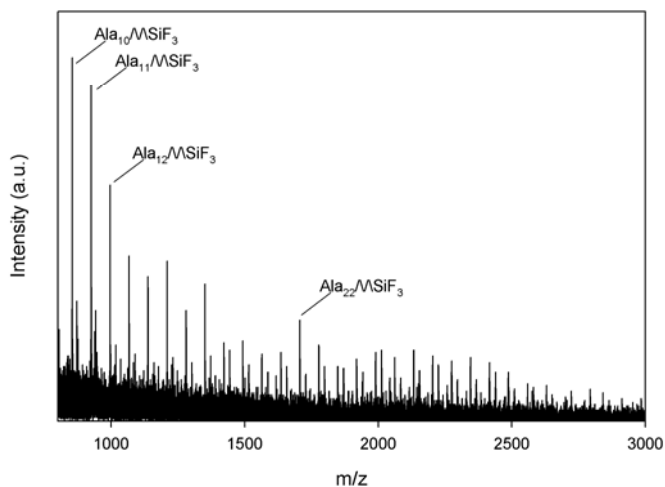


Figure 4.16 MALDI-TOF MS of peptide from the 0.75mmol APTMS/g MCM-41 Poly-L-alanine composite. Note the spacing of peaks is equivalent to the mass difference of one monomer. Only select peaks are labeled.

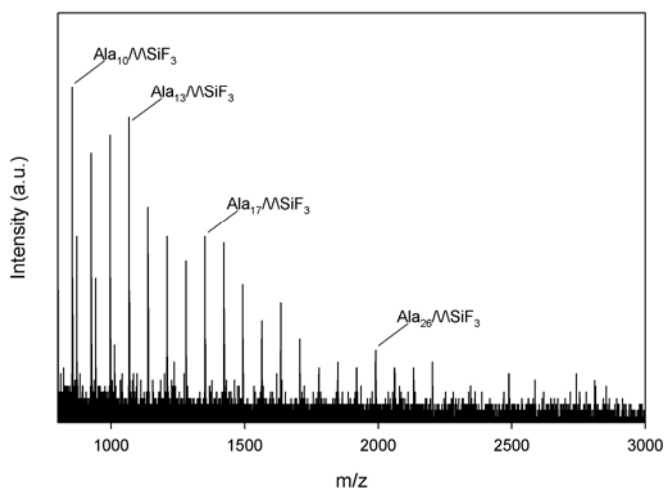


Figure 4.17 MALDI-TOF MS of peptide from the 0.75mmol APTMS/g KIT-6 Poly-L-alanine composite. Only select peaks are labeled.

4.4 Discussion

4.4.1 *Effect of Initial Amine Loading*

The overall influence of the initial amine loading is on the porosity of the samples primarily. In the PZK composites, there is a notable change in the overall organic content with changing amine loadings, but this is probably more a result of the bulky monomer and difficulty reaching high molecular weights than strictly on amine loading. In the PA samples, which show no content differences by TGA, the effect of the amine loading can be seen more clearly. In these samples, as in the PZK composites, the porosity increases with decreasing amine loading. The authors believe this has to do with the increase in spacing of polymers with equal or similar lengths inside the pores, with longer polymers on the external surface for the low initiator loadings to make up for the difference in weight. Our mass spectrometry results, which show similar results for various amine loadings in the same OMS material are evidence of this conclusion.

4.4.2 *Effect of Pore Size (MCM-41 vs. SBA-15)*

In the PZK composites, the pore size seems to have little effect in terms of the MW of the polymer obtained by MALDI-TOF MS. In terms of the amount of organic in the pores, SBA-15 was able to accommodate more organic, likely due to its higher pore volume. In the PA composites, we see a clear difference in the MW of the polymer between SBA-15 and MCM-41: SBA-15 affords longer polymers and MCM-41 shorter polymers. A simple way to interpret this result is that the OMS mesopores provide confinement effects that influence the final polymer MW.

4.4.3 Effect of Pore Topology (SBA-15 vs. KIT-6)

The effect of the pore topology is fairly dramatic, especially in the case of the PZK composites: the organic contents in the PZK composites of KIT-6 are very low and the porosities are quite high compared with those on SBA-15. In the case of PA, the organic contents and porosity are almost the same for the 0.5mmol APTMS/g SiO₂ composites of SBA-15 and KIT-6. We do, however, see smaller MWs in the MALDI-TOF MS for the PA KIT-6 composite synthesized. Though the exact reason for the differences between peptide growth on KIT-6 and SBA-15 and between PZK and PA on KIT-6 remains elusive, it is fairly clear that it is related purely to topological differences as KIT-6 and SBA-15 have roughly the same pore diameter and surface area. Some factors that may play roles include: pore dimensionality (2D vs. 3D), local/overall pore curvature and local/overall surface silanol densities,

4.4.4 Effect of Monomer Identity (L-Lys(Z) NCA vs. L-Ala NCA)

As evident from the TGA and MALDI-TOF showing the accommodation of much longer chains in the pores, PA packs significantly better than the PZK due to its substantially smaller side chain. The longer peptide chains may also be attributed to folding of the polymer. Another notable difference between the two systems is that the PA composites maintain some porosity at high organic loadings while the PZK composites do not.

4.5 Conclusions

The results show that NCA polymerization chemistry can be used to synthesize well-defined composite materials with ordered mesoporous silica. The properties of the composite and the attached polymer can be tuned by altering the surface initiator loading, pore size, pore topology and monomer identity. For the poly-Z-L-lysine composites, it has been demonstrated that the polymer can be deprotected to yield the active side chain amine without deterioration of the polymer. This result also evidences the accessibility of the side chain groups despite the high organic loadings and the lack of porosity by nitrogen adsorption. In addition, the presented catalytic data of the deprotected composites demonstrates accessibility to larger molecules for composites with slightly more porosity. For the poly-L-alanine—SBA-15 composites, the porosity can be tuned by changing the initiator loading while having no ill effect on overall organic content and minimal effect on the polymer MW obtained.

CHAPTER V

SURFACE SELECTIVE GRAFTING*

5.1 Introduction

In the previous chapter, we described the synthesis of OMS-polypeptide hybrids *via* the use of surface-tethered amines as initiators for the ring-opening polymerization of *N*-carboxyanhydride (NCA) amino acids.²⁴⁶ Building off that work, here we demonstrate the ability to selectively functionalize the outer or inner surface of SBA-15 with poly-L-lysine while grafting a different functional group, here thiols, to the opposite surface (Figure 5.1). We believe the ability to graft different organic architectures surface-selectively will extend the scope of OMS hybrids in a diverse field of scientific interests. In the current work, amines and thiols were chosen given their potential interest in catalysis, sensing, and controlled release, and their well-developed/orthogonal chemistries that permit subsequent reactions/use as chemical handles.

Recently, there has been increasing interest in developing such multifunctional materials. An array of different approaches have been reported in the literature. One method utilizes the OMS-templating agent as a barrier to selectively graft organics to the outer surface followed by template extraction.^{222,247-249} A second approach uses sequential co-condensation in radially growing OMS

* Modified from Lunn, J.D.; Shantz, D. F. *Chemical Communications* **2010**, 46, 2926-2928, DOI: 10.1039/b927487a (www.rsc.org/ej/CC/2010/b927487a.pdf) – Reproduced by permission of The Royal Society of Chemistry (RSC).

nanoparticles to incorporate one or more functional groups.²⁵⁰⁻²⁵² Other methods employing diffusion-limited deprotection²²⁵ and surface tension differences²⁵³ have also been reported. Though likely less domain specific than “designer” methods used for OMS nanoparticles, the “barrier” approach yields high external organosilane concentrations and uses traditional OMS synthesis protocols applicable to a wide variety of common systems. For these reasons, it is the method of choice here.

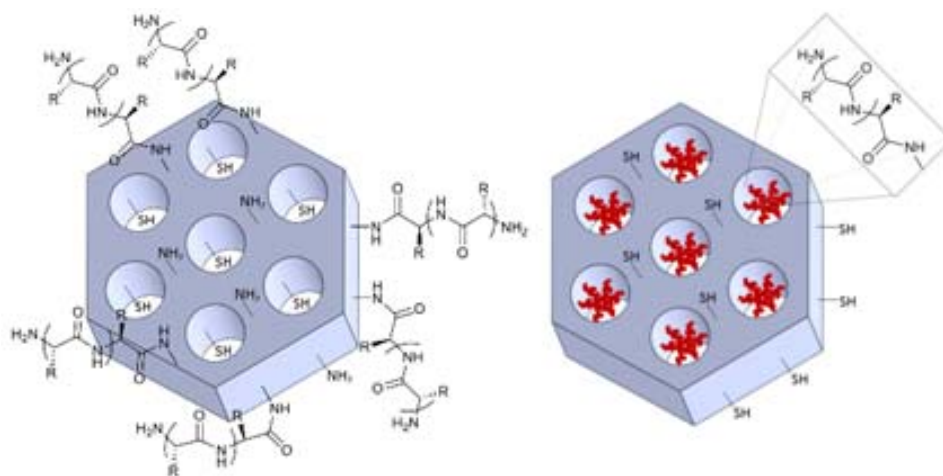


Figure 5.1 Pictorial representations of externally (left) and internally (right) grafted poly-Z-L-lysine SBA-15 hybrids with thiols grafted to the opposite surface; R = $-\text{CH}_2\text{CH}_2\text{CH}_2\text{CH}_2\text{NHCbz}$.

5.2 Selective Grafting of Polylysine Only

We initially started by preparing polylysine only hybrids using a traditional organosilane grafting approach, similar to that described in Chapter V. As they serve as

a reference point for our later investigations incorporating two functional groups, these studies will be discussed first.

5.2.1 *Synthesis*

SBA-15 was synthesized and filtered without washing or calcination. The as-made SBA-15 was divided into two 1 g batches; both were vacuum-dried. The external surface of one batch was reacted with 3-aminopropyltrimethoxysilane (APTMS) in toluene (**X1**), while the other was capped with hexamethyldisilazane (HMDS). The Pluronic template in both samples was extracted using refluxing ethanol and HCl. The HMDS-capped sample was further functionalized with 0.5mmol/g APTMS (**I1**). 0.5g of each were vacuum-dried and reacted with 50ml of 0.1M NCA in THF (10mmol NCA/g **X1** or **I1**). The resulting hybrids will be referred to as **PZK-X1** and **PZK-I1**. Deprotection and neutralization followed (**PK-X1** and **PK-I1**). The detailed synthetic procedures are located in Chapter II (Sublevel 2.2.2).

5.2.2 *Results*

XPS spectra taken after organosilane functionalization show the effective incorporation of the aminosilane (Figure 5.2). As might be expected, the N 1s peak for the externally grafted sample (**X1**) is more intense relative to the silicon peaks than its internally grafted counterpart (**I1**). For **I1**, the additional C1s signal is likely due to the HMDS-capped surface. Nitrogen adsorption of the precursor materials shows that **X1** has significantly less porosity than **I1** (Table 5.1). The lower pore

volume and estimated pore diameter are likely due to a combination of two factors: partial pore mouth blockage from the amines on the surface and the resulting decreased efficiency toward Pluronic removal. It should be noted, however, that even for bare SBA-15, the extraction efficiency is low ($\sim 75\%$).²⁵⁴ TGA, similarly, shows a significant amount of organic left after extraction in **X1** (Table 5.1). Unfortunately, insufficient sample remained to run TGA on **I1**; however, based on its higher porosity, it seems reasonable to assume that the organic content is lower (i.e. less residual Pluronic).

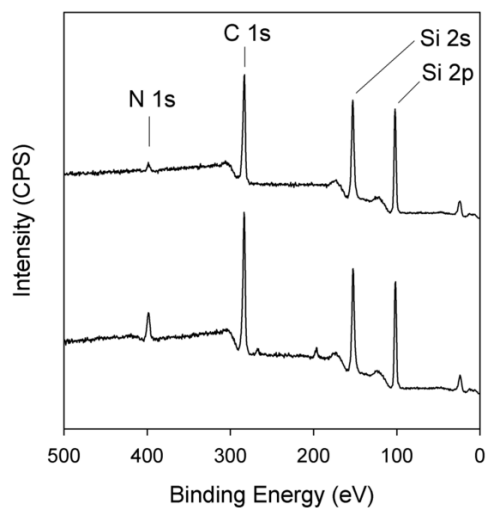


Figure 5.2 XPS spectra of **I1** (top) and **X1** (bottom).

Table 5.1 Adsorption and TGA data of hybrids synthesized from **X1** and **I1**.

Sample	$S(\alpha_s)$ [m ² /g]	V_p^a [cm ³ /g]	$d_p(\text{BJH})$ [nm]	Organic [wt%]	N/Si _{XPS} [mol/mol]	C/Si _{XPS} [mol/mol]
X1	537	0.56	7.1	16.9	0.24	1.74
I1	874	0.87	7.5	---- ^b	0.06	1.35
PZK-X1	----	n.p.	----	59.6	4.3	41.9
PK-X1	----	n.p.	----	53.8		
PZK-I1	----	n.p.	----	49.0	1.8	17.3
PK-I1	223	0.29	6.2	41.7		

^a Recorded at $p/p_0 = 0.9$; n.p. = non-porous

^b No sample was available for this measurement

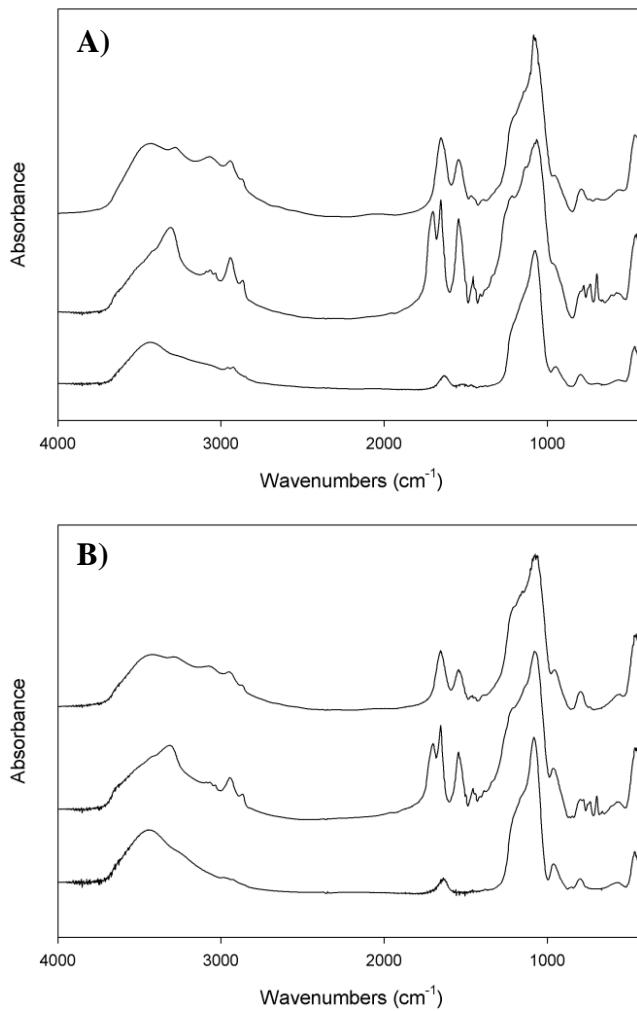


Figure 5.3 IR spectra of the externally (A) and internally (B) poly-Z-L-lysine grafted SBA-15, showing spectra for the precursor materials (bottom), and both protected (middle) and deprotected hybrids (top).

As in Chapter IV, we found that the ring-opening polymerization of *N*-carboxyanhydride amino acids proceeds from the surface of amine-functionalized SBA-15. IR (Figure 5.3) indicates significant amounts of polypeptide are formed in both sets of materials, evident from the amide peak intensities ($\sim 1650\text{cm}^{-1}$ & $\sim 1550\text{cm}^{-1}$) relative to the Si-O-Si bending peak ($\sim 1100\text{cm}^{-1}$). It is similarly apparent that the polymer can be deprotected with ease in HBr, shown by the disappearance of the carbamate peak ($\sim 1700\text{cm}^{-1}$). TGA data corroborates the IR results showing large amounts of organic in both samples (Table 5.1). TGA shows larger weight losses (i.e. larger amounts of peptide) compared to the 0.5mmol APTMS/ g SBA-15 hybrid achieved in Chapter IV (Table 5.1).^{*} This result will be further explored below in the discussion for the polylysine/thiol hybrids. XPS, corroborating the TGA and IR, shows dramatic increases in the C 1s and N 1s peaks relative to Si 2p in both samples (Appendix B) when compared to the amine-functionalized materials (Figure 5.2). As anticipated, the C/Si and N/Si ratios are much larger for the externally grafted samples (Table 5.1), strong evidence for selective grafting.

Nitrogen adsorption isotherms for the precursor materials and polymerized samples are shown in Figure 5.4 (See also Table 5.1). Upon polymerization, both externally and internally grafted samples show complete loss of porosity. However, upon deprotection of the polymer, the internally grafted sample regains considerable

^{*} Molar quantities of peptide were not calculated for the lack of **II** TGA data.

porosity while the externally grafted sample regains none. The lack of porosity in **PK-X1** is likely due to pore mouth blockage.

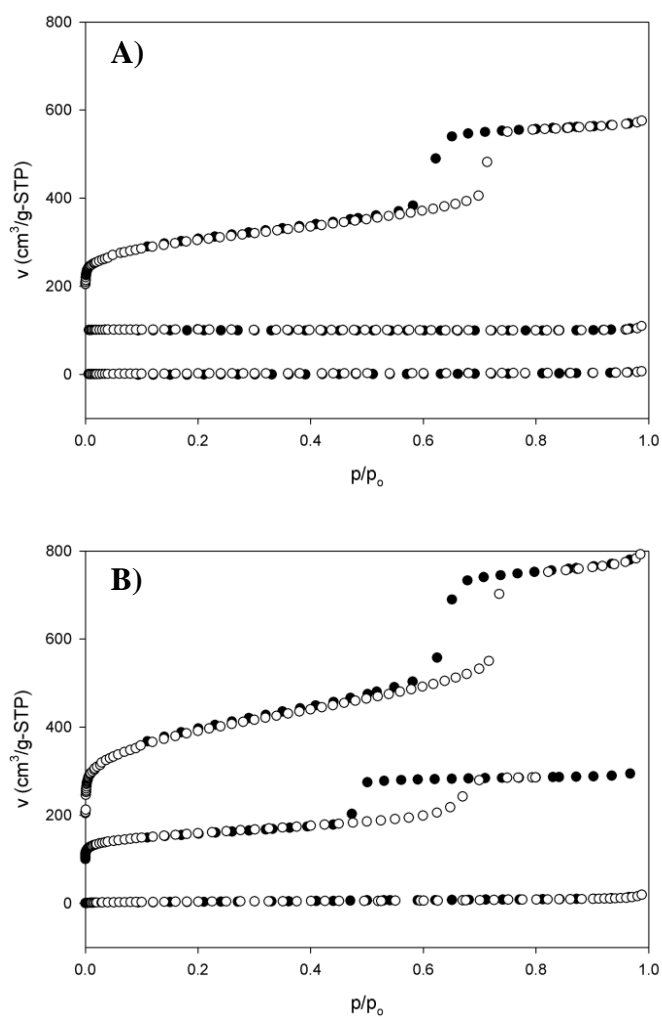


Figure 5.4. Nitrogen adsorption isotherms of the externally (A) and internally (B) poly-Z-L-lysine grafted SBA-15; Top to bottom – functionalized SBA-15, PK-SBA15 hybrid, and PZK-SBA15 hybrid.

5.3 Selective Grafting of Polylysine and Thiols

As stated above, our principal objective was to selectively graft thiols and polylysine on opposite surfaces (i.e. external/internal). In order to do so, thiols needed to be grafted opposite of the initiating amines prior to polymerization. Though we found above that amines graft easily to the external surface of SBA-15 through traditional reaction in toluene, thiols proved much less reactive, requiring high temperatures, long reaction times, and the addition of water. Figure 5.5 shows the XPS spectra of thiol-functionalized SBA-15 synthesized by various approaches.

We first attempted grafting thiols to the outer surface in the same manner as the amines above: 1ml 3-mercaptopropyl trimethoxysilane (MPTMS) in 25ml dry toluene for 0.5 g as-made SBA-15 for 2 hours. This approach, however, yielded no observable S 2s or S 2p peaks by XPS (bottom spectra in Figure 5.5). Increasing the reaction time to 24 hours also failed to graft observable thiol. By refluxing for 24 hours and adding 1ml of water, only a small amount of grafted thiol was observed (middle spectra in Figure 5.5). The use of water, reflux conditions, and a long reaction time, however, is undesirable due to possible Pluronic extraction. Polylysine/thiol—SBA-15 hybrids prepared using this approach when combined with extraction difficulties were messy and hard to interpret (Appendix B).

Considering these difficulties, a new approach was sought. It was discovered that by using microwaves²⁵⁵ to promote the reaction of neat MPTMS with as-made SBA-15, a much higher degree of functionalization could be achieved in only 15 minutes (top spectra in Figure 5.5). We also found microwaves could be used to assist in the ethanol extraction

of the Pluronic template.²⁵⁶ This microwave-assisted functionalization and extraction was consequently used to synthesize the polylysine/thiol—SBA-15 hybrids described below.

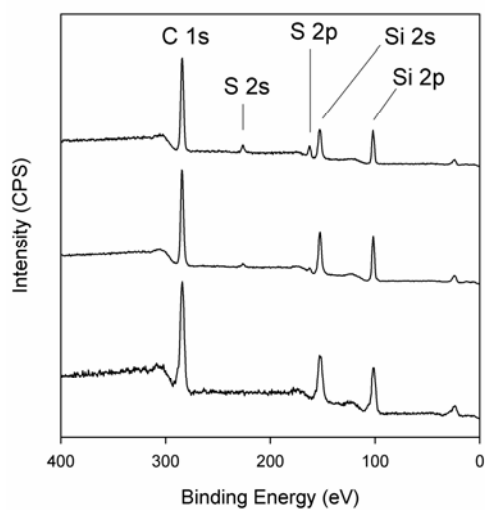


Figure 5.5 XPS spectra of externally grafted MPTMS to SBA-15 by various methods: (top) MW approach; (middle) 24 hours reflux w/ water; and (bottom) 2h stirring at RT.

5.3.1 Synthesis

SBA-15 was synthesized as described previously. External surface functionalization was achieved by reacting as-made SBA-15 in neat organosilane while stirring and irradiating with microwaves (300W) for 15 minutes.* The Pluronic template was then removed by a rapid three step ethanol extraction which was assisted by microwaves (100W). Extraction was followed by a traditional post-synthetic grafting of 0.5mmol/g functionalized SiO₂ (FS) of the orthogonal silane. In this manner, two samples were prepared: one with amines externally and thiols internally (**X2**) and another with thiols externally and amines internally (**I2**). Poly-Z-L-lysine was grafted from the amine-functionalized surface, deprotected using HBr, and neutralized (See Figure 5.1 above). High and low monomer loading (10 and 5 mmol NCA/g functionalized SiO₂) syntheses were performed to observe the effect of the polypeptide loading: **PZK-X2 10** & **PZK-I2 10** and **PZK-X2 5** & **PZK-I2 5**, for high and low, respectively. The detailed synthetic procedures are located in Chapter II (Sublevel 2.2.2).

* A comparison of the as-made functionalized samples with as-made SBA-15 indicates some Pluronic is likely extracted into the silane phase during functionalization (Appendix B); however, it does not seem to have a large effect on the resulting samples based on the following results and its impact is probably limited to pore mouth functionalization.

5.3.2 *Results*

XPS spectra taken after the second functionalization step show the effective incorporation of both silanes (Figure 5.6C). As expected, the silane on the external surface shows more intense peak(s) at the characteristic binding energy/energies. Additionally, NHS-fluorescein (amine selective) and BODIPY-TMR thiosulfate (thiol selective) dyes were used to visualize the degree of surface segregation of the amines and thiols by Confocal Microscopy. Despite limits in optical resolution, images of these samples show amine and thiol-selective dyes occupying separate domains (Figures 5.6A & B), again suggesting successful selective functionalization in both materials. Again, the NCA-polymerization effectively grafted poly-Z-L-lysine from the amine-functionalized surface, as evidenced by IR (Figure 5.7), demonstrating that the amines are accessible and the thiols do not inhibit the polymerization. The polymer was likewise easily deprotected in HBr as above.

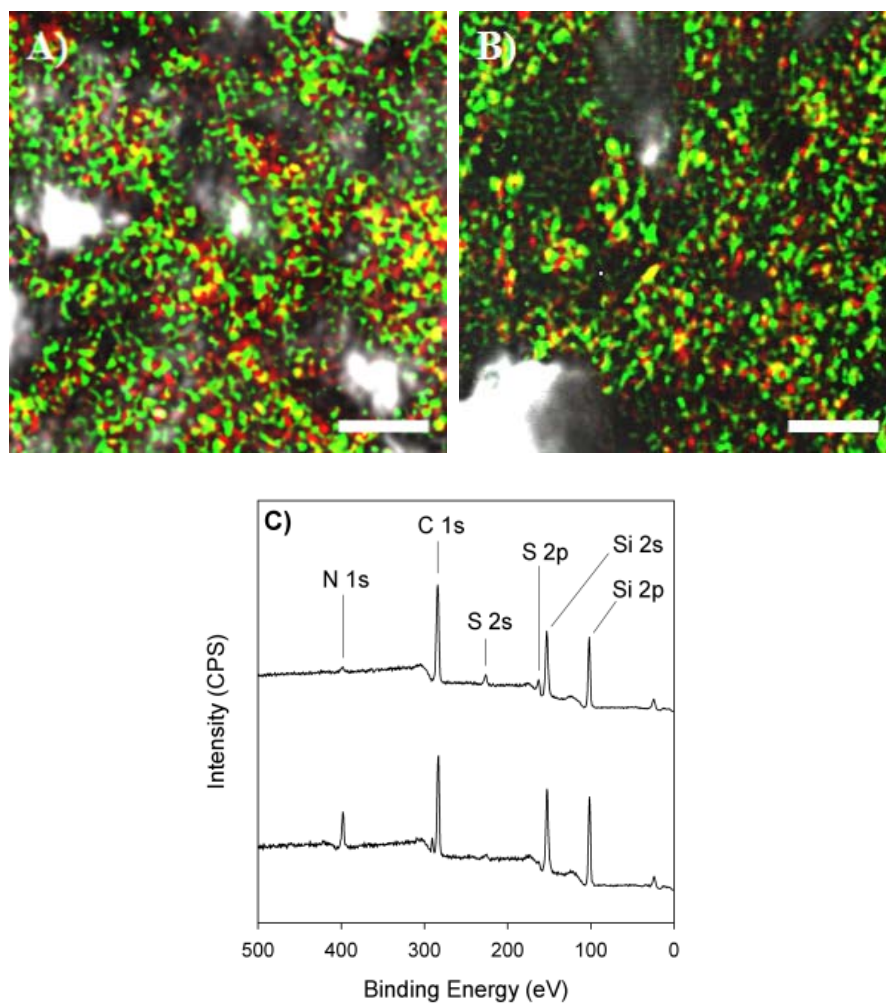


Figure 5.6 Confocal images of A) **I2** and B) **X2** dyed with NHS-fluorescein (green, amine selective) and BODIPY-TMR thiosulfate (red, thiol selective). The scale bar represents 5 μm. C) XPS spectra of **I2** (top) and **X2** (bottom).

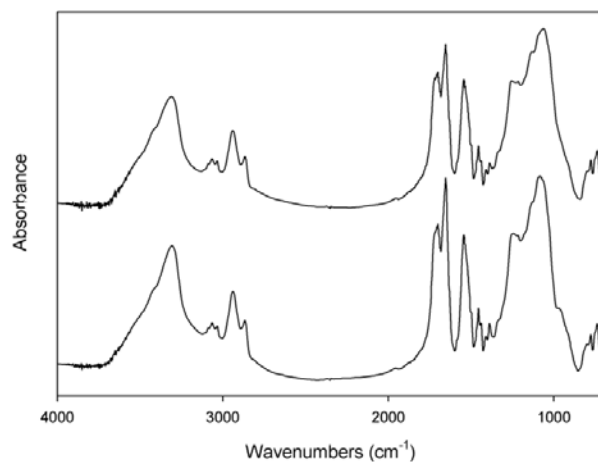


Figure 5.7 IR spectra of **PZK-X2-10** (top) and **PZK-I2-10** (bottom).

Table 5.2 Adsorption and TGA data of MW samples

Sample	$S(\alpha_s)$ [m ² /g]	V_p^a [cm ³ /g]	$d_p(\text{BJH})$ [nm]	Organic [wt%]	Lysine ^b [mmol/g FS]
SBA-15				9.4	----
X2	660	0.66	7.5	19.6	----
I2	651	0.65	7.4	24.5	----
PZK-X2-10	----	n.p.	----	68.9	6.04
PK-X2-10	33	0.02	5.6	53.7	5.74
PK-X2-10 H+	----	n.p.	----		
PZK-X2-5	----	n.p.	----	63.8	4.66
PK-X2-5	34	0.02	5.9	49.7	4.68
PZK-I2-10	----	n.p.	----	68.0	5.18
PK-I2-10	204	0.18	6.2	52.7	4.66
PK-I2-10 H+	60	0.03	6.2		
PZK-I2-5	----	n.p.	----	61.8	3.73
PK-I2-5	256	0.23	6.6	45.8	3.07

^a Recorded at $p/p_0 = 0.9$; n.p. = non-porous

^b Calculated from TGA data after subtracting organosilane and residual Pluronic contributions.

As in the polylysine-only hybrids, TGA shows, with the exception of **PZK-I2-5**, much larger amounts of peptide are formed compared to the ~ 3.5 mmol lysine/g FS maximum achieved in Chapter IV (Table 5.2). For the externally grafted samples, this result may be explained by a lack of pore wall confinement on polymer growth. The externally grafted peptide samples for both monomer loadings, as above, show larger amounts of polymer relative to their internally grafted counterparts. SEM shows large amounts of polymer on the external surface of the elementary SBA-15 particles ($d \sim 0.5 \mu\text{m}$) for these samples (Figure 5.8). For the internally grafted samples, polymer chains close to the pore mouth likely continue to grow outward without external interference leading to larger than expected polymer loadings; SEM, in support, shows polymer on the outer surface of **PZK-I2-10**. SEM images of **PZK-I2-5**, in contrast, show smaller and more defined particles indicative of much less or no polymer on the outer surface. Weight losses recorded for the deprotected samples are in excellent agreement with estimated values for complete deprotection and neutralization as noted by the calculated mmol lysine/g FS in Table 5.2.

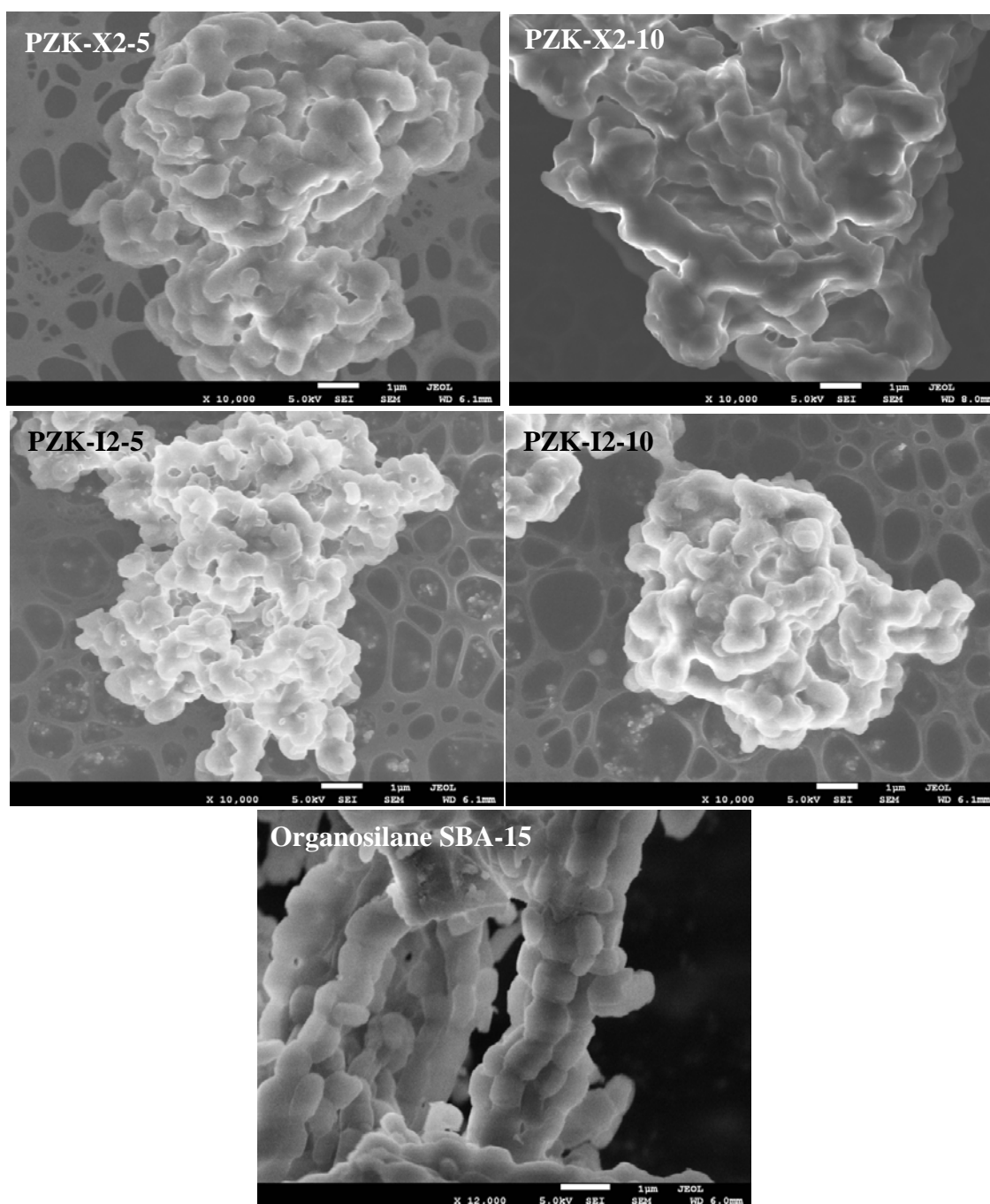


Figure 5.8 SEM images of the samples prepared *via* microwaves. The white scale bar represents 1 micron. Note: The magnification on the bottom image is 12K while the others are 10K.

Complementary to SEM, XPS shows a dramatic decreasing trend in the C/Si and N/Si atomic ratios from **PZK-X2-10** to **PZK-I2-5** (Figure 5.9A). **PZK-X2-10** has C/Si and N/Si ratios of 425 and 28, respectively, whereas, **PZK-I2-5** has ratios of 60 and 6. The much lower contribution of N and C in the **PZK-I2-5** spectra provides strong evidence for more internally confined polypeptide. **PZK-X2-5** and **PZK-I2-10** show similar ratios, again suggesting that excess peptide is exiting the pores in **PZK-I2-10**. These results compare well to the hybrids without thiols. Another notable difference is observed in the spectra of the deprotected samples: the S 2s and S 2p peaks are visible for the internally grafted samples contrary to the externally grafted samples where none are observed (Figure 5.9B).

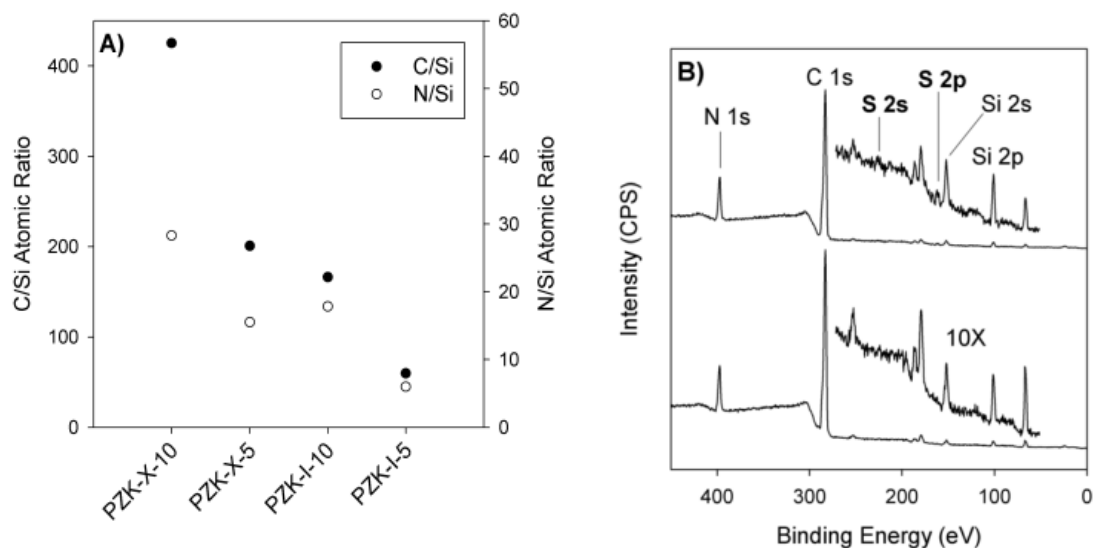


Figure 5.9 A) Plot of N/Si and C/Si atomic ratios for poly-Z-L-lysine grafted samples; B) XPS spectra of **PZK-I2-5** (top) and **PZK-X2-5** (bottom)

Nitrogen adsorption shows that upon polymerization there is a complete loss of porosity in all samples (Table 5.2). However, there is a significant difference in the porosity after deprotection of the polymer: the internally grafted samples regain a third of their porosity, while the externally grafted samples regain little to none (See also Figures 5.10 & 5.11). This trend, again, compares very well with the samples without thiols.

As there are numerous studies on polyelectrolyte brush swelling,²⁵⁷ we were interested in looking at the effects of side chain protonation on the deprotected samples. **PK-I2-10** and **PK-X2-10**, neutralized after deprotection, were treated with 0.1M HCl and sonicated for 10 minutes. Nitrogen adsorption of **PK-I2-10 H+** shows a drastic decrease in porosity (Figure 5.10, Table 5.2). Similarly, though there was very little initial porosity, **PK-X2-10 H+** shows absolutely no porosity (Figure 5.11, Table 5.2).

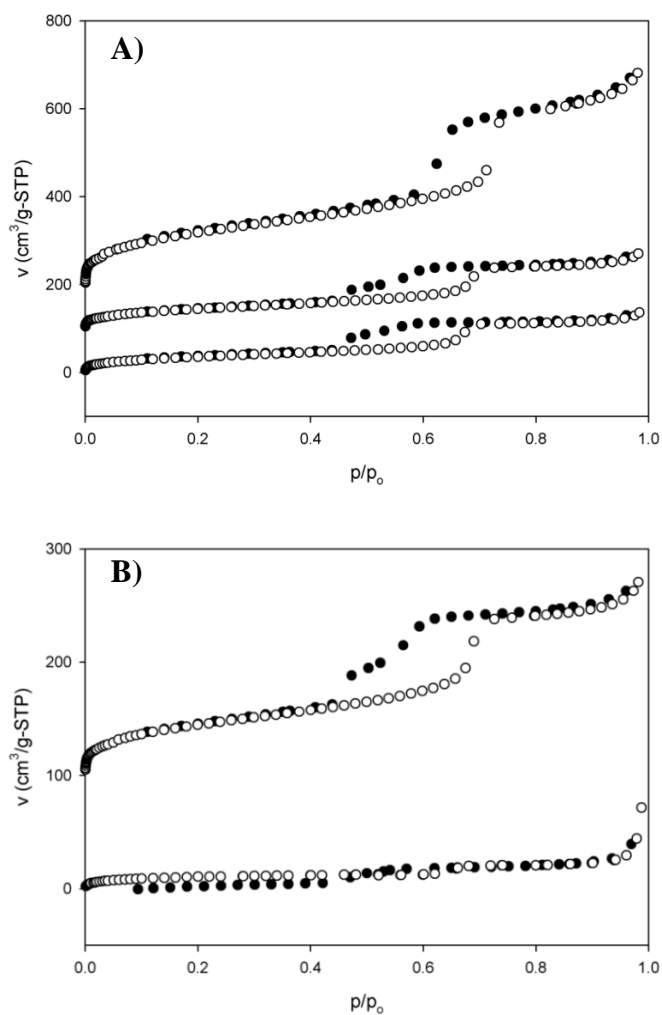


Figure 5.10 A) Nitrogen adsorption isotherms of **I2**, **PK-I2-5**, and **PK-I2-10** (from top to bottom); B) Nitrogen adsorption isotherms of the neutral **PK-I2-10** (top) and protonated **PK-I2-10 H+** (bottom)

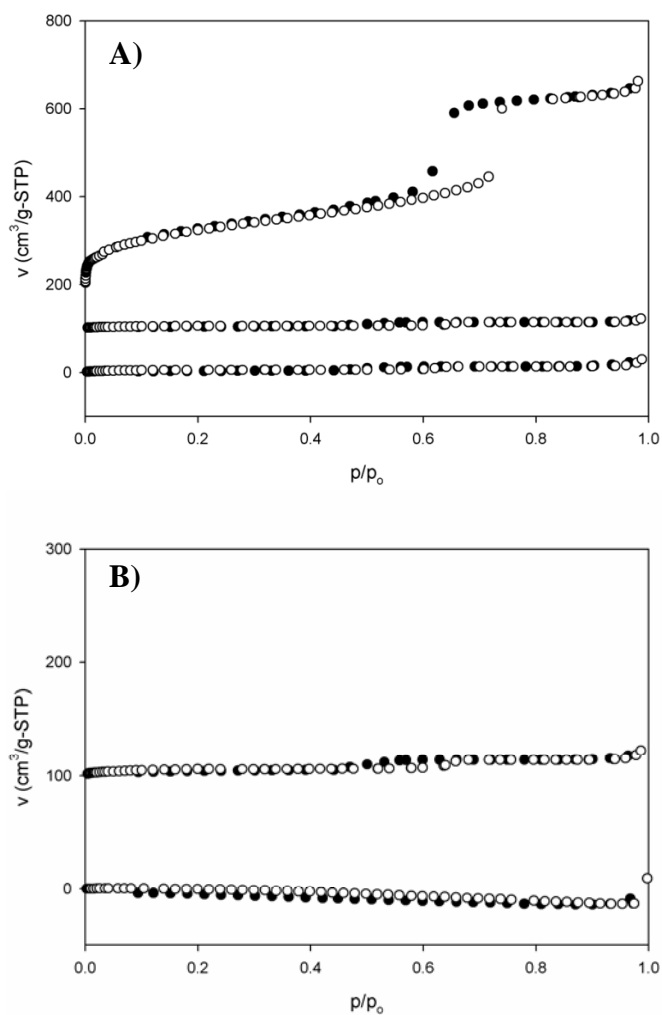


Figure 5.11 A) Nitrogen adsorption isotherms of X2, PK-X2-5, and PK-X2-10 (from top to bottom); B) Nitrogen adsorption isotherms of the neutral PK-X2-10 (top) and protonated PK-X2-10 H⁺ (bottom)

There is also a chemical change for both of these samples evidenced by IR.[§] As noted in the literature, when protonated, the amine absorption band at $\sim 3030\text{cm}^{-1}$ intensifies.²⁵⁸ Here, this intensity increase occurs significantly for **PK-X-10 H** (Figure 5A), signifying a high degree of protonation, and much less for **PK-I-10 H**, signifying a lesser degree of protonation (Figure 5B). The higher degree of protonation in the externally grafted sample is reasonable as the polymer layer has far more space to expand. The fact that the pores essentially close off in the internally grafted sample with limited protonation is evidence of a high sensitivity to pH. This feature may have very interesting implications for molecular gating. The ability to protonate the externally grafted sample easily suggests a further decrease in the monomer loading may yield a similar effect. Continuing work is investigating whether the thiol groups of the externally grafted samples are accessible to chemical probes in solution under various conditions.

5.4 Summary

In summary, it has been demonstrated that amines and thiols can be selectively grafted to the exterior surface and within the pores of SBA-15 using a post-synthetic approach. Furthermore, the amines can be used as initiators in the grafting of large amounts of poly-Z-L-lysine, creating novel hybrid materials. The poly-Z-L-lysine layer is selective to the amine-functionalized surface as supported by a number of techniques. Porosity of the hybrids and the chemical state of the polymer layer are dependent on the protonation state of side chain amines.

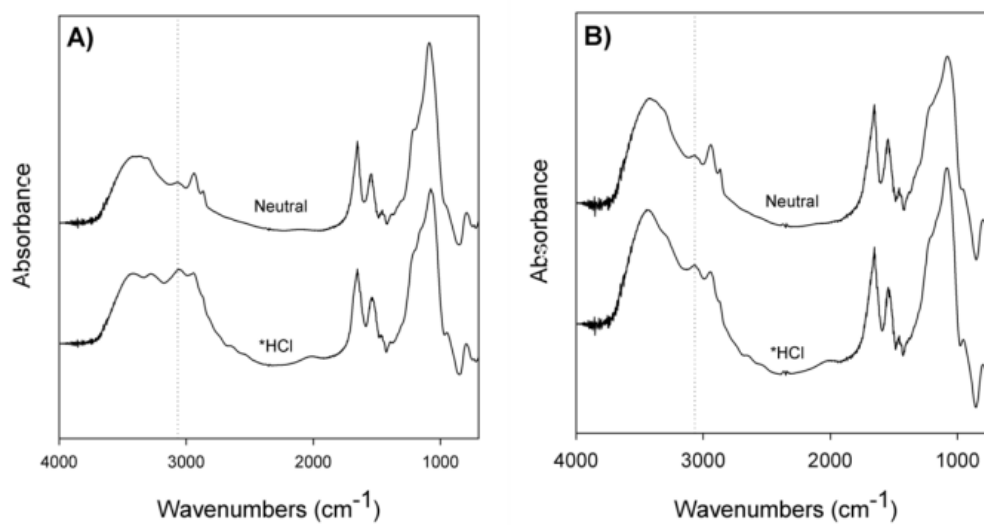


Figure 5.12 IR of neutral and protonated A) **PK-X-10** and B) **PK-I-10**. The dashed lines mark the amine absorption band at $\sim 3060\text{cm}^{-1}$.

CHAPTER VI

POLYPEPTIDE/THIOL—OMS SPHERE HYBRIDS

6.1 Introduction

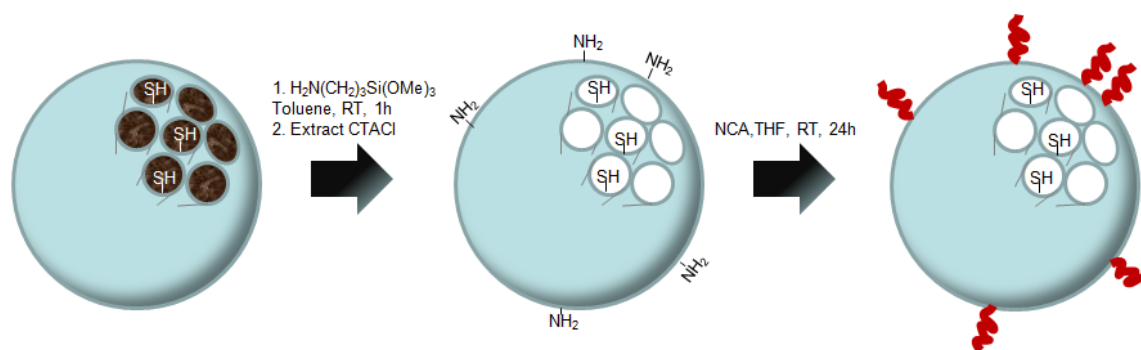
As discussed in the introduction to Chapter V, an alternative “designer” approach for selective functionalization employs sequential addition of silane mixtures in the co-condensation of radially growing OMS nanoparticles. This approach has been championed by two groups in particular, those of Thomas Bein at the University of Munich^{250,251} and Kazuhisa Yano at Toyota R&D in Japan.²⁵² Though both employ similar synthesis procedures and the resulting nanoparticles are hexagonally ordered with radially aligned pores, Yano’s procedure yields monodisperse spheres rather than irregular polydisperse ellipsoids. The sizes of Yano’s spheres are also larger, typically around 0.6 μm . As a result of these favorable properties, monodisperse mesoporous silica spheres (MMSS) serve as a model material for the continued study of selective grafting.

Here, we present the results of our investigations grafting polypeptides selectively to the external surface of monodisperse OMS spheres with thiols grafted at the core. This effort employed a two-pronged approach: thiol-functionalization of the core through sequential co-condensation and subsequent amine-functionalization of the outer surface through the traditional “barrier” approach described in the previous chapter. Our principal goals for this work were a) selectively graft polypeptides which behave differently to external stimuli and b) show that the interior thiols are accessible to

a chemical probe as might be relevant for the uptake and release of a drug or chemical agent under specified external conditions. In this line of reasoning, polylysine and polyglutamic acid were chosen as the polypeptides: polylysine swelling at low pHs due to the positive charge of the amine side chain; and polyglutamic acid swelling at high pHs having a deprotonated carboxylic acid side chain. Additionally, we desired to show a copolymer of the two may be grafted that may have other interesting properties.

6.2 Experimental

Monodisperse OMS spheres with a thiol functionalized core were synthesized according to the procedure developed by Yano et al. with a core/shell silane ratio of 2 to 1. 1g of the as-made spheres was vacuum-dried for 24 hours and reacted under argon for 1 hour in a solution of 50ml dry toluene and 2ml distilled APTMS. Extraction of the CTACl template was performed by refluxing in an ethanol/HCl solution for 3 hours. The amine-functionalized OMS spheres (**NH₂/SH-MMSS**) were divided into three 250mg portions, vacuum dried, and dispersed in 10ml dry THF. 15ml 0.1M NCA (6mmol NCA/g starting material) were added to each flask: one with L-Lys(Z)-NCA, another with L-Glu(Bz)-NCA, and the last with a 1:1 mixture. The reaction was carried out at room temperature for 24 hours. Deprotection and neutralization were performed as above with HBr and DIPEA. Detailed synthetic procedures can be found in Chapter II (Sublevel 2.2.3).



Scheme 6.1 Pictorial representation of polypeptide/thiol-OMS sphere hybrid synthesis

6.3 Results

6.3.1 Amine-functionalized OMS Spheres

Powder X-ray diffraction was performed on the as-made OMS spheres prior to amine-functionalization to confirm successful mesophase synthesis. The XRD pattern in Figure 6.1A shows the three diffraction peaks as reported in the original manuscript with Miller indices of (100), (110) and (200), characteristic of a hexagonal material. SEM (Figure 6.1B) and DLS show monodisperse spheres with a diameter of 0.6 μm were successfully synthesized.

Following amine-functionalization and extraction, N_2 adsorption (Figure 6.2) and XPS (Figure 6.3) were performed to confirm the mesoporosity of the spheres and successful amine-functionalization, respectively. The N_2 adsorption isotherm matches closely to that of the OMS spheres in the original work with a total pore volume of 0.67 ml/g and a pore diameter of 2.2nm estimated from BJH analysis. XPS of the amine-functionalized spheres shows the presence of the N 1s peak confirming amine attachment (Figure 6.3A). A comparison of this sample with one not amine-

functionalized shows that this peak is not a result of unextracted surfactant. Confocal microscopy, as in the previous chapter, was used to identify the amine/thiol functionalized regions. The result, here, however, is much more clear due to the uniformity of the particles and strongly supports selective bifunctionalization. In Figure 6.3B, the red thiol-selective BODIPY-TMR dye occupies the inner portion of the spheres, while the green amine-selective NHS-fluorescein dye forms a ring on the outside.

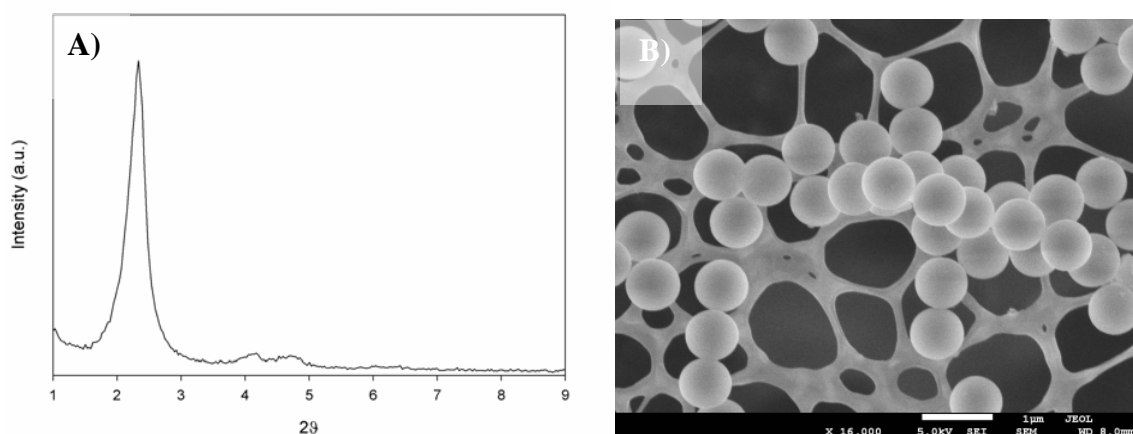


Figure 6.1 XRD and SEM of OMS spheres: A) XRD pattern of as-made OMS spheres with thiol core and B) SEM image of NH_2/SH -MMSS (The white scale bar represents 1 μm .)

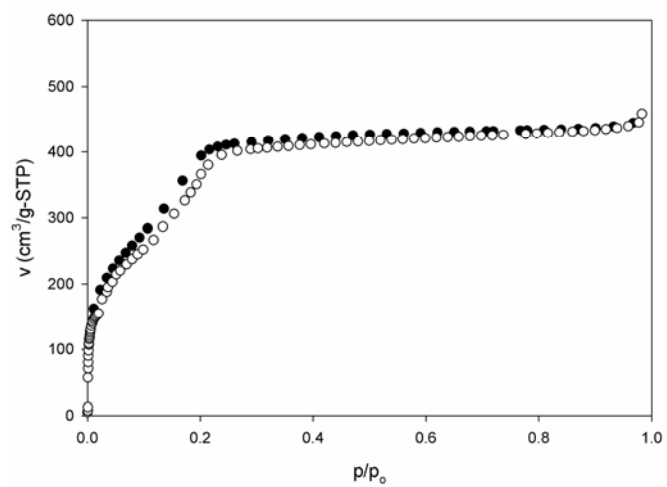


Figure 6.2 Nitrogen adsorption isotherm of NH₂/SH-MMSS.

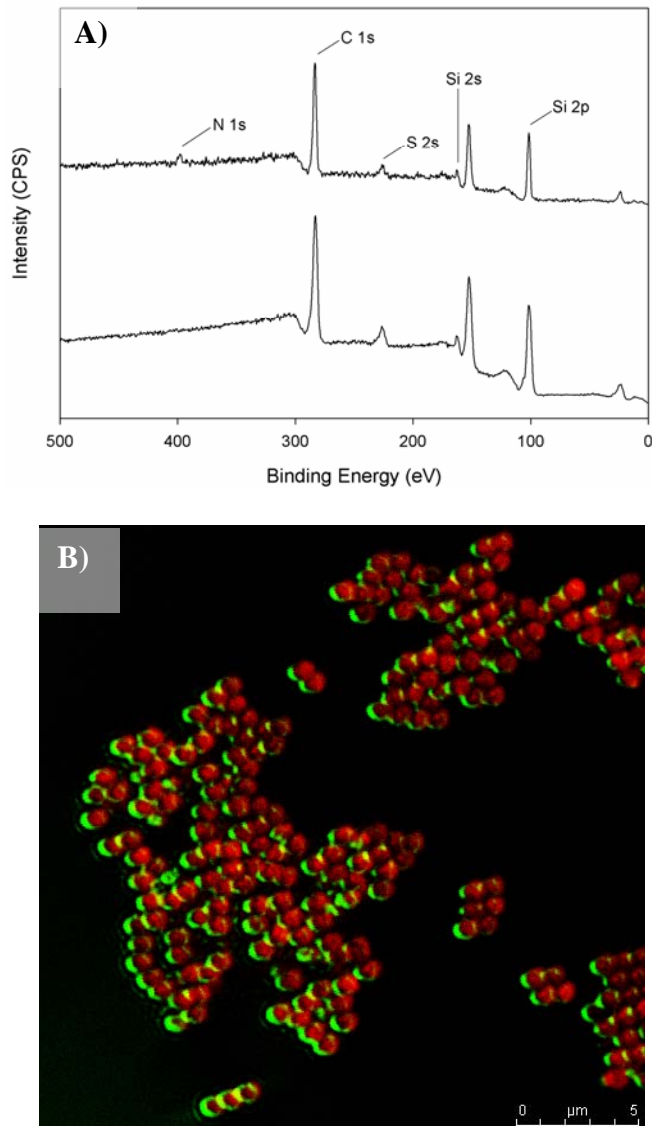


Figure 6.3 XPS spectra and confocal microscopy of $\text{NH}_2/\text{SH-MMSS}$: A) XPS spectra comparing OMS spheres that were amine-functionalized and extracted (top), with those that were extracted without additional functionalization (bottom); and B) A confocal image of spheres dyed with NHS-fluorescein (green, amine selective) and BODIPY-TMR thiosulfate (red, thiol selective) (The scale bar on the bottom right represents 5 μm).

6.3.2 Polypeptide Grafted OMS Spheres

6.3.2.1 IR and XPS

As in the previous two chapters, NCA polymerization is successfully initiated by the surface amines. IR spectroscopy of the poly-Z-L-lysine hybrid (**PZK/SH-MMSS**) shows peaks at 1655 cm^{-1} and 1550 cm^{-1} for the amide I and II modes, respectively, and a peak at 1701 cm^{-1} for the Cbz protecting group (Figure 6.4). Similarly, the poly(benzyl-L-glutamate) (**PBG/SH-MMSS**) shows the same amide peaks with the benzyl ester (OBz) protecting group showing up at 1735 cm^{-1} (Figure 6.5). **PZK&PBG/SH-MMSS** shows both protecting groups are present, evidence of copolymerization (Figure 6.6). The exact composition of the copolymer is unknown and is assumed to be random. Treatment with HBr effectively deprotects both polymers.

XPS was performed on the protected and deprotected hybrids (Figures 6.4 - 6.6). As expected, XPS shows large increases in the N 1s and C 1s peaks relative to the silicon peaks when compared to **NH₂/SH-MMSS** (Figure 6.3A above). The C/N ratios are almost double the expected values of 7 (PZK) and 12 (PBG): 13.1 and 21.1 for **PZK/SH-MMSS** and **PBE/SH-MMSS**, respectively (Atomic ratios are tabulated in Appendix C.). A similar effect was noted in the externally grafted samples in the previous chapter (Appendix B). The exact reason for this is uncertain. Upon deprotection, the C/N ratios decrease 49-62% (compared to 57-58% in the ideal case) and are accompanied by a large decrease in the O/N ratio. These reductions confirm the IR results for the deprotected samples. Another unexpected observation is the substantial increases in the N/Si and C/Si ratios in the deprotected samples compared to

their protected counterparts. These increases may be a result of polymer charging/swelling causing them to elongate. The presence of bromine in the **PK/SH-MMSS** XPS spectra indicates neutralization was not completely effective; the polyglutamic acid is also likely partially charged.

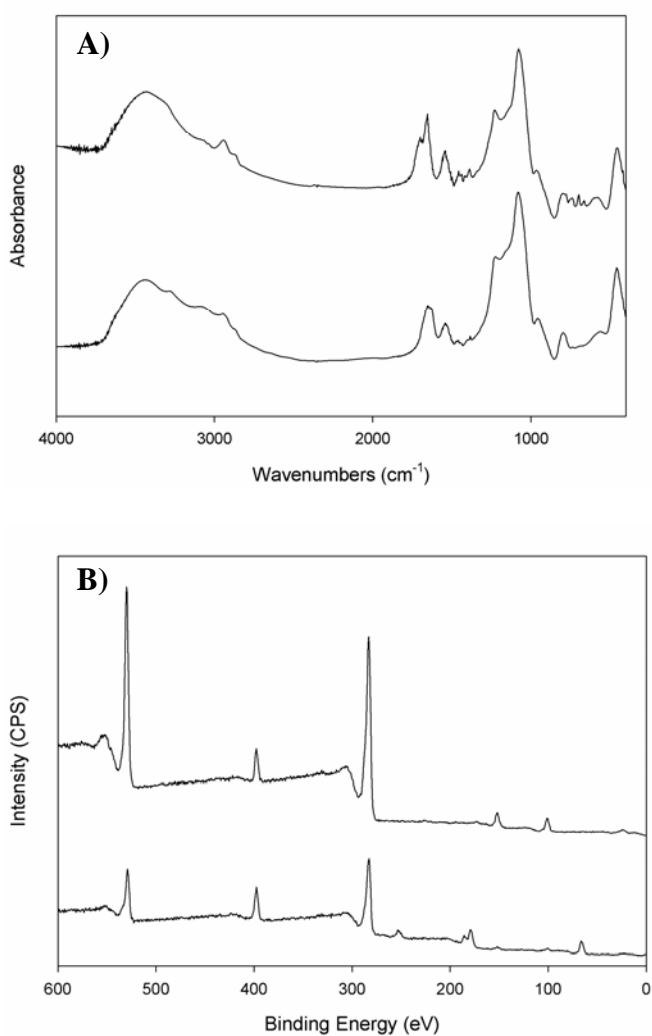


Figure 6.4 A) IR and B) XPS spectra of **PZK/SH-MMSS** before (top) and after (bottom) deprotection.

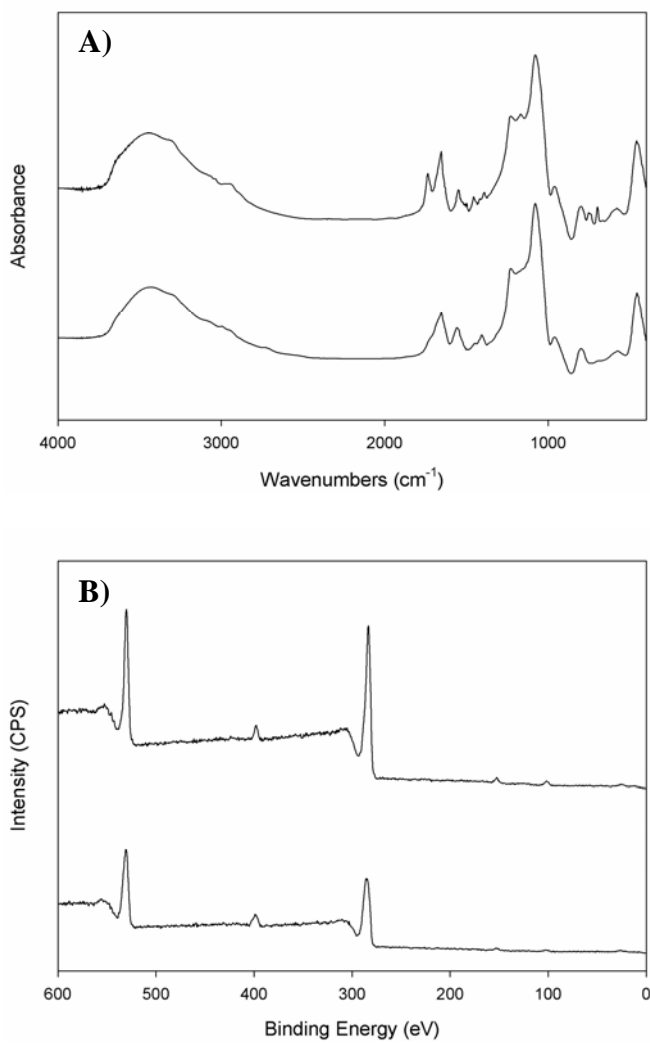


Figure 6.5 A) IR and B) XPS spectra of **PBG/SH-MMSS** before (top) and after (bottom) deprotection.

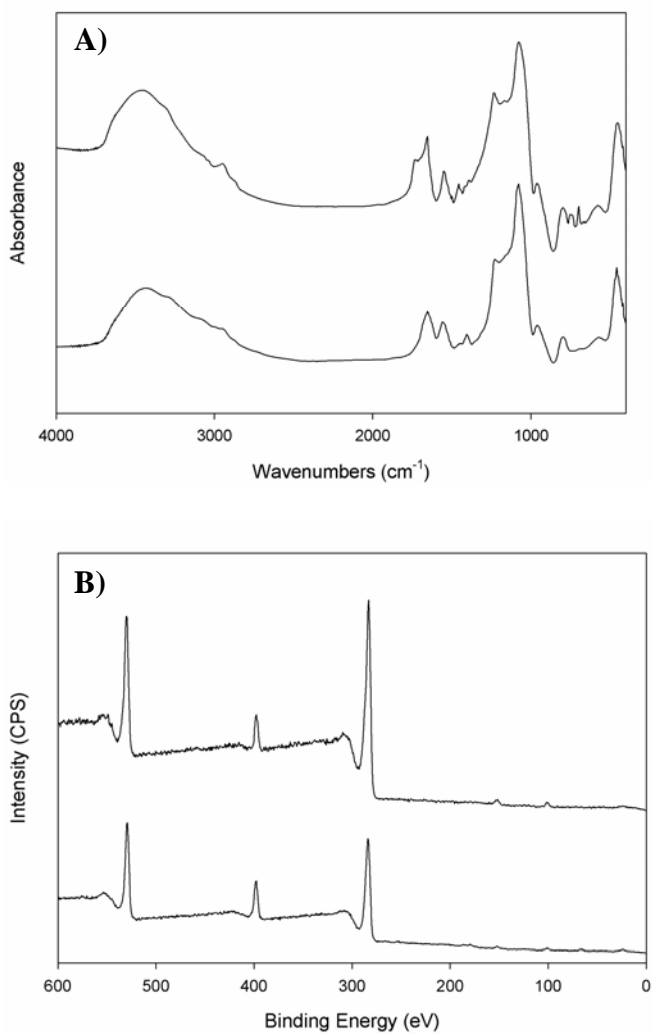


Figure 6.6 A) IR and B) XPS spectra of **PZK&PBG/SH-MMSS** before (top) and after (bottom) deprotection.

6.3.2.2 *TGA and Porosimetry*

Porosimetry and TGA results are tabulated below in Table 6.1. N₂ adsorption results show that upon polymerization there is no porosity at 77K. Following deprotection, this result persists. This result is in accord with the results on the externally grafted SBA-15 in Chapter V and is likely due to pore mouth blockage. TGA shows weight losses and mmoles of converted monomer of 42.8wt% (1.7mmol) for **PZK/SH-MMSS**, 50.4wt% (3.1mmol) for **PBG/SH-MMSS** and 42.6wt% (1.9mmol, assuming 1:1 copolymer) for **PZK&PBG/SH-MMSS**. These values are smaller than those in the previous chapter but make sense when the smaller external surface area due to the radially aligned pores is taken into account. The polymer content of the **PBG/SH-MMSS** is significantly larger than **PZK/SH-MMSS**, probably a result of the less bulky side chain of the L-Glu(OBz)-NCA. The values after deprotection are in good agreement with expectations, excluding PK/SH-MMSS, which has a higher weight loss than prior to deprotection. The reason for this is possibly due to trapped HBr in the form of amine salts or otherwise. A substantial bromine presence is observed in the XPS for this sample (Figure 6.4B).

Table 6.1 Adsorption and TGA data of OMS sphere hybrids.

Sample	S(a _s) [m ² /g]	V _p ^a [cm ³ /g]	d _p (BJH) [nm]	Organic [wt%]	NCA Covered ^b [mmol/g FS]
NH ₂ /SH-MMSS	1640	0.67	2.2	17.1	
PZK/SH-MMSS	----	n.p.	----	42.8	1.7
PK/SH-MMSS	----	n.p.	----	46.7	
PBG/SH-MMSS	----	n.p.	----	50.4	3.1
PG/SH-MMSS	----	n.p.	----	40.3	
PZK&PBG/SH-MMSS	----	n.p.	----	42.6	1.9 ^c
PK&PG/SH-MMSS	----	n.p.	----	35.2	

^a Recorded at p/p₀ = 0.9; n.p. = non-porous

^b Calculated from TGA data after subtracting organosilane and residual Pluronic contributions.

^c Assumes 1:1 monomer ratio in grafted polymer

6.3.2.3 SEM

Scanning electron microscopy images of the polypeptide grafted samples show significant polymer on the outer surface as evident by the surface deformation when compared with the smooth surfaces of **NH₂/SH-MMSS** (Figure 6.7). There is similarly noticeable interaction between the particles not present prior to polymerization. Both of these add support for the polymer layer being on the outer surface as indicated by the XPS results.

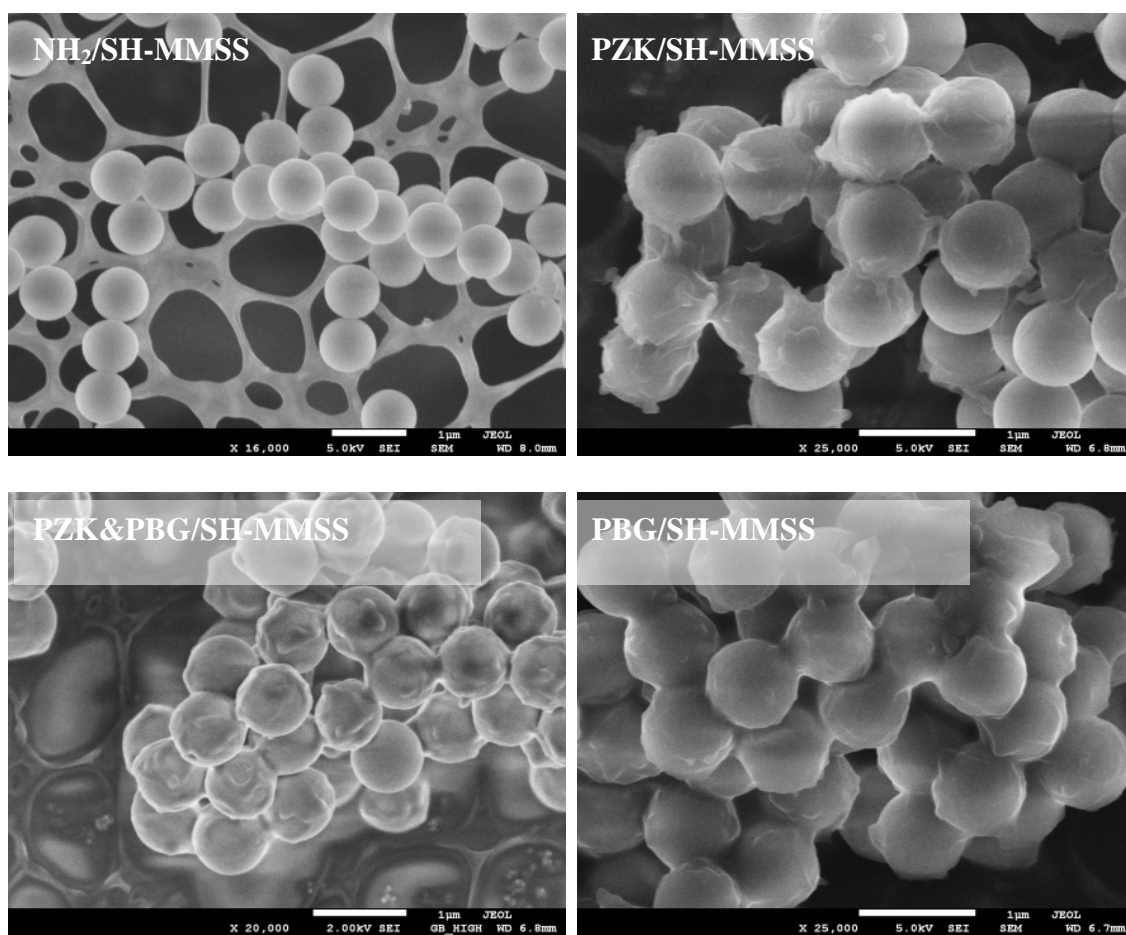


Figure 6.7 SEM images of the OMS spheres before and after polymerization. The white scale bars represent 1 μm in each image.

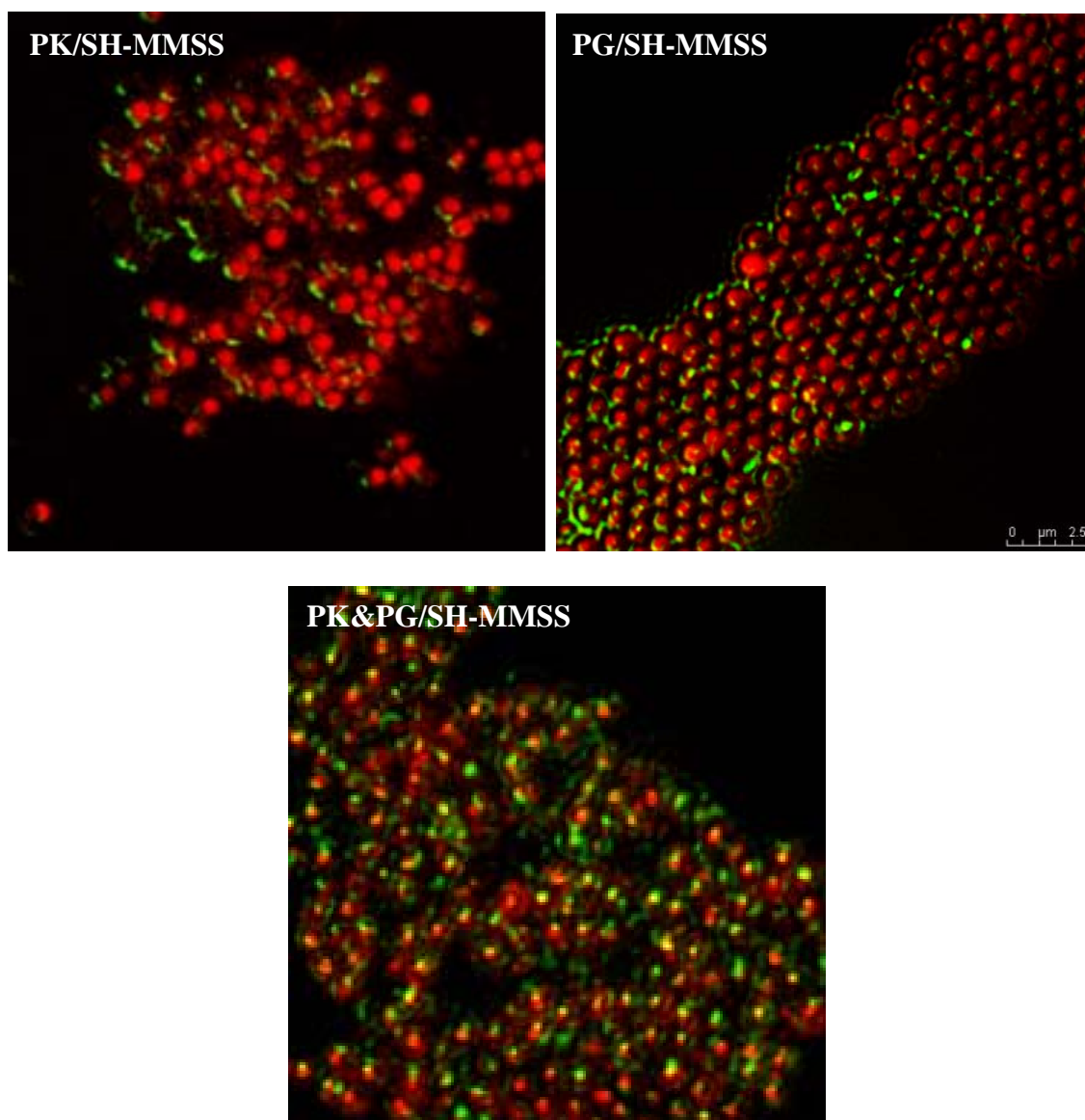


Figure 6.8 Confocal images showing the uptake of amine and thiol-selective dyes in the various hybrids. The scale bar on the upper right image applies to all three images.

6.3.2.4 *Dye Uptake by Confocal Microscopy*

BODIPY-TMR and NHS-fluorescein dyes were used again on the polymerized samples to visualize the hybrids by confocal microscopy (Figure 6.8). Their use serves two purposes: 1) to identify the regions occupied by the polypeptide and thiols; and 2) to determine whether the thiols within the pores are accessible at conditions much less extreme than those used in N₂ adsorption (i.e. RT vs. 77K). Regarding the first point, there is again a clear separation between the two dyes and thus the two functionalities, with the polypeptide being on the outer surface. The red BODIPY dye was reacted first and the images support that it infiltrates the pores of the particles. The fluorescein was added second and again only reacts with the outer surface. It is interesting that **PG-MMSS** appears to form an ordered hexagonal arrangement not present in the other two samples.

6.4 Conclusions

As reported in the literature, radially growing OMS spheres is an effective way to selectively position thiols in the particle core. In this work, it was demonstrated that amine-functionalization and subsequent NCA-polymerization of such nanoparticles yields a surface segregated bifunctional material composed of polypeptides on the outer surface and thiols in the core. Polylysine, polyglutamic acid and a random copolymer were grafted to the outer surface. The thiol-functionalized core is accessible following polymerization as evidenced by the binding of BODIPY-TMR, a thiol selective dye. As these polypeptides are polyelectrolytes with different pIs, these materials are potentially

interesting for controlled release of a drug or other agent bound to the thiol-functionalized core, as well as other applications. Future work resulting from these studies will look at the uptake and release of a dye or chemical probe under various conditions.

CHAPTER VII

CONCLUSIONS AND FUTURE WORK

7.1 Conclusions

In this dissertation, we explored the synthesis and design of polypeptide-OMS hybrid materials. By combining the properties of polypeptides and OMS through the understanding of the OMS hybrid and polymer brush literature, new and interesting materials have been synthesized. New hybrid synthesis paradigms have also been developed.

Our first objective in this regard was to demonstrate the ability to graft polypeptides to planar surfaces, colloidal particles, and ordered mesoporous silica using solution methods. This issue was addressed in Chapters III and IV. Though our initial efforts to synthesize polypeptide brushes on silicon wafers proved unsuccessful, we were able to tether polypeptides in high densities to the surfaces of colloidal silica and ordered mesoporous silica. This difference in reactivity between what should be comparable materials may be due to multiple factors, including a) the rapid formation of dense oligomeric β -sheets on planar surfaces which prevent significant growth as suggested by Chang and Frank;¹⁹⁰ b) the lower surface area and higher sensitivity to impurities of planar silicon as suggested by Schouten;¹⁹⁸ and c) chemical differences in the nature of the respective surfaces, such as surface silanol densities.

The promising results of Chapter III with respect to OMS grafts, led to the progression to work on OMS materials and the desire to be able to design polypeptide-

OMS hybrids with different properties by manipulating the synthesis parameters: the second objective of this dissertation. In Chapter IV, we investigated the effects of OMS phase/porosity, initiator density and monomer identity on polypeptide hybrid design. Hybrids were synthesized on three different OMS materials (MCM-41, SBA-15, and KIT-6) using two different monomers (Lys(Z)-NCA) and (Ala-NCA). It was demonstrated that high density grafts could be synthesized with each of the variables having a significant impact on the resulting hybrid material, particularly on porosity and organic content. For the poly-L-alanine hybrids, porosity could be controlled by altering the initial amine loading while maintaining the same polymer loading. Pore confinement effects were also noted and cited as the possible cause for the tunability of the poly-L-alanine hybrids.

The third objective related to extending this concept by developing synthesis paradigms to selectively graft polypeptides to the inner and outer surfaces of OMS. Specifically, we investigated the grafting of poly-L-lysine from the widely used SBA-15. Two sets of materials were synthesized using the OMS template barrier approach: poly-L-lysine alone and poly-L-lysine opposite thiols. A modified method using microwaves was developed for the poly-L-lysine/thiol samples to effectively graft amines or thiols to the external surface and to extract the Pluronic OMS template. A particularly interesting result was the ability to open and close the pores of these hybrids by the reversible swelling of the polypeptide layer.

The final objective was the focus of Chapter VI: synthesizing novel polypeptide grafts to monodisperse OMS spheres with thiol cores. Here, the monodisperse OMS

spheres served as a model system for the external grafting of poly-L-lysine and poly-L-glutamic acid. The effects of grafting can be more clearly seen here than in the irregularly shaped SBA-15 particles/aggregates. The accessibility of the internal thiols to a thiol-selective fluorescent dye shows the potential of these hybrids for applications such as controlled uptake/release.

7.2 Future Work

Based on the results of this dissertation, there are many possible directions future work could be taken. In the discussion below these are constructed around fundamental and application-based studies. Below, suggested future work in both of these is discussed.

7.2.1 Fundamental Studies

7.2.1.1 Conformation/Orientation

One of the most interesting characteristics of polypeptides is their ability to fold into distinct conformations (e.g. α -helices and β -sheets) in different environmental conditions. Though IR may be used to give conformation data, broad peaks, water adsorption, and small wavenumber differences between the various states make such discernments problematic. IR data for the OMS hybrids in Chapter III seem to indicate the peptides form α -helices; however, similar IR values obtained for both the acidified and neutral lysine chains were unexpected. This is likely due to the ambiguity inherent in such analyses.

Circular dichroism (CD) offers more definite conformational analysis and is thus appropriate to clarify and extend these investigations. It is for this reason CD was employed for the initial work on silicon wafers. As direct transmittance measurements on powder samples are more difficult due to lack of transparency, diffuse-reflectance CD should be used. Experiments should be performed investigating the effect of pH on conformation as well as that of the counter-ion (e.g. Cl^- , Br^- , and HSO_3^-). It would be very interesting to compare the differences in the relationship between conformation and pH of internally grafted polypeptides with those grafted externally, from planar surfaces, and free in solution. The latter two have been studied extensively in the literature, especially for polylysine and polyglutamic acid.^{195,196,198,233,234}

A feature of surface-grafted polymers, especially relevant to polypeptides in helical conformations, is the orientation relative to the surface. As noted in Chapter I, this has been studied for polypeptide grafts on planar surfaces.^{199,200} Again, it would be very interesting and useful to compare these results. In literature reports, the preferred method to determine orientation is through IR by measuring the relative intensities of the amine I and II bands. This approach requires anisotropy of the polymer layer. As such, this approach cannot be used for powder samples directly as it would sample polypeptides in every direction, regardless of preferred orientation within the pores. One possible method to make such analysis possible would be to graft polypeptides to oriented OMS thin films with pore geometry similar to those used in the samples in this dissertation. Lamellar films would be the easiest starting point and would enable the determination of orientation effects related to confinement. Later work could build upon

this work looking at hexagonal and cubic films. The use of solid state NMR with ^{13}C enriched polypeptide-OMS thin films hybrids would be another approach worthy of study.

7.2.1.2 Polymer Swelling Effects

Another area deserving further study is the polymer swelling effect noted in Chapter V as it relates to porosity. A detailed investigation should be conducted looking at how different counter-ions and pH conditions affect the porosity of the hybrids. Such studies should look at both N_2 adsorption measurements and chemical probes at RT. These measurements when performed in conjunction with the conformation studies described above would allow a very complete understanding of environmental factors on the polypeptide layer and would aid future application studies.

7.2.1.3 Other Areas

In addition to these investigations, there are a number of other areas of possible future research. One such area is the further study of the polypeptide molecular weight in the externally and internally grafted samples described in Chapters V and VI.

7.2.2 Applications

As this work has primarily centered on synthesis, characterization and design of model hybrid systems, further work should also more closely explore specific applications and incorporation of polypeptides on industrially relevant supports.

7.2.2.1 *Membrane Separations/Chromatography*

The ability to synthesize dense brushes with controllable porosity and organic content suggests membrane and separation related applications. Such studies would undoubtedly investigate the separation of chiral compounds. Initial studies could look at using capillary columns in HPLC to analyze the potential of the hybrids synthesized in Chapter IV toward chiral separations. Additionally, polypeptides could be grafted to industrially relevant supports such as Anopore™ and Membralox® membranes as has been done with dendrimers in our lab.^{259,260}

7.2.2.2 *Controlled Uptake/Release*

The investigations on selective grafting on SBA-15 and OMS spheres in Chapters V and VI suggest studies on the applicability of these hybrids in controlled release and molecular-gating. As the thiols in the OMS spheres have been shown to be accessible to chemical probes, this would be the most likely starting point. The conformational analysis described above would be very useful in these investigations. After careful selection of a reversibly bound thiol-selective probe, possible candidates include BODIPY-TMR thiosulfate and didansyl cystine, a series of experiments could be conducted investigating the effect of pH on the uptake and release of these compounds and the effects of the type of polypeptide used (polylysine, polyglutamic acid, or the random copolymer). These results should be compared with those for simple amine-grafted OMS spheres.

7.2.2.3 *Sensing*

As polypeptides are also stimuli responsive with various functionalities available, studies should also look at applications in sensing. Again, the conformational analyses described above would be invaluable to these studies. One could envision the binding of various chemical agents to the polypeptide side chain group altering the conformational state of the polypeptide and thus acting as a sensor.

7.2.2.4 *Catalysis*

A final application area of interest is catalysis. Though initial catalytic studies with the hybrids described in Chapter IV with the nitroaldol reaction showed only limited catalytic activity, the use of other solvents more capable of solvating the polymer and the testing of other reactions may yield more promising results. Similarly, it would be very interesting to observe the differences in catalytic activity due to the external and internal grafting of the polypeptides as described in Chapter V.

REFERENCES

- (1) Kitchen, K. A. *On the Reliability of the Old Testament*; Wm. B. Eerdmans: Grand Rapids, MI, 2003.
- (2) Kickelbick, G. *Hybrid Materials*; Wiley: Weinheim, 2007.
- (3) Gomez-Romero, P.; Sanchez, C. *Functional Hybrid Materials*; Wiley: Weinheim, 2004.
- (4) Leuchs, H. *Berichte Der Deutschen Chemischen Gesellschaft* **1906**, *39*, 857-861.
- (5) Leuchs, H.; Felser, H. *Berichte Der Deutschen Chemischen Gesellschaft* **1908**, *41*, 1726-1735.
- (6) Leuchs, H.; Manasse, W. *Berichte Der Deutschen Chemischen Gesellschaft* **1907**, *40*, 3235-3249.
- (7) Sim, T. B.; Rapoport, H. *Journal of Organic Chemistry* **1999**, *64*, 2532-2536.
- (8) Kataoka, K.; Kwon, G. S.; Yokoyama, M.; Okano, T.; Sakurai, Y. *Journal of Controlled Release* **1993**, *24*, 119-132.
- (9) Nakanishi, T.; Fukushima, S.; Okamoto, K.; Suzuki, M.; Matsumura, Y.; Yokoyama, M.; Okano, T.; Sakurai, Y.; Kataoka, K. *Journal of Controlled Release* **2001**, *74*, 295-302.
- (10) Takaki, R.; Asami, Y.; Hunada, N. O. *Polymer Bulletin* **1987**, *18*, 105-110.
- (11) Hawkins, K. M.; Wang, S. S. S.; Ford, D. M.; Shantz, D. F. *Journal of the American Chemical Society* **2004**, *126*, 9112-9119.
- (12) Jan, J. S.; Lee, S. J.; Carr, C. S.; Shantz, D. F. *Chemistry of Materials* **2005**, *17*, 4310-4317.
- (13) Jan, J. S.; Shantz, D. F. *Chemical Communications* **2005**, 2137-2139.
- (14) Jan, J. S.; Shantz, D. F. *Advanced Materials* **2007**, *19*, 2951-2956.
- (15) Brinker, C. J.; Scherer, G. W. *Sol-gel Science: The Physics and Chemistry of Sol-gel Processing*; Academic Press: San Diego, CA, 1990.
- (16) Iler, R. K. *The Chemistry of Silica*; Wiley: New York, 1979.
- (17) Meakin, P. *Journal of Sol-Gel Science and Technology* **1999**, *15*, 97-117.

- (18) Stober, W.; Fink, A.; Bohn, E. *Journal of Colloid and Interface Science* **1968**, *26*, 62.
- (19) Barrer, R. M.; Denny, P. J. *Journal of the Chemical Society* **1961**, 971-982.
- (20) Davis, M. E.; Lobo, R. F. *Chemistry of Materials* **1992**, *4*, 756-768.
- (21) Cheng, C. H.; Shantz, D. F. *Current Opinion in Colloid & Interface Science* **2005**, *10*, 188-194.
- (22) Cheng, C. H.; Shantz, D. F. *Journal of Physical Chemistry B* **2005**, *109*, 13912-13920.
- (23) Cheng, C. H.; Shantz, D. F. *Journal of Physical Chemistry B* **2006**, *110*, 313-318.
- (24) Fedeyko, J. M.; Egolf-Fox, H.; Fickel, D. W.; Vlachos, D. G.; Lobo, R. F. *Langmuir* **2007**, *23*, 4532-4540.
- (25) Drews, T. O.; Tsapatsis, M. *Microporous and Mesoporous Materials* **2007**, *101*, 97-107.
- (26) Kumar, S.; Davis, T. M.; Ramanan, H.; Penn, R. L.; Tsapatsis, M. *Journal of Physical Chemistry B* **2007**, *111*, 3398-3403.
- (27) Alfredsson, V.; Anderson, M. W. *Chemistry of Materials* **1996**, *8*, 1141-1146.
- (28) Beck, J. S.; Vartuli, J. C.; Roth, W. J.; Leonowicz, M. E.; Kresge, C. T.; Schmitt, K. D.; Chu, C. T. W.; Olson, D. H.; Sheppard, E. W.; McCullen, S. B.; Higgins, J. B.; Schlenker, J. L. *Journal of the American Chemical Society* **1992**, *114*, 10834-10843.
- (29) Zhao, D. Y.; Feng, J. L.; Huo, Q. S.; Melosh, N.; Fredrickson, G. H.; Chmelka, B. F.; Stucky, G. D. *Science* **1998**, *279*, 548-552.
- (30) Zhao, D. Y.; Huo, Q. S.; Feng, J. L.; Chmelka, B. F.; Stucky, G. D. *Journal of the American Chemical Society* **1998**, *120*, 6024-6036.
- (31) Ford, D. M.; Simanek, E. E.; Shantz, D. F. *Nanotechnology* **2005**, *16*, S458-S475.
- (32) Kleitz, F.; Choi, S. H.; Ryoo, R. *Chemical Communications* **2003**, *17*, 2136-2137.
- (33) Wan, Y.; Zhao, D. Y. *Chemical Reviews* **2007**, *107*, 2821-2860.

- (34) Huo, Q. S.; Margolese, D. I.; Ciesla, U.; Feng, P. Y.; Gier, T. E.; Sieger, P.; Leon, R.; Petroff, P. M.; Schuth, F.; Stucky, G. D. *Nature* **1994**, *368*, 317-321.
- (35) Bagshaw, S. A.; Prouzet, E.; Pinnavaia, T. J. *Science* **1995**, *269*, 1242-1244.
- (36) Moller, K.; Bein, T. *Chemistry of Materials* **1998**, *10*, 2950-2963.
- (37) Sanchez, C.; Ribot, F. *New Journal of Chemistry* **1994**, *18*, 1007.
- (38) Hoffmann, F.; Cornelius, M.; Morell, J.; Froba, M. *Angewandte Chemie-International Edition* **2006**, *45*, 3216-3251.
- (39) Lim, M. H.; Stein, A. *Chemistry of Materials* **1999**, *11*, 3285-3295.
- (40) Burkett, S. L.; Sims, S. D.; Mann, S. *Chemical Communications* **1996**, 1367-1368.
- (41) Fowler, C. E.; Burkett, S. L.; Mann, S. *Chemical Communications* **1997**, 1769-1770.
- (42) Feng, X.; Fryxell, G. E.; Wang, L. Q.; Kim, A. Y.; Liu, J.; Kemner, K. M. *Science* **1997**, *276*, 923-926.
- (43) Lim, M. H.; Blanford, C. F.; Stein, A. *Journal of the American Chemical Society* **1997**, *119*, 4090-4091.
- (44) Lim, M. H.; Blanford, C. F.; Stein, A. *Chemistry of Materials* **1998**, *10*, 467-470.
- (45) Lim, M. H.; Stein, A. *Chemistry of Materials* **1999**, *11*, 3285-3295.
- (46) McKittrick, M. W.; Jones, C. W. *Chemistry of Materials* **2003**, *15*, 1132-1139.
- (47) Defaud, V.; Davis, M. E. *Journal of the American Chemical Society* **2003**, *125*, 9403-9413.
- (48) Margelefsky, E. L.; Zeidan, R. K.; Davis, M. E. *Chemical Society Reviews* **2008**, *37*, 1118-1126.
- (49) Bass, J. D.; Anderson, S. L.; Katz, A. *Angewandte Chemie-International Edition* **2003**, *42*, 5219-5222.
- (50) Bass, J. D.; Katz, A. *Chemistry of Materials* **2003**, *15*, 2757-2763.
- (51) Bass, J. D.; Katz, A. *Chemistry of Materials* **2006**, *18*, 1611-1620.

- (52) Huh, S.; Wiench, J. W.; Yoo, J.-C.; Pruski, M.; Lin, V. S. Y. *Chemistry of Materials* **2003**, *15*, 4247-4256.
- (53) Huh, S.; Wiench, J. W.; Yoo, J.-C.; Pruski, M.; Lin, V. S. Y. *Chemistry of Materials* **2003**, *15*, 2364-2365.
- (54) Huh, S.; Chen, H.-T.; Wiench, J. W.; Pruski, M.; Lin, V. S. Y. *Journal of the American Chemical Society* **2004**, *126*, 1010-1011.
- (55) Zhao, X. S.; Bao, X. Y.; Guo, W. P.; Lee, F. Y. *Materials Today* **2006**, *9*, 32-39.
- (56) Acosta, E. J.; Carr, C. S.; Simanek, E. E.; Shantz, D. F. *Advanced Materials* **2004**, *16*, 985-989.
- (57) Reynhardt, J. P. K.; Yang, Y.; Sayari, A.; Alper, H. *Advanced Functional Materials* **2005**, *15*, 1641-1646.
- (58) Yoo, S.; Lunn, J. D.; Gonzalez, S.; Ristich, J. A.; Simanek, E. E.; Shantz, D. F. *Chemistry of Materials* **2006**, *18*, 2935-2942.
- (59) Lunn, J. D. *Synthesis and Application of Melamine-based Dendrimer/SBA-15 Hybrid Materials*; Texas A&M University: College Station, TX, 2006.
- (60) Wang, Q. Q.; Guerrero, V. V.; Ghosh, A.; Yeu, S.; Lunn, J. D.; Shantz, D. F. *Journal of Catalysis*, *269*, 15-25.
- (61) Reynhardt, J. P. K.; Yang, Y.; Sayari, A.; Alper, H. *Chemistry of Materials* **2004**, *16*, 4095-4102.
- (62) Young, R. J. L., P. A. *Introduction to Polymers*; 2nd ed.; Nelson Thornes: Cheltenham, U.K., 1991.
- (63) Allcock, H. R. L., F. W. *Contemporary Polymerization Chemistry*; 2nd ed.; Prentice Hall: Englewood Cliffs, NJ, 1990.
- (64) Szwarc, M. *Nature* **1956**, *178*, 1168-1169.
- (65) Szwarc, M.; Levy, M.; Milkovich, R. *Journal of the American Chemical Society* **1956**, *78*, 2656-2657.
- (66) Levy, M.; Cohenbosidan, F. *Polymer* **1960**, *1*, 517-518.
- (67) Szwarc, M.; Rembaum, A. *Journal of Polymer Science* **1956**, *22*, 189-191.
- (68) Hsieh, H.; Tobolsky, A. V. *Journal of Polymer Science* **1957**, *25*, 245-247.

- (69) Hsieh, H. L. *Journal of Polymer Science Part A-General Papers* **1965**, 3, 163.
- (70) Stearns, R. S.; Forman, L. E. *Journal of Polymer Science* **1959**, 41, 381-397.
- (71) Hsieh, H.; Quirk, R. P. *Anionic Polymerization: Principles and Practical Applications*; Marcel Dekker: New York, 1996.
- (72) Baskaran, D.; Muller, A. H. E. *Progress in Polymer Science* **2007**, 32, 173-219.
- (73) Fuoss, R. M. *Journal of the American Chemical Society* **1958**, 80, 5059-5061.
- (74) Winstein, S.; Clippinger, E.; Fainberg, A. H.; Robinson, G. C. *Journal of the American Chemical Society* **1954**, 76, 2597-2598.
- (75) Barnikol, W. K.; Schulz, G. V. *Zeitschrift Fur Physikalische Chemie-Frankfurt* **1965**, 47, 89.
- (76) Shimomura, T.; Smid, J.; Szwarc, M. *Journal of the American Chemical Society* **1967**, 89, 5743-5749.
- (77) Bywater, S.; Worsfold, D. J. *Canadian Journal of Chemistry-Revue Canadienne De Chimie* **1962**, 40, 1564.
- (78) Welch, F. J. *Journal of the American Chemical Society* **1960**, 82, 6000-6005.
- (79) Carlotti, S.; Menoret, S.; Barabanova, A.; Desbois, P.; Deffieux, A. *Polymer* **2005**, 46, 6836-6843.
- (80) Desbois, P.; Fontanille, M.; Deffieux, A.; Warzelhan, V.; Latsch, S.; Schade, C. *Macromolecular Chemistry and Physics* **1999**, 200, 621-628.
- (81) Roovers, J. E. L.; Bywater, S. *Transactions of the Faraday Society* **1966**, 62, 1876.
- (82) Guyot, A.; Vialle, J. *Journal of Macromolecular Science-Chemistry* **1970**, A4, 107.
- (83) Baskaran, D.; Chakrapani, S.; Sivaram, S. *Macromolecules* **1995**, 28, 7315-7317.
- (84) Baskaran, D.; Muller, A. H. E.; Sivaram, S. *Macromolecular Chemistry and Physics* **2000**, 201, 1901-1911.
- (85) Johann, C.; Muller, A. H. E. *Makromolekulare Chemie-Rapid Communications* **1981**, 2, 687-691.

- (86) Marchal, J.; Gnanou, Y.; Fontanille, M. *Macromolecular Symposia* **1996**, *107*, 27-41.
- (87) Varshney, S. K.; Jerome, R.; Bayard, P.; Jacobs, C.; Fayt, R.; Teyssie, P. *Macromolecules* **1992**, *25*, 4457-4463.
- (88) Wang, J. S.; Jerome, R.; Bayard, P.; Baylac, L.; Patin, M.; Teyssie, P. *Macromolecules* **1994**, *27*, 4615-4620.
- (89) Baskaran, D.; Sivaram, S. *Macromolecules* **1997**, *30*, 1550-1555.
- (90) Ishizone, T.; Yoshimura, K.; Yanase, E.; Nakahama, S. *Macromolecules* **1999**, *32*, 955-957.
- (91) Kunkel, D.; Muller, A. H. E.; Janata, M.; Lochmann, L. *Makromolekulare Chemie-Macromolecular Symposia* **1992**, *60*, 315-326.
- (92) Lochmann, L.; Kolarik, J.; Doskocilova, D.; Vozka, S.; Trekoval, J. *Journal of Polymer Science Part A-Polymer Chemistry* **1979**, *17*, 1727-1737.
- (93) Lochmann, L.; Muller, A. H. E. *Makromolekulare Chemie-Macromolecular Chemistry and Physics* **1990**, *191*, 1657-1664.
- (94) Varshney, S. K.; Bayard, P.; Jacobs, C.; Jerome, R.; Fayt, R.; Teyssie, P. *Macromolecules* **1992**, *25*, 5578-5584.
- (95) Varshney, S. K.; Hautekeer, J. P.; Fayt, R.; Jerome, R.; Teyssie, P. *Macromolecules* **1990**, *23*, 2618-2622.
- (96) Marchal, J.; Fontanille, M.; Gnanou, Y. *Macromolecular Symposia* **1998**, *132*, 249-262.
- (97) Wang, J. S.; Jerome, R.; Bayard, P.; Patin, M.; Teyssie, P.; Vuillemin, B.; Heim, P. *Macromolecules* **1994**, *27*, 4635-4638.
- (98) Wang, J. S.; Jerome, R.; Bayard, P.; Teyssie, P. *Macromolecules* **1994**, *27*, 4908-4913.
- (99) Zundel, T.; Zune, C.; Teyssie, P.; Jerome, R. *Macromolecules* **1998**, *31*, 4089-4092.
- (100) Sogah, D. Y.; Hertler, W. R.; Webster, O. W.; Cohen, G. M. *Macromolecules* **1987**, *20*, 1473-1488.
- (101) Miyamoto, M.; Sawamoto, M.; Higashimura, T. *Macromolecules* **1984**, *17*, 265-268.

- (102) Higashimura, T.; Miyamoto, M.; Sawamoto, M. *Macromolecules* **1985**, *18*, 611-616.
- (103) Goethals, E. J.; Du Prez, F. *Progress in Polymer Science* **2007**, *32*, 220-246.
- (104) Kamigaito, M.; Sawamoto, M.; Higashimura, T. *Journal of Polymer Science Part A-Polymer Chemistry* **1993**, *31*, 2987-2994.
- (105) Kamigaito, M.; Yamaoka, K.; Sawamoto, M.; Higashimura, T. *Macromolecules* **1992**, *25*, 6400-6406.
- (106) Cho, C. G.; Feit, B. A.; Webster, O. W. *Macromolecules* **1990**, *23*, 1918-1923.
- (107) Cho, C. G.; Feit, B. A.; Webster, O. W. *Macromolecules* **1992**, *25*, 2081-2085.
- (108) Haucourt, N. H.; Peng, L. B.; Goethals, E. J. *Macromolecules* **1994**, *27*, 1329-1333.
- (109) Matyjaszewski, K.; Lin, C. H. *Makromolekulare Chemie-Macromolecular Symposia* **1991**, *47*, 221-237.
- (110) Cramail, H.; Deffieux, A.; Nuyken, O. *Makromolekulare Chemie-Rapid Communications* **1993**, *14*, 17-27.
- (111) Haucourt, N. H.; Kashikar, S.; Goethals, E. J. *Makromolekulare Chemie-Rapid Communications* **1993**, *14*, 489-494.
- (112) Lubnin, A. V.; Kennedy, J. P. *Polymer Bulletin* **1992**, *29*, 9-13.
- (113) Nuyken, O.; Kroner, H. *Makromolekulare Chemie-Macromolecular Chemistry and Physics* **1990**, *191*, 1-16.
- (114) Peng, L.; Haucourt, N.; Goethals, E. J. *Macromolecular Rapid Communications* **1994**, *15*, 197-202.
- (115) Kennedy, J. P.; Smith, R. A. *Journal of Polymer Science Part A-Polymer Chemistry* **1980**, *18*, 1539-1546.
- (116) Ivan, B.; Kennedy, J. P. *Macromolecules* **1990**, *23*, 2880-2885.
- (117) Paulo, C.; Puskas, J. E.; Angepat, S. *Macromolecules* **2000**, *33*, 4634-4638.
- (118) Storey, R. F.; Donnalley, A. B. *Macromolecules* **2000**, *33*, 53-59.
- (119) Penczek, S.; Cypriak, M.; Duda, A.; Kubisa, P.; Slomkowski, S. *Progress in Polymer Science* **2007**, *32*, 247-282.

- (120) Kricheldorf, H. R. *Angewandte Chemie-International Edition* **2006**, *45*, 5752-5784.
- (121) Deming, T. J. *Nature* **1997**, *390*, 386-389.
- (122) Deming, T. J. *Journal of the American Chemical Society* **1998**, *120*, 4240-4241.
- (123) Lu, H.; Cheng, J. J. *Journal of the American Chemical Society* **2008**, *130*, 12562-12563.
- (124) Richardson, W. H. O. N., H. E. *Comprehensive Chemical Kinetics*; Elsevier: Amsterdam, 1972; Vol. 5.
- (125) Georges, M. K.; Veregin, R. P. N.; Kazmaier, P. M.; Hamer, G. K. *Macromolecules* **1993**, *26*, 2987-2988.
- (126) Braunecker, W. A.; Matyjaszewski, K. *Progress in Polymer Science* **2007**, *32*, 93-146.
- (127) Benoit, D.; Chaplinski, V.; Braslau, R.; Hawker, C. J. *Journal of the American Chemical Society* **1999**, *121*, 3904-3920.
- (128) Benoit, D.; Grimaldi, S.; Robin, S.; Finet, J. P.; Tordo, P.; Gnanou, Y. *Journal of the American Chemical Society* **2000**, *122*, 5929-5939.
- (129) Bertin, D.; Chauvin, F.; Marque, S.; Tordo, P. *Macromolecules* **2002**, *35*, 3790-3791.
- (130) Studer, A.; Harms, K.; Knoop, C.; Muller, C.; Schulte, T. *Macromolecules* **2004**, *37*, 27-34.
- (131) Studer, A.; Schulte, T. *Chemical Record* **2005**, *5*, 27-35.
- (132) Hawker, C. J. *Journal of the American Chemical Society* **1994**, *116*, 11185-11186.
- (133) Hawker, C. J.; Barclay, G. G.; Orellana, A.; Dao, J.; Devonport, W. *Macromolecules* **1996**, *29*, 5245-5254.
- (134) Solomon, D. H. *Journal of Polymer Science Part A-Polymer Chemistry* **2005**, *43*, 5748-5764.
- (135) Braunecker, W. A.; Itami, Y.; Matyjaszewski, K. *Macromolecules* **2005**, *38*, 9402-9404.

- (136) Le Grogneq, E.; Claverie, R.; Poli, R. *Journal of the American Chemical Society* **2001**, *123*, 9513-9524.
- (137) Debuigne, A.; Caille, J. R.; Detrembleur, C.; Jerome, R. *Angewandte Chemie-International Edition* **2005**, *44*, 3439-3442.
- (138) Debuigne, A.; Caille, J. R.; Jerome, R. *Angewandte Chemie-International Edition* **2005**, *44*, 1101-1104.
- (139) Debuigne, A.; Caille, J. R.; Jerome, R. *Macromolecules* **2005**, *38*, 5452-5458.
- (140) Wayland, B. B.; Poszmik, G.; Mukerjee, S. L.; Fryd, M. *Journal of the American Chemical Society* **1994**, *116*, 7943-7944.
- (141) Gossage, R. A.; Van De Kuil, L. A.; Van Koten, G. *Accounts of Chemical Research* **1998**, *31*, 423-431.
- (142) Minisci, F. *Accounts of Chemical Research* **1975**, *8*, 165-171.
- (143) Pintauer, T.; McKenzie, B.; Matyjaszewski, K. In *Advances in Controlled/Living Radical Polymerization*; Matyjaszewski, K., Ed.; American Chemical Society: Washington, D.C., 2003; Vol. 854, p 130-147.
- (144) He, J. P.; Li, L.; Yang, Y. L. *Macromolecules* **2000**, *33*, 2286-2289.
- (145) Matyjaszewski, K.; Xia, J. H. *Chemical Reviews* **2001**, *101*, 2921-2990.
- (146) Tsarevsky, N. V.; Braunecker, W. A.; Tang, W.; Brooks, S. J.; Matyjaszewski, K.; Weisman, G. R.; Wong, E. H. *Journal of Molecular Catalysis A-Chemical* **2006**, *257*, 132-140.
- (147) Tang, W.; Tsarevsky, N. V.; Matyjaszewski, K. *Journal of the American Chemical Society* **2006**, *128*, 1598-1604.
- (148) Gillies, M. B.; Matyjaszewski, K.; Norrby, P. O.; Pintauer, T.; Poli, R.; Richard, P. *Macromolecules* **2003**, *36*, 8551-8559.
- (149) Gaynor, S. G.; Wang, J. S.; Matyjaszewski, K. *Macromolecules* **1995**, *28*, 8051-8056.
- (150) Iovu, M. C.; Matyjaszewski, K. *Macromolecules* **2003**, *36*, 9346-9354.
- (151) Goto, A.; Kwak, Y.; Fukuda, T.; Yamago, S.; Iida, K.; Nakajima, M.; Yoshida, J. *Journal of the American Chemical Society* **2003**, *125*, 8720-8721.

- (152) Grishin, D. F.; Moikin, A. A. *Vysokomolekulyarnye Soedineniya Seriya a & Seriya B* **1998**, *40*, 1266-1270.
- (153) Moad, C. L.; Moad, G.; Rizzardo, E.; Thang, S. H. *Macromolecules* **1996**, *29*, 7717-7726.
- (154) Chiefari, J.; Chong, Y. K.; Ercole, F.; Krstina, J.; Jeffery, J.; Le, T. P. T.; Mayadunne, R. T. A.; Meijs, G. F.; Moad, C. L.; Moad, G.; Rizzardo, E.; Thang, S. H. *Macromolecules* **1998**, *31*, 5559-5562.
- (155) Destarac, M.; Brochon, C.; Catala, J. M.; Wilczewska, A.; Zard, S. Z. *Macromolecular Chemistry and Physics* **2002**, *203*, 2281-2289.
- (156) Moad, G.; Rizzardo, E.; Thang, S. H. *Australian Journal of Chemistry* **2005**, *58*, 379-410.
- (157) Chong, Y. K.; Krstina, J.; Le, T. P. T.; Moad, G.; Postma, A.; Rizzardo, E.; Thang, S. H. *Macromolecules* **2003**, *36*, 2256-2272.
- (158) Favier, A.; Charreyre, M. T. *Macromolecular Rapid Communications* **2006**, *27*, 653-692.
- (159) Clayden, J. G., N.; Warren, S.; Wothers, P. *Organic Chemistry*; Oxford: New York, 2001.
- (160) Truett, W. L.; Johnson, D. R.; Robinson, I. M.; Montague, B. A. *Journal of the American Chemical Society* **1960**, *82*, 2337-2340.
- (161) Calderon, N.; Ofstead, E. A.; Ward, J. P.; Judy, W. A.; Scott, K. W. *Journal of the American Chemical Society* **1968**, *90*, 4133-4140.
- (162) Herisson, J. L.; Chauvin, Y. *Makromolekulare Chemie* **1971**, *141*, 161.
- (163) Bielawski, C. W.; Grubbs, R. H. *Progress in Polymer Science* **2007**, *32*, 1-29.
- (164) Bazan, G. C.; Khosravi, E.; Schrock, R. R.; Feast, W. J.; Gibson, V. C.; Oregan, M. B.; Thomas, J. K.; Davis, W. M. *Journal of the American Chemical Society* **1990**, *112*, 8378-8387.
- (165) Bazan, G. C.; Oskam, J. H.; Cho, H. N.; Park, L. Y.; Schrock, R. R. *Journal of the American Chemical Society* **1991**, *113*, 6899-6907.
- (166) Bazan, G. C.; Schrock, R. R.; Cho, H. N.; Gibson, V. C. *Macromolecules* **1991**, *24*, 4495-4502.
- (167) Khosravi, E.; Al-Hajaji, A. A. *Polymer* **1998**, *39*, 5619-5625.

- (168) Khosravi, E.; Feast, W. J.; Al-Hajaji, A. A.; Leejarkpai, T. *Journal of Molecular Catalysis a-Chemical* **2000**, *160*, 1-11.
- (169) Schaverien, C. J.; Dewan, J. C.; Schrock, R. R. *Journal of the American Chemical Society* **1986**, *108*, 2771-2773.
- (170) Schrock, R. R. *Accounts of Chemical Research* **1990**, *23*, 158-165.
- (171) Schrock, R. R.; Depue, R. T.; Feldman, J.; Schaverien, C. J.; Dewan, J. C.; Liu, A. H. *Journal of the American Chemical Society* **1988**, *110*, 1423-1435.
- (172) Schrock, R. R.; Feldman, J.; Cannizzo, L. F.; Grubbs, R. H. *Macromolecules* **1987**, *20*, 1169-1172.
- (173) Schrock, R. R.; Murdzek, J. S.; Bazan, G. C.; Robbins, J.; Dimare, M.; Oregan, M. *Journal of the American Chemical Society* **1990**, *112*, 3875-3886.
- (174) Maughon, B. R.; Grubbs, R. H. *Macromolecules* **1997**, *30*, 3459-3469.
- (175) Nguyen, S. T.; Grubbs, R. H.; Ziller, J. W. *Journal of the American Chemical Society* **1993**, *115*, 9858-9859.
- (176) Nguyen, S. T.; Johnson, L. K.; Grubbs, R. H.; Ziller, J. W. *Journal of the American Chemical Society* **1992**, *114*, 3974-3975.
- (177) Weck, M.; Schwab, P.; Grubbs, R. H. *Macromolecules* **1996**, *29*, 1789-1793.
- (178) Wu, Z.; Benedicto, A. D.; Grubbs, R. H. *Macromolecules* **1993**, *26*, 4975-4977.
- (179) Hong, S. H.; Grubbs, R. H. *Journal of the American Chemical Society* **2006**, *128*, 3508-3509.
- (180) Kirkland, T. A.; Lynn, D. M.; Grubbs, R. H. *Journal of Organic Chemistry* **1998**, *63*, 9904-9909.
- (181) Halperin, A.; Tirrell, M.; Lodge, T. P. *Advances in Polymer Science* **1992**, *100*, 31-71.
- (182) Advincula, R. *Advances in Polymer Science* **2006**, *197*, 107-136.
- (183) Bergbreiter, D. E.; Kippenberger, A. M. *Advances in Polymer Science* **2006**, *198*, 1-49.
- (184) Buchmeiser, M. R. *Advances in Polymer Science* **2006**, *197*, 137-171.
- (185) Radhakrishnan, B.; Ranjan, R.; Brittain, W. J. *Soft Matter* **2006**, *2*, 386-396.

- (186) Tsujii, Y.; Ohno, K.; Yamamoto, S.; Goto, A.; Fukuda, T. *Advances in Polymer Science* **2006**, *197*, 1-45.
- (187) Brittain, W. J.; Minko, S. *Journal of Polymer Science Part A-Polymer Chemistry* **2007**, *45*, 3505-3512.
- (188) Barbey, R.; Lavanant, L.; Paripovic, D.; Schuwer, N.; Sugnaux, C.; Tugulu, S.; Klok, H. A. *Chemical Reviews* **2009**, *109*, 5437-5527.
- (189) Edmondson, S.; Osborne, V. L.; Huck, W. T. S. *Chemical Society Reviews* **2004**, *33*, 14-22.
- (190) Chang, Y.-C.; Frank, C. W. *Langmuir* **1996**, *12*, 5824-5829.
- (191) Chang, Y.-C.; Frank, C. W. *Langmuir* **1998**, *14*, 326-334.
- (192) Fong, B.; Russo, P. S. *Langmuir* **1999**, *15*, 4421-4426.
- (193) Fong, B.; Turksen, S.; Russo, P. S.; Stryjewski, W. *Langmuir* **2004**, *20*, 266-269.
- (194) Heise, A.; Menzel, H.; Yim, H.; Foster, M. D.; Wieringa, R. H.; Schouten, A. J.; Erb, V.; Stamm, M. *Langmuir* **1997**, *13*, 723-728.
- (195) Wang, Y.; Chang, Y.-C. *Macromolecules* **2003**, *36*, 6503-6510.
- (196) Wang, Y.; Chang, Y.-C. *Macromolecules* **2003**, *36*, 6511-6518.
- (197) Wang, Y.; Chang, Y.-C. *Adv. Mater.* **2003**, *15*, 290-293.
- (198) Wieringa, R. H.; Siesling, E. A.; Geruts, P. F. M.; Werkman, P. J.; Vorenkamp, E. J.; Erb, V.; Stamm, M.; Schouten, A. J. *Langmuir* **2001**, *17*, 6477-6484.
- (199) Wieringa, R. H.; Siesling, E. A.; Geruts, P. F. M.; Werkman, P. J.; Vorenkamp, E. J.; Erb, V.; Stamm, M.; Schouten, A. J. *Langmuir* **2001**, *17*, 6485-6490.
- (200) Whitesell, J. K.; Chang, H. K. *Science* **1993**, *261*, 73-76.
- (201) Wang, Y.; Chang, Y.-C. *Journal of the American Chemical Society* **2003**, *125*, 6376-6377.
- (202) Wong, M. S.; Cha, J. N.; Choi, K. S.; Deming, T. J.; Stucky, G. D. *Nano Letters* **2002**, *2*, 583-587.
- (203) Jaworek, T.; Neher, D.; Wegner, G.; Wieringa, R. H.; Schouten, A. J. *Science* **1998**, *279*, 57-60.

- (204) Oosterling, M.; Willems, E.; Schouten, A. J. *Polymer* **1995**, *36*, 4463-4470.
- (205) Oosterling, M.; Willems, E.; Schouten, A. J. *Polymer* **1995**, *36*, 4485-4490.
- (206) Wieringa, R. H.; Schouten, A. J. *Macromolecules* **1996**, *29*, 3032-3034.
- (207) Wieringa, R. H.; Siesling, E. A.; Werkman, P. J.; Vorenkamp, E. J.; Schouten, A. J. *Langmuir* **2001**, *17*, 6491-6495.
- (208) Czaun, M.; Rahman, M. M.; Takafuji, M.; Ihara, H. *Polymer* **2008**, *49*, 5410-5416.
- (209) Shundo, A.; Sakurai, T.; Takafuji, M.; Nagaoka, S.; Ihara, H. *Journal of Chromatography A* **2005**, *1073*, 169-174.
- (210) Abelow, A. E.; Zharov, I. *Soft Matter* **2009**, *5*, 457-462.
- (211) Kruk, M.; Dufour, B.; Celer, E. B.; Kowalewski, T.; Jaroniec, M.; Matyjaszewski, K. *Macromolecules* **2008**, *41*, 8584-8591.
- (212) Audouin, F.; Blas, H.; Pasetto, P.; Beaunier, P.; Boissiere, C.; Sanchez, C.; Save, M.; Charleux, B. *Macromolecular Rapid Communications* **2008**, *29*, 914-921.
- (213) Moreno, J.; Sherrington, D. C. *Chemistry of Materials* **2008**, *20*, 4468-4474.
- (214) Lenarda, M.; Chessa, G.; Moretti, E.; Polizzi, S.; Storaro, L.; Talon, A. *Journal of Materials Science* **2006**, *41*, 6305-6312.
- (215) Moller, K.; Bein, T.; Fischer, R. X. *Chemistry of Materials* **1999**, *11*, 665-673.
- (216) Frisch, H. L.; Mark, J. E. *Chemistry of Materials* **1996**, *8*, 1735-1738.
- (217) Wu, C. G.; Bein, T. *Science* **1994**, *266*, 1013-1015.
- (218) Wu, C. G.; Bein, T. *Chemistry of Materials* **1994**, *6*, 1109-1112.
- (219) Wu, C. G.; Bein, T. *Science* **1994**, *264*, 1757-1759.
- (220) Hicks, J. C.; Drese, J. H.; Fauth, D. J.; Gray, M. L.; Qi, G. G.; Jones, C. W. *Journal of the American Chemical Society* **2008**, *130*, 2902-2903.
- (221) Rosenholm, J. M.; Duchanoy, A.; Linden, M. *Chemistry of Materials* **2008**, *20*, 1126-1133.
- (222) Rosenholm, J. M.; Penninkangas, A.; Linden, M. *Chemical Communications* **2006**, 3909-3911.

- (223) Edler, K. J.; White, J. W. *Chemistry of Materials* **1997**, *9*, 1226-1233.
- (224) Daly, W. H.; Poche, D. *Tetrahedron Letters* **1988**, *29*, 5859-5862.
- (225) Cheng, K.; Landry, C. C. *Journal of the American Chemical Society* **2007**, *129*, 9674-9685.
- (226) Ladd, M. F. C.; Palmer, R. A. *Structure Determination by X-ray Crystallography*; Plenum: New York, 1977.
- (227) Rouquerol, F.; Rouquerol, J.; Sing, K. *Adsorption by Powders and Porous Solids*; Academic: San Diego, 1999.
- (228) Barrett, E. P.; Joyner, L. G.; Halenda, P. P. *Journal of the American Chemical Society* **1951**, *73*, 373-380.
- (229) Kruk, M.; Jaroniec, M.; Sayari, A. *Langmuir* **1997**, *13*, 6267-6273.
- (230) Harris, D. C.; Bertolucci, M. D. *Symmetry and Spectroscopy: An Introduction to Vibrational and Electronic Spectroscopy*; Oxford University Press: New York, 1978.
- (231) Reinert, F.; Hufner, S. *New Journal of Physics* **2005**, *7*, 97.
- (232) Watts, J. F.; Wolstenholme, J. *An Introduction to Surface Analysis by XPS and AES*; John Wiley & Sons: New York, 2003.
- (233) Davidson, B.; Fasman, G. D. *Biochemistry* **1967**, *6*, 1616-1629.
- (234) Greenfield, N.; Fasman, G. D. *Biochemistry* **1969**, *8*, 4108-4116.
- (235) Blout, E. R.; Asadourian, A. *Journal of the American Chemical Society* **1956**, *78*, 955-961.
- (236) Doty, P.; Lundberg, R. D. *Journal of the American Chemical Society* **1956**, *78*, 4810-4812.
- (237) Idelson, M.; Blout, E. R. *Journal of the American Chemical Society* **1957**, *79*, 3948-3955.
- (238) Mitchell, J. C.; Woodward, A. E.; Doty, P. *Journal of the American Chemical Society* **1957**, *79*, 3955-3960.
- (239) Kricheldorf, H. R.; Muller, D. *Macromolecules* **1983**, *16*, 615-623.
- (240) Hicks, J. C.; Jones, C. W. *Langmuir* **2006**, *22*, 2676-2681.

- (241) Hanton, S. D. *Chemical Reviews* **2001**, *101*, 527-569.
- (242) He, M. Y.; Chen, H. *Current Organic Chemistry* **2007**, *11*, 909-923.
- (243) Ji, H. N.; Nonidez, W. K.; Advincula, R. C.; Smith, G. D.; Kilbey, S. M.; Dadmun, M. D.; Mays, J. W. *Macromolecules* **2005**, *38*, 9950-9956.
- (244) Ji, H. N.; Sakellariou, G.; Mays, J. W. *Macromolecules* **2007**, *40*, 3461-3467.
- (245) Ji, H. N.; Sato, N.; Nonidez, W. K.; Mays, J. W. *Polymer* **2002**, *43*, 7119-7123.
- (246) Lunn, J. D.; Shantz, D. F. *Chemistry of Materials* **2009**, *21*, 3638-3648.
- (247) Casasus, R.; Marcos, M. D.; Martinez-Manez, R.; Ros-Lis, J. V.; Soto, J.; Villaescusa, L. A.; Amoros, P.; Beltran, D.; Guillem, C.; Latorre, J. *Journal of the American Chemical Society* **2004**, *126*, 8612-8613.
- (248) de Juan, F.; Ruiz-Hitzky, E. *Advanced Materials* **2000**, *12*, 430-432.
- (249) Mal, N. K.; Fujiwara, M.; Tanaka, Y. *Nature* **2003**, *421*, 350-353.
- (250) Cauda, V.; Schlossbauer, A.; Kecht, J.; Zurner, A.; Bein, T. *Journal of the American Chemical Society* **2009**, *131*, 11361-11370.
- (251) Kecht, J.; Schlossbauer, A.; Bein, T. *Chemistry of Materials* **2008**, *20*, 7207-7214.
- (252) Suzuki, T. M.; Nakamura, T.; Sudo, E.; Akimoto, Y.; Yano, K. *Journal of Catalysis* **2008**, *258*, 265-272.
- (253) Kilian, K. A.; Bocking, T.; Gaus, K.; Gooding, J. J. *Angewandte Chemie-International Edition* **2008**, *47*, 2697-2699.
- (254) van Grieken, R.; Calleja, G.; Stucky, G. D.; Melero, J. A.; Garcia, R. A.; Iglesias, J. *Langmuir* **2003**, *19*, 3966-3973.
- (255) Procopio, A.; De Luca, G.; Nardi, M.; Oliverio, M.; Paonessa, R. *Green Chemistry* **2009**, *11*, 770-773.
- (256) Lai, T. L.; Shu, Y. Y.; Lin, Y. C.; Chen, W. N.; Wang, C. B. *Materials Letters* **2009**, *63*, 1693-1695.
- (257) Ruhe, J.; Ballauff, M.; Biesalski, M.; Dziezok, P.; Grohn, F.; Johannsmann, D.; Houbenov, N.; Hugenberg, N.; Konradi, R.; Minko, S.; Motornov, M.; Netz, R. R.; Schmidt, M.; Seidel, C.; Stamm, M.; Stephan, T.; Usov, D.; Zhang, H. N. *Advances in Polymer Science* **2004**, *165*, 79-150.

- (258) Rozenberg, M.; Shoham, G. *Biophysical Chemistry* **2007**, *125*, 166-171.
- (259) Yeu, S.; Lunn, J. D.; Rangel, H. M.; Shantz, D. F. *Journal of Membrane Science* **2009**, *327*, 108-117.
- (260) Yoo, S.; Yeu, S.; Sherman, R. L.; Simanek, E. E.; Shantz, D. F.; Ford, D. M. *Journal of Membrane Science* **2009**, *334*, 16-22.

APPENDIX A

ADDITIONAL FIGURES FROM CHAPTER IV

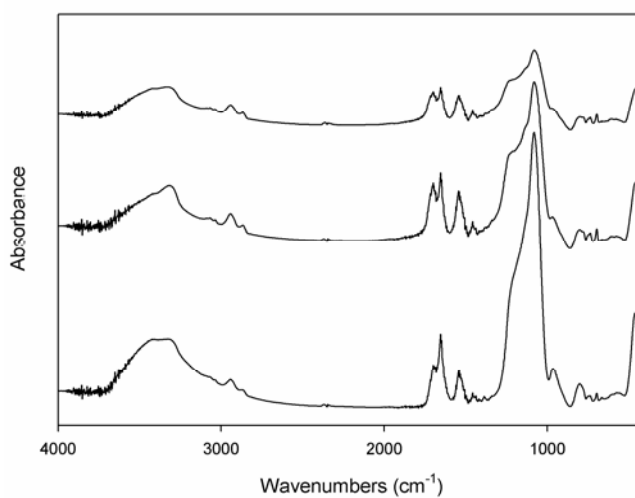


Figure A1 IR spectra of the Poly-Z-L-lysine—SBA-15 composites: 0.75mmol APTMS/g (top); 0.50mmol APTMS/g (middle); and 0.25mmol APTMS/g (bottom).

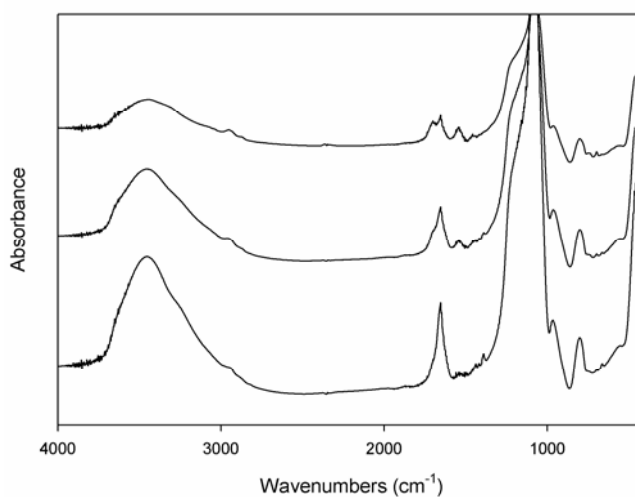


Figure A2 IR spectra of the Poly-Z-L-lysine—SBA-15 composites: 0.75mmol APTMS/g (top); 0.50mmol APTMS/g (middle); and 0.25mmol APTMS/g (bottom).

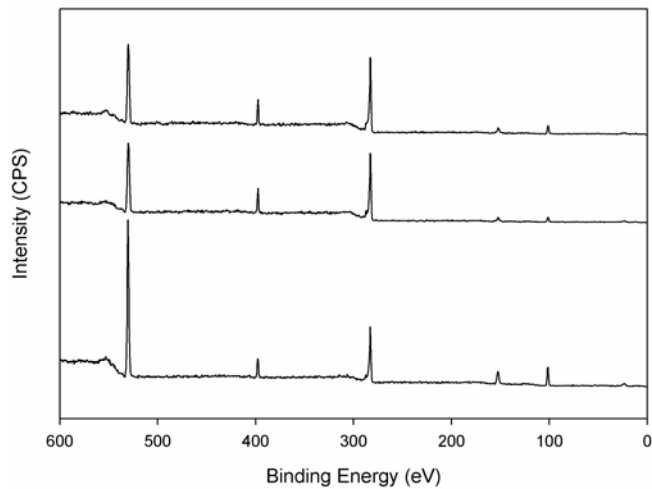


Figure A3 XPS of the Poly-Z-L-lysine—SBA-15 composites: 0.75mmol APTMS/g (top); 0.50mmol APTMS/g (middle); and 0.25mmol APTMS/g (bottom).

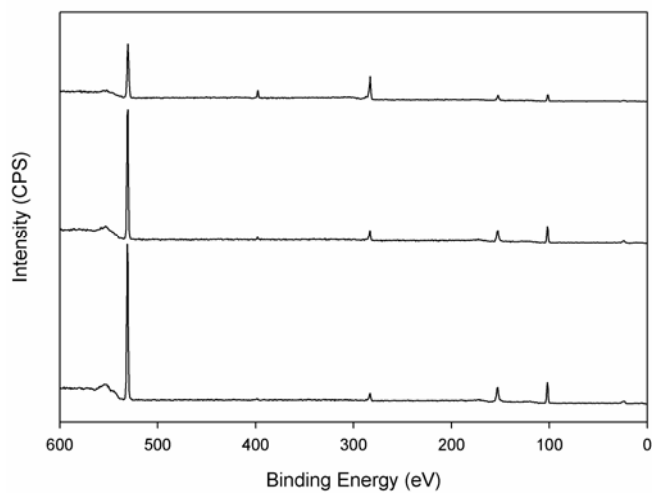


Figure A4 XPS of the Poly-Z-L-lysine—KIT-6 composites: 0.75mmol APTMS/g (top); 0.50mmol APTMS/g (middle); and 0.25mmol APTMS/g (bottom).

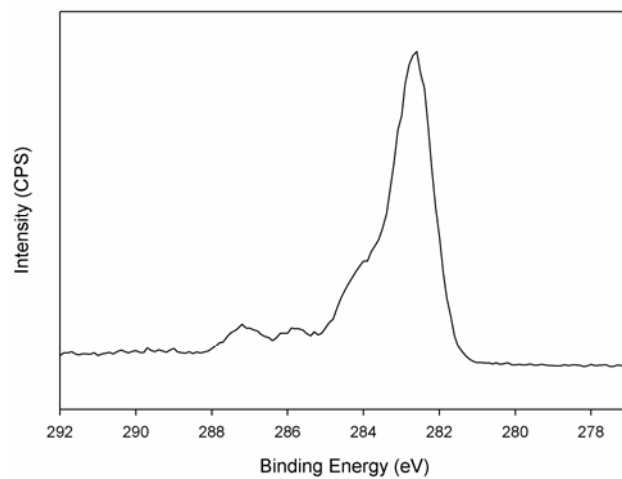


Figure A5 C1s high resolution XPS scan showing splitting due to peptide formation in the 0.75mmol/g MCM-41 Poly-Z-L-lysine composite.

Table A1 Tabulated TGA data for composite materials

Sample ID	Organic wt%
PZLK-0.75APTMS-MCM41	41.81
PZLK-0.50APTMS-MCM41	42.59
PZLK-0.25APTMS-MCM41	31.23
PZLK-0.75APTMS-SBA15	49.26
PZLK-0.50APTMS-SBA15	47.28
PZLK-0.25APTMS-SBA15	30.32
PZLK-0.75APTMS-KIT6	31.64
PZLK-0.50APTMS-KIT6	16.15
PZLK-0.25APTMS-KIT6	9.60
PLA-0.50APTMS-MCM41	40.03
PLA-0.75APTMS-SBA15	42.42
PLA-0.50APTMS-SBA15	40.19
PLA-0.25APTMS-SBA15	41.15
PLA-0.50APTMS-KIT6	36.59

Table A2 Tabulated Elemental Analysis Results: “TGA” denotes theoretical values calculated from the TGA results and “EA”, the values obtained from elemental analysis

Sample ID	C _{TGA} (wt%)	C _{EA} (wt%)	N _{TGA} (wt%)	N _{EA} (wt%)	H _{TGA} (wt%)	H _{EA} (wt%)	Si _{TGA} (wt%)	Si _{EA} (wt%)
PZLK-0.75APTMS-MCM41	26.78	25.68	4.73	5.06	3.00	3.70	27.20	23.50
PZLK-0.50APTMS-MCM41	27.29	25.71	4.66	5.07	2.99	3.67	26.84	24.60
PZLK-0.25APTMS-MCM41	20.02	19.06	3.37	3.97	2.17	3.05	32.15	28.90
PZLK-0.75APTMS-SBA15	31.56	30.76	5.49	5.50	3.50	3.91	23.72	21.90
PZLK-0.50APTMS-SBA15	30.30	29.39	5.16	5.19	3.31	3.31	24.65	24.65
PZLK-0.25APTMS-SBA15	19.43	18.55	3.27	3.40	2.11	2.78	32.57	27.80
PZLK-0.75APTMS-KIT6	20.26	13.81	3.69	2.77	2.31	2.49	31.95	30.6
PZLK-0.50APTMS-KIT6	10.34	8.50	1.90	1.87	1.19	1.19	39.20	35.10
PZLK-0.25APTMS-KIT6	6.15	5.58	1.07	1.45	0.68	1.65	42.26	37.6

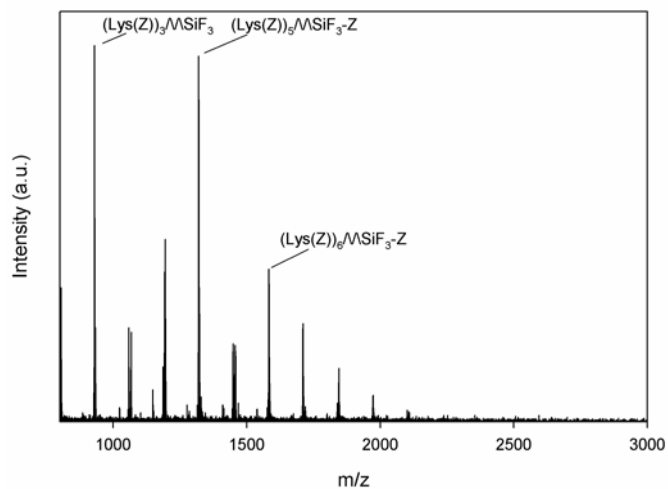


Figure A6 MALDI-TOF MS of peptide from the 0.50mmol APTMS/g MCM-41 Poly-Z-L-lysine composite.

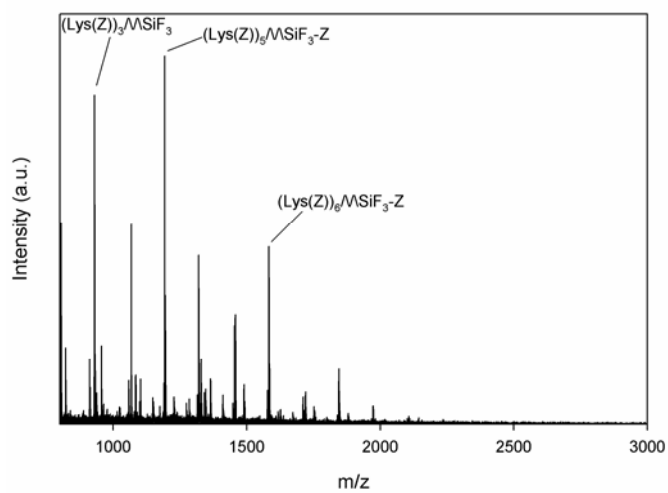


Figure A7 MALDI-TOF MS of peptide from the 0.50mmol APTMS/g KIT-6 Poly-Z-L-lysine composite.

APPENDIX B

ADDITIONAL FIGURES FROM CHAPTER V

I. Polylysine—SBA-15 Hybrids

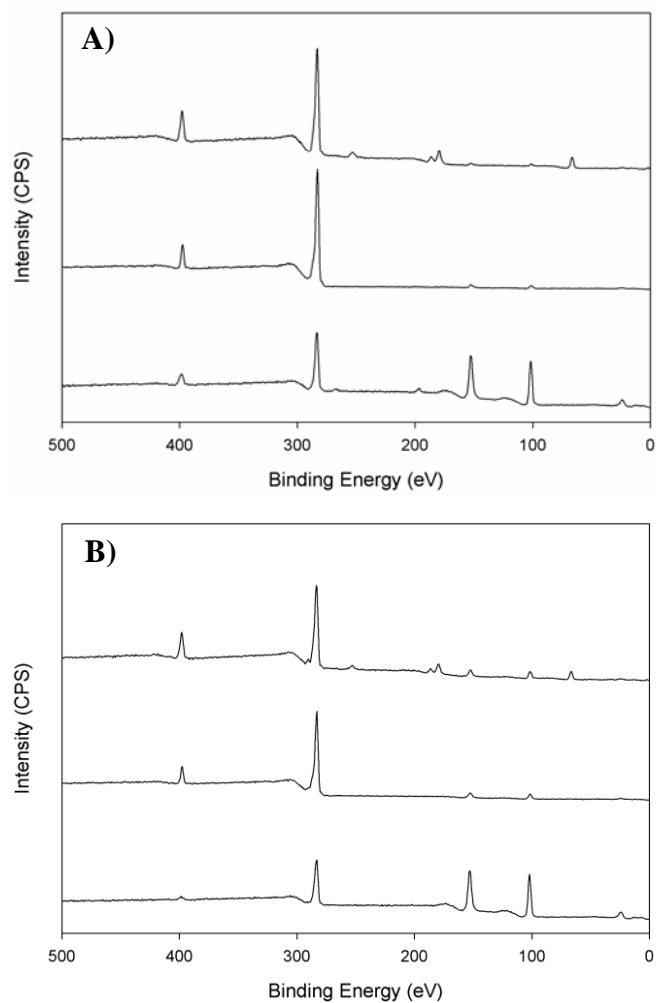


Figure B1 XPS spectra of the **X1** (A) and **I1** (B) poly-Z-L-lysine hybrids, showing spectra for the functionalized SBA-15 (bottom) and protected (middle) and deprotected hybrids (top).

II. Polylysine/thiols—SBA-15 Hybrids by traditional grafting/extraction

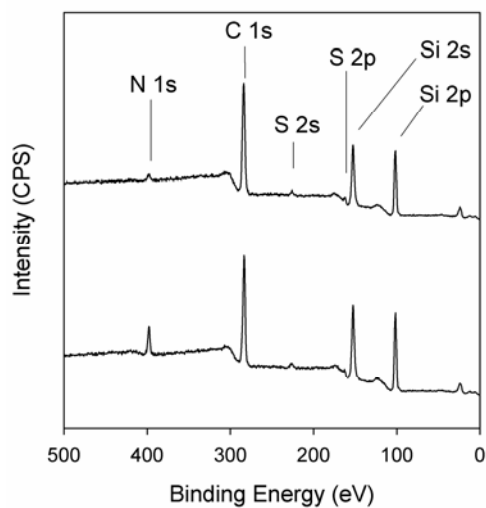


Figure B2 XPS spectra of **I2'** (top) and **X2'** (bottom).

Table B1 Adsorption and TGA data of hybrids synthesized from **X2'** and **I2'**.

Sample	$S(a_s)$ [m^2/g]	V_p^a [cm^3/g]	$d_p(BJH)$ [nm]	Organic [wt%]
SBA-15				13.2
X2'	262	0.37	6.5	21.1
I2'	492	0.53	7.0	31.7
PZK-X2'	----	n.p.	----	52.0
PK-X2'	----	n.p.	----	53.2
PZK-I2'	----	n.p.	----	71.8
PK-I2'	----	n.p.	----	54.5

^a Recorded at $p/p_0 = 0.9$; n.p. = non-porous.

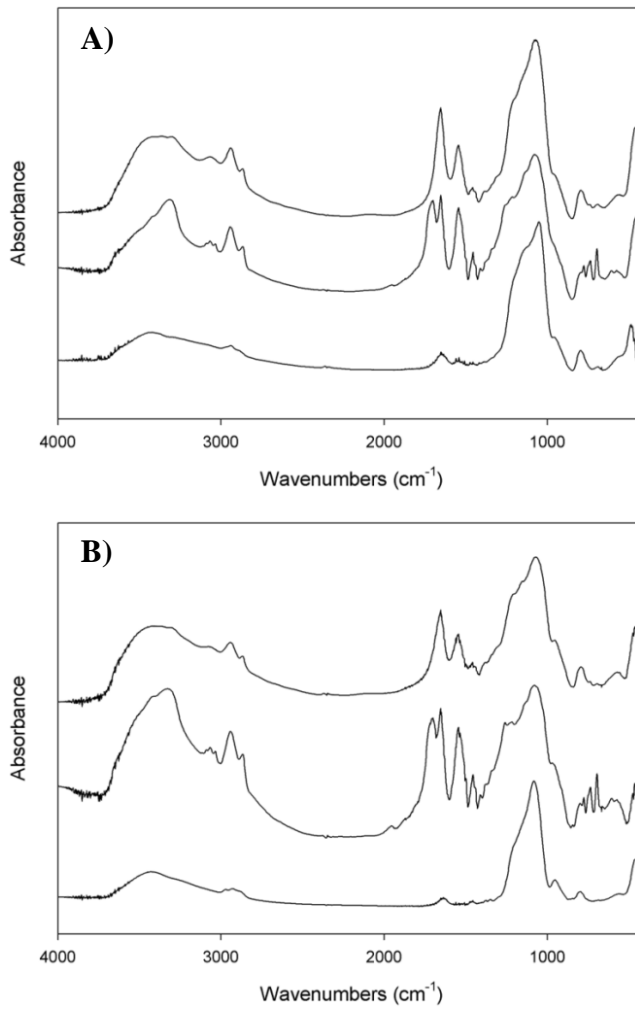


Figure B3 IR spectra of the externally (A) and internally (B) poly-Z-L-lysine grafted SBA-15, showing spectra for both protected and deprotected hybrids.

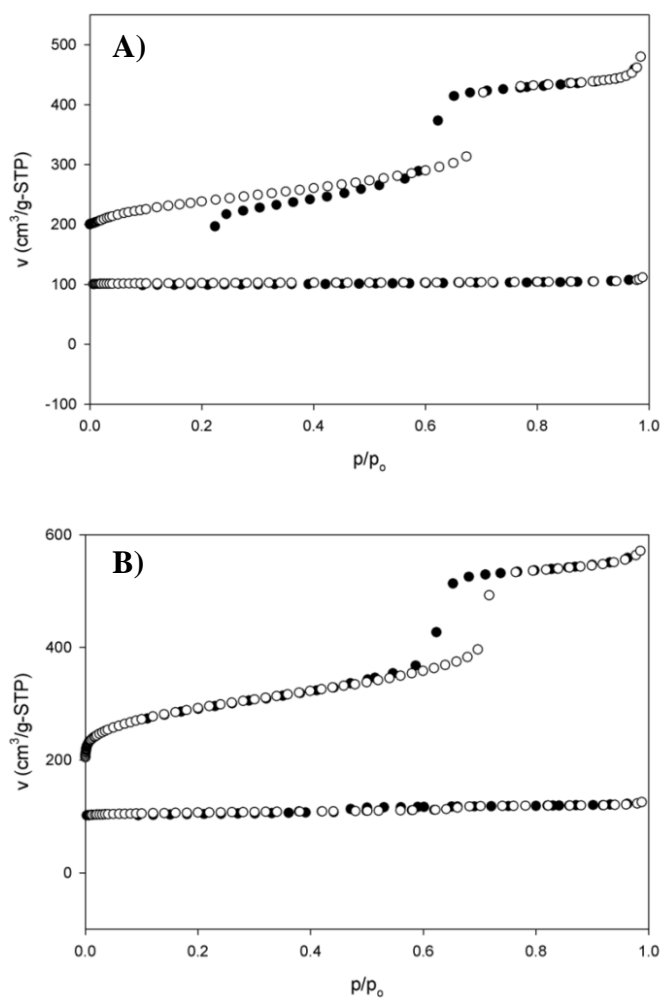


Figure B4 Nitrogen adsorption isotherms of the externally (A) and internally (B) poly-Z-L-lysine grafted SBA-15; Top to bottom – functionalized SBA-15 and PK-SBA15 hybrid.

III. Polylysine/thiols—SBA-15 Hybrids by microwave grafting/extraction

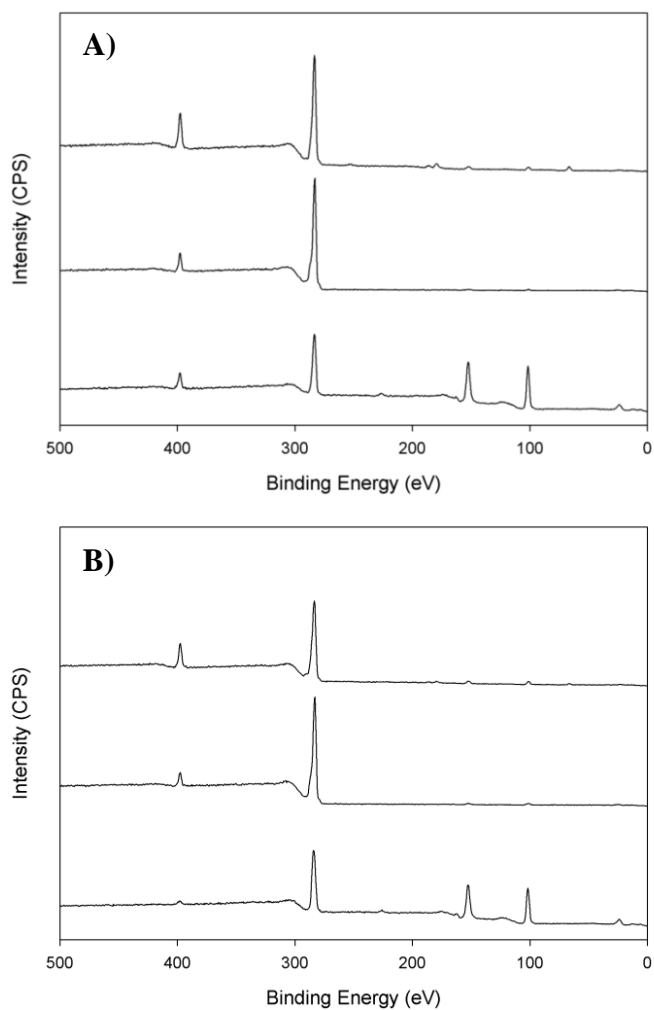


Figure B5 XPS spectra of the **X2** (A) and **I2** (B) poly-Z-L-lysine hybrids, showing spectra for the functionalized SBA-15 (bottom) and protected (middle) and deprotected hybrids (top).

Table B2 Adsorption and TGA data of as-made and extracted samples using microwave grafting approach.

Sample	V_p^a [cm ³ /g]	Organic [wt%]
SBA-15 as-made	0.24	47.8
SBA-15 extracted	0.90	9.4
NH ₂ -SBA-15 as-made	0.35	28.8
NH ₂ (X)-SH(I)-SBA-15 ^b	0.66	19.6

^a Recorded at p/p₀ = 0.9
^b X2

Table B3 Atomic ratios determined by XPS.

Sample	N/Si _{XPS} [mol/mol]	C/Si _{XPS} [mol/mol]	C/N _{XPS} [mol/mol]
X2	0.28	1.43 ^a	5.11 ^a
I2	0.06	0.17 ^a	2.99 ^a
PZK-X2-10	28.3	425.2	15.0
PZK-X2-5	15.5	200.9	12.9
PZK-I2-10	17.8	166.3	9.3
PZK-I2-5	6.0	59.7	10.0

^a Includes C 1s contribution from mercaptosilane

APPENDIX C

ADDITIONAL FIGURES FOR CHAPTER VI

Table C1 XPS atomic ratio data of OMS sphere hybrids.

Sample	N/Si _{XPS} [mol/mol]	C/Si _{XPS} [mol/mol]	C/N _{XPS} [mol/mol]
NH ₂ /SH-MMS	0.12	2.21 ^a	19.1 ^a
PZK/SH-MMS	1.5	20.0	13.1
PK/SH-MMS	8.5	42.3	5.0
PBG/SH-MMS	1.8	38.8	21.1
PG/SH-MMS	5.3	56.6	10.8
PZK&PBG/SH-MMS	5.0	66.4	13.2
PK&PG/SH-MMS	12.5	69.8	5.6

^a Includes C 1s contribution from mercaptosilane

VITA

Name: Jonathan David Lunn

Address: The Dow Chemical Company
1776 Building
Midland, MI 48674

Email Address: jdlunn@tamu.edu

Education: B.S., Chemical Engineering, Texas A&M University, 2004
M.S., Chemical Engineering, Texas A&M University, 2006
Ph.D., Chemical Engineering, Texas A&M University, 2010